

**Selective Oxidation of Propane Over Cation  
Exchanged Zeolites**

*Jiang Xu*

## Promotion Committee

Chairman:	Prof. dr. C. Hoede	University of Twente
Promotor:	Prof. dr. ir L. Lefferts	University of Twente
Assistant promotor:	Dr. B. L. Mojet	University of Twente
Member:	Prof. dr. P. J. Kelly	University of Twente
	Dr. J. G. van Ommen	University of Twente
	Prof. dr. D. de Vos	Katholieke Universiteit Leuven
	Dr. H. J. M. Bouwmeester	University of Twente
	Dr. G. Mul	Technische Universiteit Delft
	Prof. dr. R. A. van Santen	Technische Universiteit Eindhoven

The research described in this thesis was performed under the auspices of the Dutch Institute for Research in Catalysis (NIOK). Financial support from CW/STW for the project No. 790-36-057 is gratefully acknowledged.

ISBN 90 365 2199 8

Copyright © 2005 by Jiang Xu, Enschede, The Netherlands

Printed by Printpartners Ipskamp, Enschede

No part of this book may be reproduced in any form of print, photo print, microfilm or any other means without permission from the author / publisher

# **SELECTIVE OXIDATION OF PROPANE OVER CATION EXCHANGED ZEOLITES**

DISSERTATION

to obtain  
the doctor's degree at University of Twente,  
on the authority of the rector magnificus,  
prof. dr. W.H.M. Zijm,  
on account of the decision of the graduation committee  
to be publicly defended  
on Thursday, 9<sup>th</sup> June, 2005 at 15.00

by

**Jiang Xu**

born on 12 March, 1972  
in Changshu, P. R. China

This dissertation has been approved by the promoter

**Prof. dr. ir. L. Lefferts**

And the assistant promoter

**Dr. B. L. Mojet**

## Contents

<b>Summary</b> .....	2
<b>Summary in Dutch</b> .....	5
<b>Summary in Chinese</b> .....	8
<b>Chapter 1 Background and motivation</b> .....	11
<b>Chapter 2 Propane selective oxidation on alkaline-earth exchanged Y zeolite at room temperature</b> .....	22
<b>Chapter 3 Desorption of acetone from alkaline-earth exchanged Y zeolite after propane selective oxidation</b> .....	38
<b>Chapter 4 The effect of Ca<sup>2+</sup> position in zeolite Y on selective oxidation of propane at room temperature</b> .....	51
<b>Chapter 5 The effects of Brönsted acidity in the mechanism of selective oxidation of propane to acetone on CaY zeolite at room temperature</b> .....	67
<b>Chapter 6 Formation of M<sup>2+</sup>(O<sub>2</sub>)(C<sub>3</sub>H<sub>8</sub>) species in alkaline-earth exchanged Y zeolite during propane selective oxidation</b> .....	88
<b>Chapter 7 Effect of zeolite geometry for propane selective oxidation on cation electrostatic field of Ca<sup>2+</sup> exchanged zeolites</b> .....	108
<b>Chapter 8 Epitome</b> .....	124
<b>Acknowledgements</b> .....	130
<b>List of Publications</b> .....	131
<b>Curriculum Vita</b> .....	132

## Summary

This thesis focuses on investigation of the fundamental knowledge on a new method for selective oxidation of propane with O<sub>2</sub> at low temperature (< 100°C). The relation between propane catalytic selective oxidation and physicochemical properties of cation exchanged Y zeolite has been studied. An attempt has been made to determine how propane oxidation activity and selectivity are influenced by charge-compensating cations, acidity and geometry of zeolites.

In **Chapter 1**, a literature overview on the new method for selective oxidation of hydrocarbons by oxygen at low temperature on cation-exchanged zeolites was summarized. Following the overview, the questions and challenges for this novel method were presented, and objectives for this thesis were provided.

First, the effect of charge-compensating cations on propane selective oxidation at room temperature was studied with *in-situ* infrared spectroscopy in **Chapter 2**. The reaction rate was observed to increase in the order BaY < MgY < SrY < CaY based on the rate of formation of adsorbed acetone. The observed lower acetone growth rate for MgY, not expected based on its higher electrostatic field, was explained by a higher hydrolysis degree of cations, results in a lower amount of available Mg<sup>2+</sup> ions. Isopropylhydroperoxide (IHP) was observed as a reaction intermediate which could be decomposed into acetone and water. The acetone/water ratio was found to increase with cation size, while no other products could be detected. Moreover, the acetone/IHP ratio decreased with decreasing number of Brönsted acid sites. Both observations mark the importance of Brönsted acid sites for this reaction, in addition to alkaline-earth cations. Based on the infrared spectra data, water and IHP are adsorbed on or close to the cations in the zeolite, while acetone adsorbed on Brönsted acid sites, pointing to a two-step mechanism in which different active sites are involved. Conversion of propane into IHP takes place on cations, while the decomposition into acetone occurs by Brönsted acid sites.

Since the acetone produced from propane selective oxidation on cation exchanged Y zeolite adsorbed strongly on the catalyst surface, the catalytic cycle is not yet closed. Thus, desorption of products from a series of alkaline-earth exchanged Y zeolites after room temperature propane selective oxidation was investigated by *in-situ* infrared and mass spectroscopy in **chapter 3**. It was found that the intermediate product, isopropylhydroperoxide (IHP), did not desorb during temperature-programmed-desorption experiments, but converted into acetone and water. Decomposition rate of IHP into acetone increased in the order BaY < SrY < CaY (< MgY) which was attributed to the number of acid sites in the samples. TPD results on CaY zeolite pointed to two acetone adsorption sites, which are tentatively assigned to

Brönsted acid sites and  $\text{Ca(OH)}_x$  species. Acetone mainly desorbed at higher temperatures ( $> 250\text{ }^\circ\text{C}$ ) under dry conditions. Addition of water, however, resulted in gas phase acetone already at room temperature. Further, upon addition of water, both desorption peaks were shifted to lower temperature and showed increased intensities. From the results it can be concluded that water clearly facilitates acetone desorption, most likely *via* shielding of the electrostatic field and creation of additional sites.

The positions of cation in zeolite Y could strongly affect the electrostatic field, as well as the accessibility to the reactant molecules. Therefore, the effects of cation location on the selective oxidation of propane on calcium exchanged Y zeolite were investigated in **chapter 4**. Increasing the  $\text{Ca}^{2+}$  exchange level in CaNaY zeolites resulted in altered properties for the zeolites: the amount of Brönsted and Lewis acid sites increased, the adsorbed propane quantity increased, the initial acetone formation rate increased and the amount of desorbed acetone decreased. Moreover, all these properties showed a sudden change above 50%  $\text{Na}^+$  exchange levels with  $\text{Ca}^{2+}$ , which can be fully attributed to the location of  $\text{Ca}^{2+}$  in the Y-zeolite framework. Clearly, only  $\text{Ca}^{2+}$  ions located in the supercage contribute to the formation of Brönsted and Lewis acidity as well as propane oxidation activity at room temperature.

In order to clarify whether the cation and Brönsted acid sites act independently in the propane selective oxidation on CaY zeolite, or that a cooperation of both sites is need, a series of CaY with a systematic variation of concentration of Brönsted acid sites were prepared, and propane selective oxidation was studied on these catalysts in **Chapter 5**. It was observed that increasing concentration of Brönsted acid sites on calcium exchanged Y zeolite, volcano type of plots are observed for: (1) amount of adsorbed propane; (2) initial acetone formation rate; (3) total amount of acetone produced after 20 hours of reaction; (4) acetone selectivity. The observations strongly point out that increasing proton concentration speeds up IHP formation *via* a proton abstraction step. Formation of a minor by-product (2-propanol) was observed when decreasing or increasing Brönsted acidity. This was attributed to the parallel reaction pathway of IHP homolytic decomposition in addition to IHP decomposition into acetone and water. The kinetics of IHP decomposition into acetone and water showed a second order in IHP.

In **Chapter 6** we extensively studied  $\text{d}_2$ -propane and oxygen adsorption on earth alkaline cation exchanged Y zeolite by infrared spectra at room temperature. The results showed that oxygen and propane are activated by simultaneous adsorption at the cation site to form a  $\text{M}^{2+}(\text{O}_2)(\text{C}_3\text{H}_8)$  species *via* exclusive electrostatic cation-adsorbate interactions. In the thermal reaction, this species facilitates both molecules to interaction to form a transition state to IHP. In perfect agreement with the oxygen

activation induced by the electrostatic field of the  $M^{2+}$  cation, the activity of propane selective oxidation to acetone was observed to increase in order  $BaY < MgY < SrY < CaY$ .

The effects of shape and size of  $Ca^{2+}$  exchanged zeolites on activity and selectivity of propane oxidation reaction were further investigated in **Chapter 7**. Based on FTIR spectra of oxygen and propane adsorption at room temperature, the electrostatic field of  $Ca^{2+}$  was found to increase in the order  $CaY < CaMOR < CaZSM5$ . The electrostatic field and Lewis acidity of  $Ca^{2+}$  cation on CaY and CaZSM5 correlate strongly with propane selective oxidation activity and selectivity. Low activity but high selectivity to acetone was observed for propane oxidation on CaY zeolite due to the main reaction path of heterolytic  $H_2O$  elimination of reaction intermediate IHP. On CaZSM5, an unusual high electrostatic field and Lewis acidity of  $Ca^{2+}$  cation resulted in high activity, but homolytic IHP decomposition was favoured, which formed a 2:1 mixture of 2-propanol and acetone in the products. On CaMOR, the steric restriction for accommodating isopropylhydroperoxide (IHP) resulted in the lowest activity of acetone formation. Further, the high Brönsted acid concentration with high propane polarization on CaMOR resulted in propane cracking and further oxidation into CO and  $CO_2$ . It was convincingly shown that the electrostatic field of the  $Ca^{2+}$  cation, the structures of the zeolites and the presence of Brönsted acid sites play important roles in the overall mechanism of propane partial oxidation on  $Ca^{2+}$  exchanged zeolites.

Finally, all results are summarized in **Chapter 8**, where also recommendations for future work are given.



## Samenvatting

Dit proefschrift richt zich op het verkrijgen van fundamentele kennis over een nieuwe methode voor selectieve oxidatie van propaan met O<sub>2</sub> bij lage temperaturen (< 100°C). Onderzocht is de relatie tussen de (selectieve katalytische) propaanoxidatie en de fysische chemische eigenschappen van kation uitgewisseld Y zeoliet. Een poging is gedaan om vast te stellen hoe de propaanoxidatie (activiteit en selectiviteit) wordt beïnvloed door ladingscompenserende kationen, zuurgraad en geometrie van de zeolieten.

In hoofdstuk 1, wordt en literatuur overzicht gegeven van de nieuwe methode voor selectieve oxidatie van koolwaterstoffen door zuurstof bij lage temperatuur op kation uitgewisselde zeolieten. In vervolg op dit overzicht worden de vragen en uitdagingen van deze nieuwe methode gepresenteerd en de doelen voor dit proefschrift geformuleerd.

In hoofdstuk 2 wordt het effect van lading compenserende kationen op de selectieve propaan oxidatie bij kamertemperatuur met in situ ir bestudeerd. De waargenomen reactiesnelheid, gebaseerd op de acetonvorming, nam toe in volgorde BaY < MgY < SrY < CaY. De waargenomen lage groeisnelheid van aceton voor MgY, welke niet wordt verwacht op basis van het hogere elektrostatische veld, wordt verklaard door de hogere graad van hydrolyse van de kationen, dat resulteert in een geringere hoeveelheid beschikbare Mg<sup>2+</sup> ionen. Isopropylhydroperoxide (IHP) werd waargenomen als een reactie intermediair, welke kan ontleden in aceton en water. De aceton/water verhouding nam toe met de grootte van het kation, terwijl geen ander product kon worden gedetecteerd. Bovendien nam de aceton/IHP verhouding af met de afname van het aantal aanwezige Brönsted zure sites. Beide waarnemingen markeren het belang van Brönsted zure plaatsen voor deze reactie, naast die van aardalkali kationen. Gebaseerd op data uit infrarood spectra, worden water en IHP beide geadsorbeerd op of dichtbij de kationen in de zeoliet, terwijl aceton wordt geadsorbeerd op Brönsted zure plaatsen, hetgeen wijst op een tweestap mechanisme, waarbij verschillende actieve plaatsen zijn betrokken. Omzetting van propaan in IHP vindt plaats op kationen, terwijl de ontleding in aceton plaatsvindt op Brönsted zure plaatsen.

Omdat het door propaan oxidatie geproduceerde aceton zeer sterk adsorbeert op kation uitgewisselde Y zeoliet, is de katalytische cirkel nog niet gesloten. Om die reden werd de desorptie van producten van een serie van aardalkali uitgewisselde Y zeolieten, na selectieve propaan oxidatie bij kamertemperatuur, met behulp van in situ infrarood en massa spectrometrie bestudeerd in hoofdstuk 3. Er werd gevonden

dat het intermediair isopropylhydroperoxide (IHP), niet desorbeerde gedurende een temperatuur geprogrammeerd desorptie experiment, maar omgezet werd in aceton en water. De ontledingssnelheid van IHP naar aceton nam toe in de volgorde BaY < SrY < CaY (< MgY), hetgeen werd toegeschreven aan het aantal actieve plaatsen in het monster. TPD resultaten van het CaY zeoliet wijzen op twee aceton adsorptie plaatsen, die mogelijk kunnen worden toegeschreven aan Brönsted zure plaatsen en  $\text{Ca}(\text{OH})_x$  vormen. Aceton desorbeert voornamelijk bij hoge temperaturen ( $>250^\circ\text{C}$ ) onder droge condities. Het toevoegen van water resulteert echter in gasfase aceton bij kamertemperatuur. Bij toevoegen van meer water, schuiven beide desorptie pieken naar lagere temperatuur en nemen toe in intensiteit. Uit deze resultaten kan duidelijk worden geconcludeerd, dat water de desorptie van aceton vereenvoudigt, hoogst waarschijnlijk via afscherming van het elektrostatische veld.

De positie van kationen in het Y zeoliet kan het elektrostatische veld en de toegankelijkheid van de reagerende moleculen sterk beïnvloeden. Daarom werden de effecten van de kationlocatie op de selectieve propaan oxidatie op calcium Y zeoliet onderzocht in Hoofdstuk 4. Verhogen van het  $\text{Ca}^{2+}$  uitwisselingsniveau in CaNaY zeolieten resulteert in veranderde eigenschappen van het zeoliet: de hoeveelheid Brönsted en Lewis zure plaatsen neemt toe, de geadsorbeerde hoeveelheid propaan neemt toe, de initiële aceton vormingssnelheid en de hoeveelheid gedesorbeerde aceton nemen af. Bovendien vertonen al deze eigenschappen een plotselinge verandering boven de 50%  $\text{Na}^+$  uitwisselingsniveaus met  $\text{Ca}^{2+}$ , hetgeen volledig kan worden toegeschreven aan de locatie van  $\text{Ca}^{2+}$  in het Y-zeoliet rooster. Het is duidelijk dat alleen de  $\text{Ca}^{2+}$  ionen in de superkooien bijdragen aan de vorming van Brönsted en Lewis zure plaatsen en aan de propaan oxidatie activiteit bij kamertemperatuur.

Om vast te stellen of het kation en de Brönsted zure plaats, onafhankelijk van elkaar werken bij de propaan selectieve oxidatie op CaY zeoliet, of dat samenwerking van beide plaatsen is vereist, is een serie CaY bereid met een systematische variatie van de concentratie van de Brönsted zure plaatsen en werd de propaan oxidatie over deze katalysatoren bestudeerd in Hoofdstuk 5. Waargenomen werd dat toenemende concentraties van Brönsted zure plaatsen op calcium uitgewisselde Y zeolieten, resulteerde in vulkaan curves voor: (1) hoeveelheid geadsorbeerd propaan; (2) initiële aceton vormingssnelheid; (3) totale hoeveelheid aceton geproduceerd na 20 uur reactie en (4) aceton selectiviteit. De waarneming suggereert, dat een toenemende proton concentratie de IHP vorming versnelt via proton abstractie. De vorming van een kleine hoeveelheid bijproduct (2-propanol) werd waargenomen, wanneer de Brönsted zuursterkte veranderde (toename of afname). Dit werd toegeschreven aan een parallel reactiepad van homolytische IHP ontleding, naast de ontleding van IHP in aceton en water.

In hoofdstuk 6 hebben we uitvoerig de  $\text{d}_2$ -propaan en zuurstof adsorptie op aardalkali kation

uitgewisselde Y zeoliet bestudeerd, met behulp van infrarood spectroscopie bij kamertemperatuur. De resultaten tonen dat zuurstof en propaan worden geactiveerd door gelijktijdige adsorptie op de kation plaats onder de vorming van  $M^{2+}(O_2)(C_3H_8)$  deeltjes via exclusieve elektrostatische kation adsorbaat interacties. Bij de thermische reactie stelt dit deeltje beide moleculen in staat tot een interactie, waarbij de overgangstoestand naar IHP kan worden gevormd. In prima overeenstemming met de zuurstof activering veroorzaakt door het elektrostatische veld van het  $M^{2+}$  kation, wordt waargenomen dat de activiteit van propaanselectieve oxidatie naar aceton toeneemt in de volgorde  $BaY < MgY < SrY < CaY$ .

De effecten van de structuur en de grootte van kanalen en kooien in de  $Ca^{2+}$ uitgewisselde zeolieten op activiteit en selectiviteit van de propaan oxidatie reactie werd verder bestudeerd in hoofdstuk 7. Gebaseerd op FTIR spectra van zuurstof en propaan adsorptie bij kamertemperatuur, werd gevonden dat het elektrostatische veld van  $Ca^{2+}$  toeneemt in de volgorde van  $CaY < CaMOR < CaZSM5$ . Het elektrostatische veld en de Lewis zuursterkte van  $Ca^{2+}$  in  $CaY$  en  $CaZSM5$  komt sterk overeen met de propaan oxidatie activiteit en selectiviteit. Lage activiteit maar hoge selectiviteit naar aceton werd waargenomen voor de propaan oxidatie op  $CaY$  zeoliet tengevolge van het hoofdreactiepad van de heterolytische  $H_2O$  eliminatie uit het reactie-intermediair IHP. Op  $CaZSM5$  resulteert een ongebruikelijk hoog elektrostatisch veld en Lewis zuursterkte van het  $Ca^{2+}$  kation in een hoge activiteit, maar homolytische IHP ontleding, welke leidt tot een 2:1 mengsel van 2-propanol en aceton in het product. Op  $CaMOR$  resulteren de sterische beperkingen voor onderbrenging van IHP in de laagste activiteit voor aceton vorming. Verder resulteert de hoge Brönsted zuur concentratie, samen met de hoge propaan polarisatie op  $CaMOR$ , in het kraken en oxideren van propaan tot  $CO$  en  $CO_2$ . Het is duidelijk aangetoond dat het elektrostatische veld van de  $Ca^{2+}$  kationen, de structuur van de zeolieten en de aanwezigheid van Brönsted zure plaatsen, belangrijke rollen spelen in het totaal mechanisme van de partiele oxidatie van propaan op  $Ca^{2+}$  uitgewisselde zeolieten.

Tenslotte worden alle resultaten samengevat in Hoofdstuk 8, waar ook de verdere aanbevelingen voor toekomstig werk worden gegeven.

## 概述

本篇论文着重研究了低温( $<100^{\circ}\text{C}$ )下丙烷在改进型分子筛催化剂上的选择氧化机理,系统地研究了催化剂的物理和化学性能对丙烷选择氧化活性和选择性的影响.这些物化性能包括分子筛的几何构造,酸性和阳离子类型.

在第一章里,作者对分子筛低温催化选择氧化烷烃的新工艺做了系统的综述,同时列出了新工艺中存在的问题和面临的挑战.

作者首先运用原位红外光谱技术对Y分子筛中阳离子类型对丙烷选择氧化活性和选择性的影响进行了研究.结果表明丙烷选择氧化活性顺序为  $\text{BaY} < \text{MgY} < \text{SrY} < \text{CaY}$ ,并不象理论预期的那样, $\text{MgY}$  会表现出较高的催化活性.这个差异被归结为分子筛中 $\text{Mg}^{2+}$ 离子易水解而导致低浓度 $\text{Mg}^{2+}$ 离子的存在.研究发现反应通过中间体异丙烷过氧化氢而最终分解产生终级产物丙酮和水.红外光谱显示水和异丙烷过氧化氢吸附于金属阳离子上,而丙酮吸附在B酸中心.基于此推断出反应通过两步催化实现.丙烷选择氧化形成异丙烷过氧化氢发生在金属阳离子中心,而异丙烷过氧化氢分解形成丙酮和水在B酸中心实现.

第三章详细研究了反应生成的丙酮的脱附条件.在反应条件下,丙酮强吸附于分子筛中.程序升温结果显示丙酮脱附需要高于  $250^{\circ}\text{C}$ .但是在反应后的催化剂上吸附少量水,丙酮即可在室温下脱附.由此推断水的加入减少了分子筛中静电场对丙酮的吸附作用,同时可能生成别的丙酮吸附位而减弱了丙酮的吸附强度.

第四章对丙烷选择氧化活性受金属阳离子在分子筛中的分布进行了系统的研究. 结果表明只有当金属阳离子交换度高于 50% 时, 丙烷选择氧化活性才获得显著提升. 研究表明只有位于大孔内的金属阳离子才是反应活性中心.

第五章就丙烷选择氧化活性受 B 酸浓度的影响进行了系统的研究. 结果表明当金属阳离子和 B 酸活性中心的浓度达到一定程度时, 丙烷选择氧化活性达到最高. 改变金属阳离子和 B 酸活性中心的比例, 对于丙烷吸附量; 丙酮起始反应速度; 丙酮生成量和丙酮选择性都呈现火山型曲线变化趋势. 同时发现异丙烷过氧化氢除了可通过分解形成丙酮和水外, 还可均裂生成自由基而进一步反应形成异丙醇. 动力学研究发现异丙烷过氧化氢分解形成丙酮和水是二级反应.

第六章对丙烷和氧气在分子筛催化剂上的吸附活化进行了详细的研究. 结果表明丙烷和氧气能够同时吸附与金属阳离子中心而形成反应活性中间体  $M^{2+}(O_2)(C_3H_8)$ . 区别于常规吸附, 这种吸附完全通过静电场作用而实现对反应物的活化. 丙烷选择氧化活性顺序为  $BaY < MgY < SrY < CaY$ , 这与氧气受活化程度相一致.

第七章是关于丙烷选择氧化活性和选择性受分子筛类型的影响的研究. 氧气吸附红外光谱表明分子筛中静电场随分子筛类型而改变. 静电场强度的递增顺序为  $CaY < CaMOR < CaZSM5$ . 丙烷选择氧化活性和选择性与分子筛中静电场强度和 L 酸有密切关系. 在  $CaY$  分子筛上, 异丙烷过氧化氢分解形成丙酮和水是主要反应. 而在  $CaMOR$  分子筛上, 异丙烷过氧化氢均裂生成自由基而进一步反应形成异丙醇占主导地位. 一维结构  $MOR$  分子筛由于位阻效应而呈现较低丙烷选择氧化活性. 同时高含量 B 酸中心还导致丙烷过度氧化形成  $CO$  和  $CO_2$ .

第八章对所有的得到的结果作了总结,并提出了今后的研究方向.

# Chapter 1

## Background and Motivation

---

### 1.1 Challenges of selective oxidation of hydrocarbon

Selective partial oxidation of hydrocarbons (alkanes, alkenes and aromatics) is one of the important types of processes in chemical industry. The products are used as building blocks for plastic and synthetic fibres as well as industrial intermediates in the manufacture of fine chemicals<sup>1-11</sup>. Oxidation of low alkanes plays a central role in the utilization of natural gas and volatile petroleum fractions as new feedstocks for important industrial chemicals.

For most of these large-scale processes, molecular oxygen is the most economically viable oxidant. The selective oxidation processes using gaseous oxygen as an oxidizing agent can be classified in two groups. The first group covers high-temperature processes using mixed oxide catalysts (gas-solid reaction). Reactions occur typically *via* a Mars-van Krevelen mechanism<sup>7</sup>. In this mechanism, the active oxygen species are lattice oxygen and gaseous oxygen simply re-oxidizes the catalyst to close the catalytic cycle<sup>1-4</sup>. A typical example is n-butane oxidation to maleic anhydride on Vanadium/Phosphorus oxides (VPO catalyst)<sup>12;13</sup>, where a lattice oxygen defect site of vanadium is considered as active site for the activation of oxygen molecule. The second group consists of low-temperature processes in liquid phase, usually involving a radical type mechanism with oxygen activated by a homogeneous catalyst such as  $\text{Co}^{2+}$  salts or through hydrocarbon auto-oxidation processes<sup>1</sup>. A typical example is cyclohexane oxidation to cyclohexanone and cyclohexanol in a cyclohexane solution of soluble Co(II) carboxylate, such as 2-ethylhexanoate or naphthenate<sup>14;15</sup>. In order to achieve a high selectivity with a reasonable conversion, the processes still require relatively high temperature (80-180°C) and pressures (0.8-2MPa)<sup>7</sup>.

Unfortunately, direct oxidation of small hydrocarbons by  $O_2$  is very unselective. Unrestricted mobility of the free radical intermediates results often in indiscriminate attack on both hydrocarbon and primary oxidation products<sup>1;7</sup>. Activation of oxygen-containing bond in partially oxidized products is easier than C-H bond of starting hydrocarbon. Therefore, under reaction conditions in the liquid or gas phase, oxygen attacks partially oxidized products more easily than the starting hydrocarbon, which results in over-oxidation to CO and  $CO_2$ <sup>7;16</sup>. For instance, oxidation of n-butane to maleic anhydride results in selectivity below 70%<sup>7</sup>. As a result, existing methods generate large amounts of unwanted by-products, such as  $CO_x$ . High selectivity can be obtained in general at very low conversion level, e.g. cyclohexane oxidation to cyclohexanone and cyclohexanol with selectivity of 90% at conversion of 10%<sup>15;16</sup>. But a heavy penalty is caused by cost for separation and recycling. The inefficiency associated with low conversion has motivated the search for solid catalysts that are highly active and selective for the oxidation of hydrocarbons.

### 1.2 New method for selective oxidation of hydrocarbon using $O_2$ at low temperature

The results first presented by Frei and co-workers are based on a completely different selective oxidation concept<sup>17-25</sup>. Under mild conditions (room temperature and atmospheric pressure), the hydrocarbon and oxygen are confined in a restricted environment inside zeolite catalyst. In the presence of a strong electrostatic field, caused by charge compensation cation (e.g.  $Na^+$  or  $Ba^{2+}$ ), hydrocarbon and oxygen react with each other when irradiated with visible light, selectively (100% selectivity in some cases) forming oxidation products (for example, toluene and oxygen to give benzaldehyde)<sup>22</sup>. Even light alkanes are selectively oxidized under these conditions. In some cases, even under thermal condition reaction occurred (e.g. cyclohexane and oxygen to cyclohexanone)<sup>23</sup>. The high selectivity of these reactions can be attributed to several factors: (1) using low reaction temperatures inhibits free radical chemistry; (2) use of visible light rather than UV light provides a low-energy pathway; (3) zeolite cavity results in a caging effect (details see below).

#### 1.2.1 Proposal mechanism

The electrostatic field of charge compensation cations in the zeolite pores is believed to be of crucial importance in the process suggested by Frei<sup>18;20-22</sup>. The reaction is initiated with a help of visible light, whereas in a limited number of cases thermal activation also gives access to a selective reaction path. The reaction involves the formation of an activated complex by electron transfer from the hydrocarbon



$C_xH_y$  to the  $O_2$  molecule yielding an ion pair of  $[C_xH_y^+ \cdot O_2^-]$ . The electron transfer occurs spontaneously when the hydrocarbon- $O_2$  collisional complex is in a strong electrostatic field, which stabilizes the charge transfer complex. A zeolitic cage creates the ideal medium for confining the hydrocarbon and oxygen in a restricted environment that favors the formation of the hydrocarbon- $O_2$  collisional complex in the electrostatic field of alkali or alkaline earth metal cations.

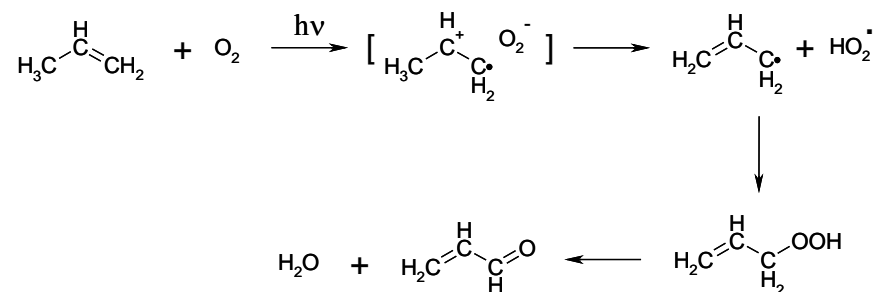


It was observed that the tail of the absorption band of the hydrocarbon- $O_2$  charge transfer complex is shifted from UV to the visible region in the presence of a strong electrostatic field<sup>18;20;23</sup>. Therefore, the electron transfer can be induced at room temperature by visible photons, or even spontaneously occurs thermally at room temperature. Produced alkane or alkene radical cations are extremely acidic and, therefore, have a strong tendency to transfer a proton to  $O_2^-$  to yield allyl (or alkyl) and HOO radicals. Generating both radicals at ambient temperature in a restricted environment (zeolite cavities) offers a way to tightly control their mobility, and consequently recombination of both allyl (or alkyl) and HOO radicals yields allyl (or alkyl) hydroperoxide. Further, based on the results obtained, Frei proposed that unlike in gas or liquid phase autoxidation, the use of low-energy photons and a low temperature environment inhibits homolysis of the peroxide bond in the zeolite<sup>21</sup>. Elimination of  $H_2O$  from hydroperoxide results in the formation of a carbonyl containing product exclusively.

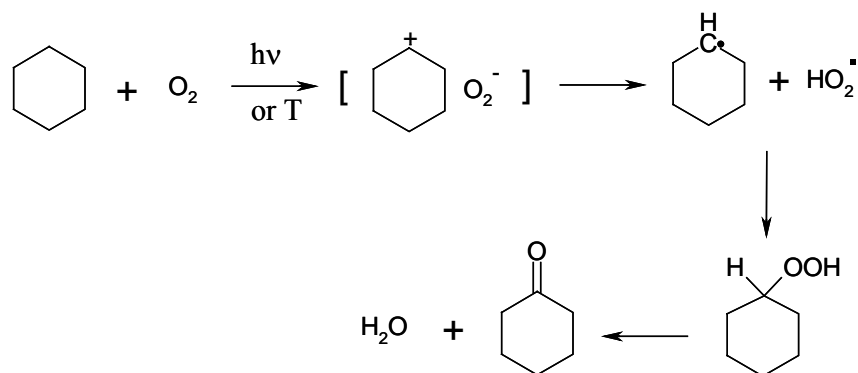
It is worth noting that only alkanes can undergo selective oxidation in cation exchanged zeolites via thermal activation. Unsaturated hydrocarbons such as short alkenes or toluene do not exhibit thermal oxidation despite the fact that the ionization potentials and C-H bond energies are appreciably smaller than those of low alkanes<sup>21</sup>. This is explained by the strong interaction of alkenes and benzenes with exchanged cations in the zeolite cage<sup>21</sup>. As a result, the unsaturated hydrocarbons reside at these cations, especially the ones that are most poorly shielded by the zeolite framework oxygens. Thus these unsaturated hydrocarbons adsorbed on cations are unable to give charge transfer with  $O_2$  because the dipole of the resulting ion-pair would be antiparallel to the electrostatic field<sup>21-23</sup>. The diminished electrostatic fields of alkenes and benzenes-shielded cations may be too weak to promote thermal charge transfer between these unsaturated hydrocarbons and oxygen. But the weaker adsorption of alkanes lead to alkane- $O_2$  collisional pairs to experience the full electrostatic field of the unshielded cations<sup>21</sup>. Therefore, it would allow electron transfer from the alkane molecule to oxygen, resulting in formation of the charge-transfer complex and consequently stabilization in the electrostatic field in the zeolites.

The reaction schemes for three typical examples of olefin (propylene)<sup>18</sup>, alkane (cyclohexane)<sup>23</sup> and alkyl substituted benzene (tolene)<sup>22</sup> are shown below.

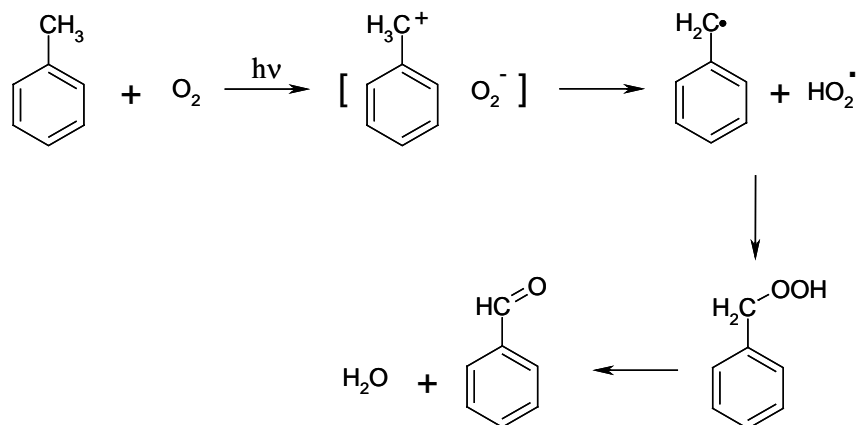
## Scheme a)



## Scheme b)



## Scheme c)



**Scheme 1-1.** Reaction pathway according to Frei for a) alkenes; b) Alkanes and c) aromatics. (thermal oxidation occur only with alkanes)

## 1.2.2 Catalysts

The catalyst used in reactions mentioned above by Frei's group is a so-called faujasite zeolite, specifically the synthetic analogue of type Y with a Si to Al ratio between 1.5 and 3. The structure consists of a three dimensional array of spherical supercages 1.3nm in diameter. These spheres are connected by 0.74nm windows (Figure 1-1)<sup>26;27</sup>. Hence, small molecules can easily enter inside the supercage network, and a high steady-state concentration of the hydrocarbon-O<sub>2</sub> collisional complex can be achieved. Most importantly, aluminum-containing zeolites have a negatively charged framework, which results from AlO<sub>2</sub><sup>-</sup> units replacing neutral SiO<sub>2</sub> units. The negative charge is balanced by an equivalent number of extra-framework cations, often alkali or alkaline-earth metal cations<sup>27;28</sup>. The material used in most of studies by Frei are Na<sup>+</sup> and Ba<sup>2+</sup> exchanged zeolite Y. There are two or four cations located in each supercage<sup>29-34</sup>. An important characteristic of these cations is the high electrostatic field inside the supercage<sup>27;35-38</sup>. Fields on the orders of 10V/nm have been predicted and confirmed experimentally by low temperature N<sub>2</sub> adsorption<sup>21</sup>.

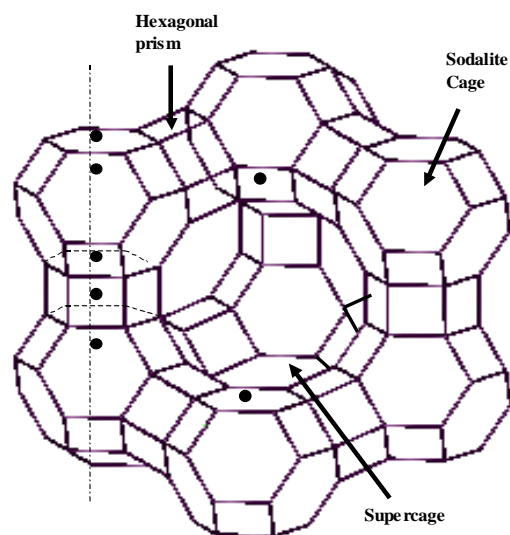


**Figure 1-1** Geometrical structure of zeolite Y  
(Cation positions indicated with solid circles)

The crucial functions of this alkali and alkaline earth exchanged supermolecular host (zeolite) proposed by Frei are the following. First, adsorption/confinement of the reactants results in a high steady state concentration of the hydrocarbon-O<sub>2</sub> collisional complex. Second, high electrostatic field in the vicinity of exchanged alkali or alkaline earth cations allows hydrocarbon-O<sub>2</sub> collisional complex to be excited by low-energy visible photons, and consequently stabilizes the excited charge transfer state. Third, motional constraints imposed on the proposed primary radical products [alkyl (allyl, benzyl) radical, HOO radical] suppresses random radical coupling reactions, which otherwise would destroy product selectivity.

Aside from these electrostatic fields, it was also suggested by Frei that the zeolites should be deliberately prepared free of acid sites (Brønsted acid sites). These catalytic sites normally play a crucial role in hydrocarbon cracking in the petroleum industry and in the synthetic applications in the chemical industry<sup>28;39-46</sup>. The presence of such sites can lead to a decrease in selectivity, especially in the olefin and alkyl substituted benzene system due to isomeration and condensation reactions of peroxide or

carbonyl products catalyzed by Brönsted acids.

It should be noted that increased concentration of residual H<sub>2</sub>O gradually quenches the reaction<sup>25</sup>. It was explained based on the fact that water molecules adsorb inside the zeolites. As a result, this would shield the Coulombic interaction of reactants with cations. Thus, to make the cages accessible to organics and O<sub>2</sub>, the zeolites used in Frei's work were dehydrated before the reactants are loaded from the gas phase.

### 1.3 Research by the other groups

#### 1.3.1 Effects of reactivity and selectivity on cation exchanged Y zeolite for cyclohexane oxidation

Since the electrostatic field is believed to play an essential role in such oxidation reactions, higher reaction rates could be achieved by using cations with larger electric field. Cyclohexane partial oxidation both in the gas phase and liquid phase was studied by Jacobs et al. on series cation exchanged Y zeolites by varying the charge and radius of cations (Na<sup>+</sup>, Ba<sup>2+</sup>, Sr<sup>2+</sup> and Ca<sup>2+</sup>)<sup>34;47</sup>. In both phases, activity was observed to increase in the order NaY < BaY < SrY < CaY. In the gas phase, the results were consistent with the mechanism proposed by Frei involving the formation of an alkane-oxygen charge transfer complex<sup>34</sup>. However, in the liquid phase it turned out that a classical autoxidation mechanism is operative based on the reaction kinetics<sup>47</sup>. A 2:1 ratio of cyclohexanol /cyclohexanone mixture was observed in the products. Thus, the authors suggested that in the liquid phase, the reaction mechanism was different from that of the gas phase system. The difference in the reaction mechanism was attributed to the low mobility of reactant molecules within the zeolite pores at the high loading characteristic of the liquid phase system. In this case, cations act as Lewis acid sites to enhance homolytic hydroperoxide decomposition.

By comparing the reaction rate of cyclohexane and deuterated cyclohexane-d<sub>12</sub> at low cyclohexane loading, a pronounced deuterium kinetic isotope effect in both thermal and photochemical oxidation reactions was observed by group of Grassian and Larsen<sup>48</sup>. Thus, the authors claimed that a proton transfer step is the rate-limiting step in the reaction mechanism. Based on the activation energies measured over BaY and NaY, a potential energy diagram for the thermal oxidation of cyclohexane was proposed (As shown in Figure 1-2)<sup>48</sup>. Neglecting the energies of diffusional processes and assuming a fast pre-equilibrium of reaction precursor, the apparent activation energy can be expressed as  $E_{a, \text{apparent}} = E_{a, \text{CT}} + E_{a, \text{PT}} - E_{a, \text{-CT}}$ , where  $E_{a, \text{CT}}$ ,  $E_{a, \text{PT}}$ , and  $E_{a, \text{-CT}}$  represent the energy of charge transfer, proton transfer and back-charge transfer, respectively. The difference in activation energy between NaY and

BaY was explained by the lower energy of the charge transfer complex in BaY as compared with in NaY, which is due to the relatively high electric field at the  $\text{Ba}^{2+}$  cation (6.1V/nm) as compared to the  $\text{Na}^+$  cation (5.0V/nm). However, a product mixture of 90% cyclohexanone and 10% cyclohexanol was obtained by group of Grassian and Larsen<sup>48</sup>, in contrast to completely selectivity to cyclohexanone reported by Frei et al.<sup>23</sup>.

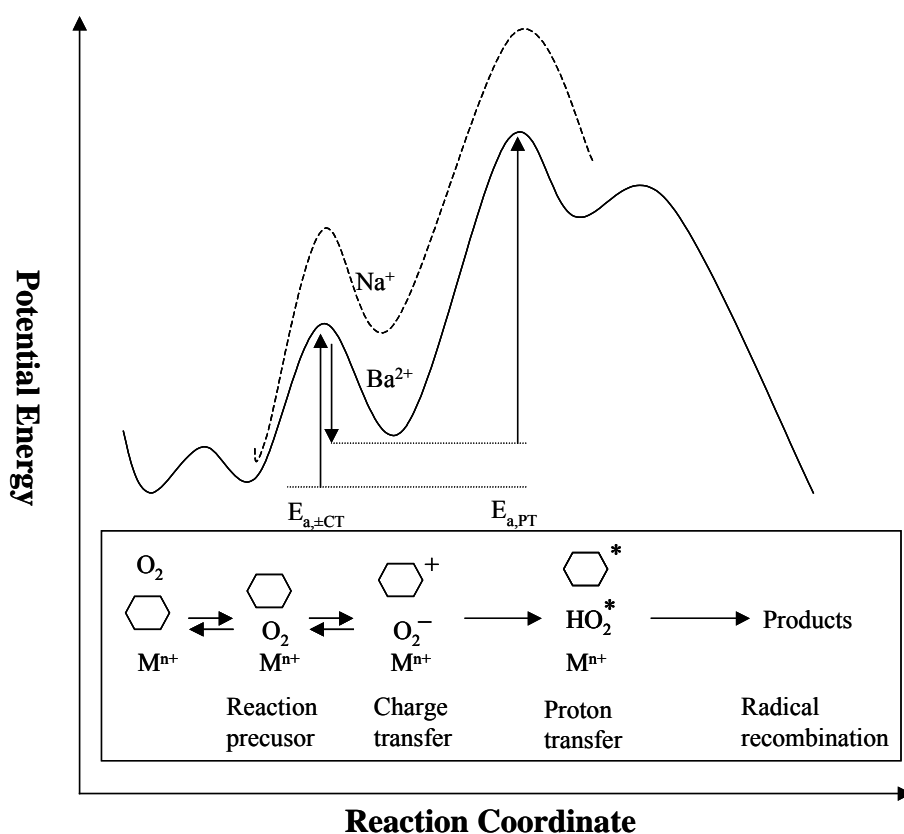


**Figure 1-2.** A potential energy diagram for the thermal oxidation of cyclohexane in BaY (NaY) shows the relative potential energies for the equilibrium configuration, the reaction precursor, the charge transfer complex, the proton transfer step, and the radical recombination step. Arrows indicate the relevant activation energies. The apparent activation energy is given by  $E_a$ , apparent =  $E_{a,CT} + E_{a,PT} - E_{a,-CT}$  (Ref. 48)

### 1.3.2 Effects of zeolite hosts for olefin and alkyl substituted benzene in photooxidation

Zeolites with different Si/Al ratios (chemical composition), namely X, Y, Beta and ZSM5 exchanged with  $\text{Na}^+$  and  $\text{Ba}^{2+}$  cation were investigated for 1-alkenes, toluene and p-xylene photooxidation by Grassian and Larsen<sup>34;49;50</sup>. CO adsorption experiments revealed that the electrostatic field increased with increasing Si/Al ratio in the order  $\text{NaX} < \text{BaX} < \text{NaY} < \text{BaY} < \text{BaBeta} < \text{BaZSM5}$ <sup>34;38</sup>. The

measured electrostatic field was found to correlate with the product yield, and was the highest for divalent cation exchanged zeolites with high Si/Al ratios, such as Ba-ZSM5 and Ba-Beta. However, selectivity was found to dramatically decrease in the order  $X > Y > \text{Beta} > \text{ZSM5}$ , which was attributed to the presence of residual Brønsted acid sites in these zeolites. These reactions include: (1) epoxide ring opening; (2) double bond migration; (3) condensation reaction. Moreover, acidic zeolites with large pores, like Y and Beta, enhanced the formation of condensation products. Thus, the authors concluded that shape selectivity also played an important role in determining product selectivities due to side reactions<sup>50</sup>. Based on the results, it was concluded that in order to achieve a higher selectivity in the host with high electrostatic field, a preparation method should be pursued to decrease the concentration of Brønsted acid sites<sup>50;51</sup>.

### 1.4 Challenges and objectives

This research opens new projects in the field of selective oxidation. However, it should be emphasized that oxidation products have been detected only with spectroscopy or after organic solvent extraction. Thermal desorption of products has not yet been reported. Stabilization of products may, however, seriously affect the overall selectivity because the stabilization also implies that high temperatures will be needed for desorption to occur. As a consequence, the overall selectivity might decrease because of both decomposition of product as well as further oxidation of the products during diffusion of the product molecules leaving the catalyst. This is being recognized to be one of the essential hurdles for taking this concept towards practical technology. From an industrial point of view, the thermal route is obviously more appealing than the photochemistry route. Therefore, it is worthwhile to know whether the high activity and selectivity obtained in photo-oxidation can also be achieved in thermal oxidation of alkanes in cation-exchanged zeolites. Further, the details of the mechanism should be better clarified. For examples, the driving force for the charge transfer is not yet clear in the case of thermal activation. The active sites of thermal decomposition of the alkylhydroperoxide intermediate are not well defined. Zeolite NaY can be prepared free of acid sites, whereas this is not possible for higher electrostatic field of Y zeolite exchanged with alkaline-earth cations<sup>25;27;45</sup>. The latter inevitably contain Brønsted acid sites, but their importance for this type of reaction has not yet been studied. Therefore, further knowledge is required in order to design better active and selective catalyst.

In this thesis, we focus on the thermal selective oxidation of small alkanes to oxygenates by cation exchanged zeolites. Alkanes are very important in perspective of application, and can be activated thermally. Propane was selected, as model compound in the reaction studies, since it is simple in

chemical composition, which leads to simple IR spectra interpretation. Moreover, it contains both methyl and methylene group. An attempt has been made to determine the relationship between the activity and selectivity of catalytic selective oxidation of propane on cation-exchanged zeolites and their physicochemical properties. The objectives are:

- (1) To reveal the active sites based on the species observed by infrared spectroscopy during the selective oxidation (**Chapter 2**).
- (2) To investigate thermal desorption of strongly adsorbed products in order to close the catalytic selective oxidation cycle (**Chapter 3**).
- (3) To determine the active sites in relation to the cation location (**Chapter 4**).
- (4) To demonstrate the importance of suitable balance between cation and Brönsted acid sites for good performance of catalytic selective oxidation (**Chapter 5**).
- (5) To confirm the activation of both reactants based on adsorption results by infrared spectroscopy (**Chapter 6**).
- (6) To correlate catalytic oxidation and geometry of zeolites (**Chapter 7**).
- (7) To come a step closer in understanding the mechanism of alkane selective oxidation catalyzed by cation exchanged zeolites (**Chapter 8**).

#### Reference List

1. Centi, G.; Corberan, V. C.; Perathoner, S.; Ruiz, P. *Catalysis Today* **2000**, *61*, 1.
2. Centi, G.; Perathoner, S. *Current Opinion in Solid State & Materials Science* **1999**, *4*, 74-79.
3. Centi, G.; Misono, M. *Catalysis Today* **1998**, *41*, 287-296.
4. Hodnett, B. K. *Heterogeneous catalytic oxidation*, Jone Wiley & Sons Ltd, Chichester: 2000.
5. Dartt, C. B.; Davis, M. E. *Ind.Eng.Chem.Res.* **1994**, *33*, 2887.
6. LYONS, J. E.; PARSHALL, G. W. *Catalysis Today* **1994**, *22*, 313-333.
7. Centi, G.; Cavani, F.; Trifiro, F. *Selective oxidation by heterogeneous catalysis*, Kluwer Academic/Plenum Publishers: New York, 2000.
8. Chaar, M. A.; Patel, C.; Kung, H. H. *Journal of Catalysis* **1988**, *109*, 463-467.
9. Ai, M. *Catalysis Today* **1998**, *42*, 297-301.
10. Lin Luo; Jay A.Labinger; Mark E.Davis. *Journal of Catalysis* **2001**, *200*, 222-231.

11. Centi, G.; Trifiro, F. *Appl.Catal.A-Gen.* **1996**, *143*, 3-16.
12. Herrmann, J. M.; Vernoux, P.; Bere, K. E.; Abon, M. *Journal of Catalysis* **1997**, *167*, 106.
13. Bordes, E. *Catalysis Today* **1993**, *16*, 27.
14. Schuchardt, U.; Cardoso, D.; Sercheli, R. *Appl.Catal.A-Gen.* **2001**, *211*, 1-17.
15. Schuchardt, U.; Carvalho, W. A.; Spinace, E. V. *Synlett* **1993**, *10*, 713.
16. Mijs, W. J.; De Jonge, C. R. H. I. *Organic syntheses by oxidation with metal compounds*, Plenum Press, New York: 1986.
17. Blatter, F.; MOREAU, F.; Frei, H. *Journal of Physical Chemistry* **1994**, *98*, 13403-13407.
18. Blatter, F.; Sun, H.; Frei, H. *Catalysis Letters* **1995**, *35*, 1-12.
19. Blatter, F.; Sun, H.; Frei, H. *Chemistry-A European Journal* **1996**, *2*, 385-389.
20. Blatter, F.; Sun, H.; Vasenkov, S.; Frei, H. *Catalysis Today* **1998**, *41*, 297-309.
21. Frei, H. *3Rd World Congress on Oxidation Catalysis* **1997**, *110*, 1041-1050.
22. Sun, H.; Blatter, F.; Frei, H. *Journal of the American Chemical Society* **1994**, *116*, 7951-7952.
23. Sun, H.; Blatter, F.; Frei, H. *Journal of the American Chemical Society* **1996**, *118*, 6873-6879.
24. Sun, H.; Blatter, F.; Frei, H. *Abstracts of Papers of the American Chemical Society* **1996**, *211*, 3-ORGN.
25. Sun, H.; Blatter, F.; Frei, H. *Catalysis Letters* **1997**, *44*, 247-253.
26. H.van Bekkum *Introduction to zeolite science and practice*, Elsevier: Amsterdam, 2001.
27. Donald W.Breck *Zeolite molecular sieves: structure, chemistry, and use*, Wiley: New York, 1974.
28. Subhash Bhatia *Zeolite catalysis : principles and applications*, CRC Press: Boca Raton, FA, 1990.
29. Bajusz, I. G.; Goodwin, J. G. *Langmuir* **1998**, *14*, 2876-2883.
30. Bordiga, S.; Scarano, D.; Spoto, G.; Zecchina, A.; Lamberti, C.; Otero Arean, C. *Vib.Spectrosc.* **1993**, *5*, 69.
31. Costenoble, M. L.; Mortier, W. J.; Uytterhoeven, J. B. *J.C.S.Faraday I* **1975**, *71*, 1877-1883.
32. Costenoble, M. L.; Mortier, W. J.; Uytterhoeven, J. B. *J.C.S.Faraday I* **1977**, *73*, 477-483.
33. Costenoble, M. L.; Mortier, W. J.; Uytterhoven, J. B. *J.C.S.Faraday I* **1977**, *73*, 466-476.
34. Vanoppen, D. L.; DeVos, D. E.; Jacobs, P. A. *Progress in Zeolite and Microporous Materials, Pts A-C* **1997**, *105*, 1045-1051.
35. Smudde, G. H.; Slager, T. L.; Weigel, S. J. *Applied Spectroscopy* **1995**, *49*, 1747-1755.
36. Jousse, F.; Lara, E. C. D. *Journal of Physical Chemistry* **1996**, *100*, 238-244.
37. Jousse, F.; Lara, E. C. D. *Journal of Physical Chemistry* **1996**, *100*, 233-237.



38. Li, P.; Xiang, Y.; Grassian, V. H.; Larsen, S. C. *Journal of Physical Chemistry B* **1999**, *103*, 5058-5062.
39. Smirniotis, P. G.; Davydov Lev. *Catal.Rev.Sci-Eng.* **1999**, *41*, 43-113.
40. Panov, A.; Fripiat, J. J. *Journal of Catalysis* **1998**, *178*, 188-197.
41. Kao, H. M.; Grey, C. P.; Ramamurthy, V. *Journal of Physical Chemistry* **1998**, *102*, 5627-5638.
42. Barthomeuf, D. *Catal.Rev.Sci-Eng.* **1996**, *38*, 521-613.
43. Ward, J. W. *Journal of Catalysis* **1968**, *10*, 34-46.
44. Ward, J. W. *Journal of Catalysis* **1967**, *9*, 225-236.
45. Ward, J. W. *Journal of Physical Chemistry* **1968**, *72*, 4211-4223.
46. Uytterhoeven, J. B.; Schoonheydt, R. *Journal of Catalysis* **1969**, *13*, 425-434.
47. Vanoppen, D. L.; De Vos, D. E.; Jacobs, P. A. *Journal of Catalysis* **1998**, *177*, 22-28.
48. Larsen, R. G.; Saladino, A. C.; Hunt, T. A.; Mann, J. E.; Xu, M.; Grassian, V. H.; Larsen, S. C. *Journal of Catalysis* **2001**, *204*, 440-449.
49. Larsen, S. C.; Xiang, Y.; Grassian, V. H. *Abstracts of Papers of the American Chemical Society* **1998**, *216*, 447-PHYS.
50. Panov, A. G.; Larsen, R. G.; Totah, N. I.; Larsen, S. C.; Grassian, V. H. *Journal of Physical Chemistry B* **2000**, *104*, 5706-5714.
51. Xiang, Y.; Larsen, S. C.; Grassian, V. H. *Journal of the American Chemical Society* **1999**, *121*, 5063-5072.

## Chapter 2

### **Propane Selective Oxidation on Alkaline-earth Exchanged Y Zeolite at Room Temperature**

---

***Abstract:** The effect of zeolite Y ion-exchanged with a series of alkaline-earth cations on selective propane oxidation at room temperature was studied with in-situ infrared spectroscopy. Isopropylhydroperoxide (IHP) was observed as a reaction intermediate and can be decomposed into acetone and water. The reaction rate increased in the order BaY < MgY < SrY < CaY based on the rate of formation of adsorbed acetone. Surprisingly, the acetone/water ratio was found to increase with cation size, while no other products could be detected. Moreover, the acetone/IHP ratio decreased with decreasing number of Brönsted acid sites. Both observations mark the importance of Brönsted acid sites for this reaction, in addition to (earth) alkali cations. A two-step mechanism with two different active sites is proposed. Conversion of propane into isopropylhydroperoxide takes place on cations, while the decomposition into acetone occurs by Brönsted acid sites.*

## 2.1 Introduction

About a quarter of the industrial production of monomers and chemical intermediates is made by catalytic selective oxidation processes. Most catalysts used in these industrial processes are based on mixed metal oxides. Typically, direct oxidation of hydrocarbons by O<sub>2</sub> gives poor selectivity at high conversion, which limits conversion to a few percent in most practical processes. The inefficiency associated with low conversion has motivated the search for solid catalysts with higher activity in selective oxidation of hydrocarbons<sup>1</sup>. Driving forces for new breakthroughs are: (i) Use of cheaper and easier available raw materials, like small-saturated hydrocarbons such as methane, ethane and propane. The underlying motivation is better use of natural gas and volatile petroleum fractions<sup>2-4</sup>. (ii) Selectivity control. Lack of selectivity is severe if conversion is pushed beyond a few percent due to over-oxidation of partial oxidized products<sup>4,5</sup>. (iii) Environmental constraints. Development is needed of processes that produce less waste and have greater safety.

Recently, Frei et al. demonstrated that oxidation of ethane, propane, isobutane and cyclohexane with molecular oxygen to corresponding oxygenates occurs with very high selectivity under mild thermal and photochemical conditions in cation exchanged zeolites, such as NaY and BaY<sup>6-11</sup>. The reaction mechanism proposed by Frei's group involved a charge transfer complex, [(C<sub>n</sub>H<sub>2n+2</sub>)<sup>+</sup>O<sub>2</sub><sup>-</sup>]. The hypothesis is that the electrostatic field of the exchanged cation stabilizes the charge transfer complex. In the next step, a proton from hydrocarbon cation radical is abstracted by O<sub>2</sub><sup>-</sup> to form HO<sub>2</sub> and a hydrocarbon radical. Subsequently, the HO<sub>2</sub> radical attacks the hydrocarbon radical to form alkylhydroperoxide. Using FTIR spectroscopy, it was observed that alkylhydroperoxide reacts thermally to form oxygenates and water. Complete selectivity was reported at conversions as high as about 35%, based on *in situ* FTIR measurements.

If the electrostatic field is the main factor determining activity, the rate of reaction should increase with increasing electrostatic field when changing cation size and charge. Vanoppen et al.<sup>12</sup> found that reaction activity increased in order CaY > SrY > BaY > NaY during cyclohexane oxidation in gas and liquid phase. Based on cation dependence, the results in gas phase were consistent with the mechanism proposed by Frei involving the formation of an alkane-oxygen charge transfer complex. However, a classical auto-oxidation process was proposed after analysis of the reaction kinetics in the liquid phase. To link the change in reaction mechanism from gas to liquid phase, Larsen et al.<sup>13</sup> investigated the kinetics of thermal and photochemical oxidation of cyclohexane in zeolite NaY and BaY. The overall conversion was found to dramatically decrease at cyclohexane loading higher than three molecules per supercage, attributed to limited diffusion of cyclohexane and oxygen in the zeolite pores. Pronounced

deuterium kinetic isotope effects indicated the proton transfer as rate-limiting step for both the thermal and photochemical reaction.

With zeolite NaY, selective oxidation did not occur for hydrocarbons with higher ionization potential (IP), such as propane, as was reported by Frei et al.<sup>8</sup>. Based on the charge transfer mechanism, they explained this by the lower electrostatic field of sodium cation. So, if the electrostatic field governs this reaction, higher reaction rates may be achieved by using cations with large field (e.g. Mg<sup>2+</sup>). Further, the mechanism of thermal decomposition of the alkylhydroperoxide intermediate is not yet clear. While zeolite NaY and BaY can be prepared free of acid sites, this is not possible for CaY and SrY<sup>14;15</sup>. The latter inevitably contain Brønsted acid sites, but their importance for this reaction has not yet been clarified.

Frei et al. have examined the propane thermal oxidation on CaY and BaY. At room temperature the reaction was found to occur only on CaY. The objective of the current work is to extend propane thermal oxidation to a series of alkaline-earth exchanged zeolite (MgY, CaY, SrY and BaY) using *in-situ* FTIR spectroscopy at low propane and oxygen pressure. This approach allows us to deeper investigate the effect of cations, and especially of acid sites on propane adsorption and selective oxidation via analysis of adsorbed species on the catalyst surface.

**Table 2-1. Zeolite, Chemical composition (Determined by XRF)**

	chemical composition (wt%)				
	Al <sub>2</sub> O <sub>3</sub>	SiO <sub>2</sub>	Na <sub>2</sub> O	MO	M <sup>2+</sup> /Al (molar ratio)
<b>MgY</b>	22.78	67.34	3.80	6.15	0.34
<b>CaY</b>	22.18	65.79	1.58	10.39	0.43
<b>SrY</b>	20.22	59.65	1.48	18.61	0.45
<b>BaY</b>	19.41	57.83	2.76	20.47	0.35

M is alkaline earth cation; Iron content <0.02wt%.

## 2.2 Experimental

### 2.2.1 Materials

Alkaline-earth cation (Mg, Ca, Sr, and Ba) exchanged Y-zeolites were prepared from NaY (Akzo Nobel, sample code: 1122-207). The parent zeolite was exchanged three times with 0.1M solution of respectively magnesium chloride, calcium chloride, strontium nitrate, or barium chloride (Merck) for 20 hours at 90°C under stirring. The resulting alkaline-earth exchanged Y zeolite was washed three times with distilled water, filtered and dried at 100°C overnight. The chemical composition of catalysts was analyzed by X-ray fluorescence (Table 2-1). Power X-ray diffraction gave no indication for collapse of the zeolite structure, even not after calcination at 650°C.

### 2.2.2 Infrared Spectroscopy Studies

The zeolite powder was pressed into a self-supporting wafer and analyzed *in-situ* during all treatments (i.e. activation, adsorption and reaction process) by means of transmission FTIR spectroscopy using a Bruker Vector22 FTIR spectrometer with a MCT detector. A miniature cell, equipped with transparent CaF<sub>2</sub> windows, which can be evacuated to pressures below 10<sup>-7</sup> mbar was used for the *in-situ* experiments. The temperature is variable from room temperature to 500°C. Each spectrum consists of 32 scans taken at 4cm<sup>-1</sup> resolution. The spectra were corrected for absorption of the activated zeolite.

The samples were activated in vacuum (< 10<sup>-7</sup> mbar) at 500°C (ramp 10°C/minute) for 2 hours, subsequently cooled down to 200°C (dwell 10 hours), and cooled to room temperature. Loading of reactants (propane and oxygen) was controlled by gas pressure. Propane was introduced into the IR cell until equilibrium was reached at 1 mbar in the gas phase, followed by addition of 40 mbar of oxygen.

Blank experiments were carried out for an empty cell and the parent NaY zeolite. In both cases, no reaction between propane and oxygen occurred at room temperature.

### 2.2.3 Ex-situ <sup>1</sup>H-NMR

*Ex situ* NMR spectroscopy was used to analyze product formation. For this the reaction was carried out in a closed glass reactor with 0.2bar propane, 0.8bar oxygen and 100mg CaY zeolite. After 48 hours reaction the sample was flushed with argon for 10 minutes and subsequently CDCl<sub>3</sub> was added. The suspension was filtered and the filtrate was analyzed on a Varian Inova NMR spectrometer with chemical shifts relative to CDCl<sub>3</sub>.

## 2.3 Results

### 2.3.1 Catalyst characterization

Transmission FTIR spectra of the activated samples are given in Figure 2-1. All samples exhibited an isolated silanol peak at  $3744\text{ cm}^{-1}$ . The band can be attributed to SiOH groups either on the outer surface of zeolite crystals or on silica impurities<sup>14,16-18</sup>. Further, absorption bands at  $3645\text{ cm}^{-1}$  for MgY, CaY, SrY and at  $3555\text{ cm}^{-1}$  for MgY indicated the formation of Brönsted acid sites, which is in agreement with literature<sup>14-16</sup>. The intensity of Brönsted acid sites at  $3645\text{ cm}^{-1}$  was almost the same for CaY and MgY, and only a small amount was observed for SrY. BaY did not exhibit any Brönsted acid sites. Further, additional bands at  $3695\text{ cm}^{-1}$  for MgY,  $3590\text{ cm}^{-1}$  for CaY and  $3570\text{ cm}^{-1}$  for SrY can be attributed to  $\text{M}(\text{OH})_x$  species<sup>16,18</sup>. The intensity of this species is obviously higher on MgY zeolite.

The T-O-T overtone vibrations in the  $1700\text{-}1900\text{ cm}^{-1}$  regions showed a clear shift with changing cation, in agreement with literature<sup>19</sup>.

### 2.3.2 Adsorption of Propane

Figure 2-2a presents the FTIR spectra of adsorbed propane for the different alkaline-earth exchanged Y zeolites. Interestingly, propane adsorption quantities were observed to increase with increasing cation radius as can be seen from the band intensity of methyl and methylene stretch (between  $3100\text{ cm}^{-1}$  and  $2700\text{ cm}^{-1}$ ) and deformation vibrations (between  $1500\text{ cm}^{-1}$  and  $1300\text{ cm}^{-1}$ )<sup>20</sup>. Two main peaks can be observed in the range of  $3100\text{ cm}^{-1}$  to  $2700\text{ cm}^{-1}$ . The position of the high frequency peak ( $2970\text{ cm}^{-1}$ ) was not affected by exchanging cations, but the low frequency band (from  $2795$  to  $2849\text{ cm}^{-1}$ ) shifted towards higher wavenumber with increasing cation radius. Further, the intensity ratio of the high to low frequency band decreased with increasing the cation radius.

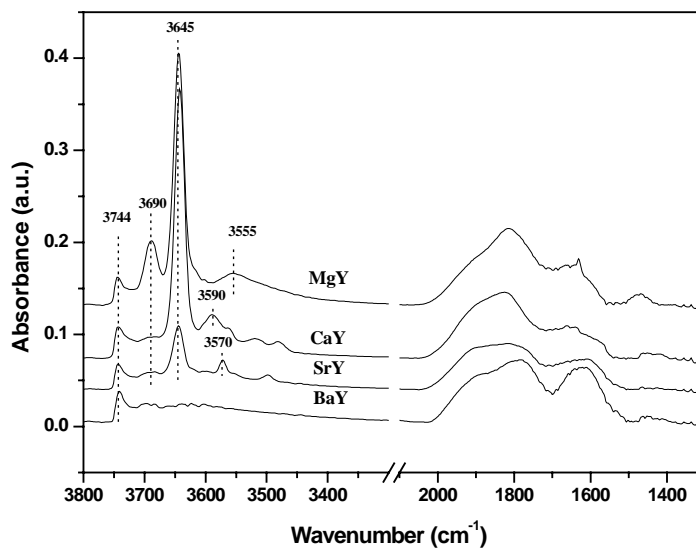
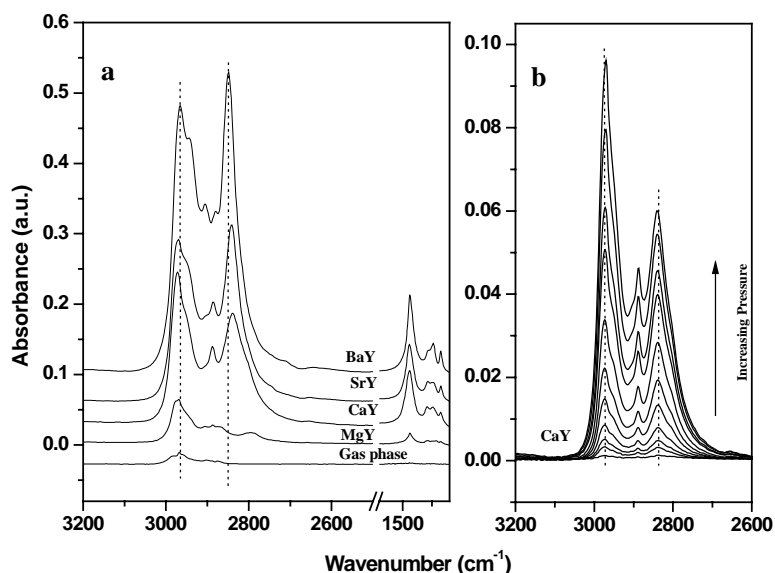


Figure 2-1. FTIR spectra of activated catalysts

In Figure 2-2b it can be seen for CaY that the ratio of the high to low frequency band is a function of propane coverage. However, no shift was detected for the low frequency band upon increasing propane pressure. Similar spectra were observed for the other catalysts.

Propane adsorption did not affect the vibrations in the hydroxyl region. Moreover, after admission oxygen, no spectral changes of adsorbed propane were found. Evacuation at room temperature resulted in disappearance of the propane signals, indicating propane was weakly adsorbed.



**Figure 2-2.** FTIR spectra of a) propane adsorption on different cation exchanged Y zeolite; b) propane adsorption as function of partial pressure (from 0.0013mbar to 1mbar) on CaY zeolite

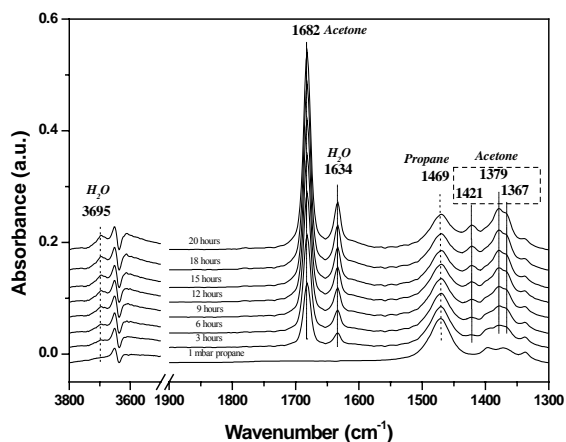


**Figure 2-3.** FTIR spectra of CaY zeolite after loading 1mbar propane and 40mbar oxygen at room temperature as a function of time.

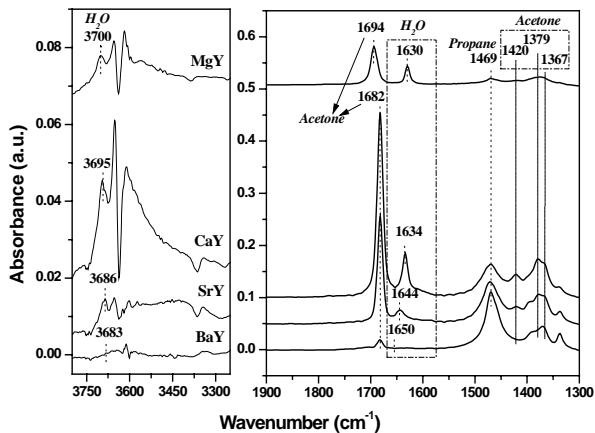


**Figure 2-4.** FTIR spectra of 1mbar propane and 40mbar oxygen oxidation at room temperature on MgY, SrY and BaY after 20 hours reaction.

### 2.3.3 Reaction Studies

After loading 1 mbar propane and 40 mbar oxygen on activated CaY, infrared spectra showed reactant depletion and product growth as function of time (Figure 2-3). Bands at  $1682\text{cm}^{-1}$ ,  $1420\text{cm}^{-1}$ ,  $1379\text{cm}^{-1}$ , and  $1367\text{cm}^{-1}$  can be attributed to acetone as confirmed by comparison with the infrared spectrum of adsorbed acetone on CaY and by literature data<sup>8;21</sup>. The growing band at  $1634\text{cm}^{-1}$  is due to bending of adsorbed water molecules, while at the same time a band at  $3695\text{cm}^{-1}$  develops, which is attributed to the isolated OH vibration of adsorbed water molecules<sup>14-16;22</sup>.

Infrared spectra of alkaline-earth exchanged zeolites after 20 hours reaction are presented in Figure 2-4. Oxidation of propane to acetone was observed for all zeolites. Acetone and water were the only products detected by infrared spectrum under the applied reaction conditions. Infrared frequencies of products and assignment are collected in Table 2-2. Interestingly the C=O stretch of acetone was found at  $1682\text{cm}^{-1}$  for CaY, SrY and BaY while a shift to  $1694\text{cm}^{-1}$  was observed on MgY. Further, with increasing cation radius a shift to lower frequency for water O-H stretch and a shift to higher wavenumber for H-O-H bending was observed. No  $\text{CO}_2$  or other oxygenates were detected in the spectra or in the gas phase as analyzed with online mass spectrometry for all catalysts.

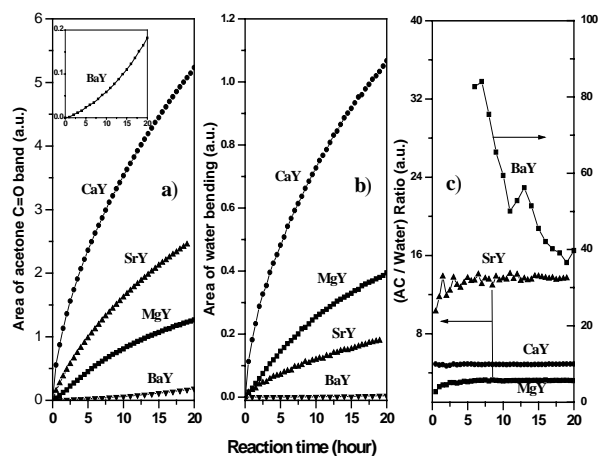


**Figure 2-5.** Integrated intensity of a) acetone ( $\nu_{\text{C=O}}$ ), b) water ( $\delta_{\text{H}_2\text{O}}$ ) and c) acetone/water ratio as function of reaction time during exposure of 1mbar propane and 40mbar oxygen on alkaline earth exchanged Y zeolite at room temperature

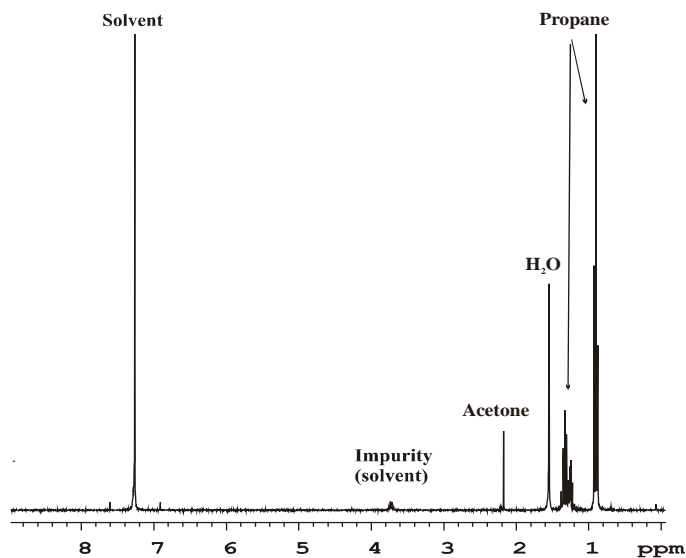


**Figure 2-6.** Proton NMR spectrum of the products extracted in  $\text{CDCl}_3$  after 48hours loading 0.2bar propane and 0.8bar oxygen at temperature  $30^\circ\text{C}$ .

Figure 2-5 displays the growth of acetone ( $\nu_{\text{C=O}}$ ) (a) and water ( $\delta_{\text{H}_2\text{O}}$ ) (b) infrared bands (integrated area) as a function of time. Acetone formation rate was found to decrease in the order of  $\text{CaY} > \text{SrY} >$



MgY > BaY. Water formation rate turned out to decrease according to CaY > MgY > SrY > BaY. In the case of BaY (insert Figure 2-5a), the reaction rate accelerated with reaction time. Moreover, Figure 2-5c shows the acetone/water ratio based on the data in Figure 2-5a and 2-5b. The ratio of acetone to water increases with increasing cation radius. In BaY, the ratio decreases with reaction time.

Figure 2-6 shows the room temperature  $^1\text{H-NMR}$  spectrum after extraction of the products by  $\text{CDCl}_3$ . The peaks showed that only acetone and water could be extracted from the zeolite<sup>23</sup>.

### 2.3.4 Evacuation after reaction

After 20 hours reaction, the samples were evacuated for 5 minutes at room temperature. The infrared spectra clearly showed that adsorbed species remained on the zeolites (Figure 2-7), also no desorption of any product molecules was detected by on-line MS analysis. After removal of adsorbed propane, new bands around  $2990 - 2980 \text{ cm}^{-1}$  and between  $1470 - 1300^{-1}$  were detected that were previously masked by propane, which could be attributed to isopropylhydroperoxide<sup>8;10</sup> (Table 2-2). No isopropylhydroperoxide was observed for MgY after 20 hours of reaction. The peak at  $2925\text{cm}^{-1}$  on all

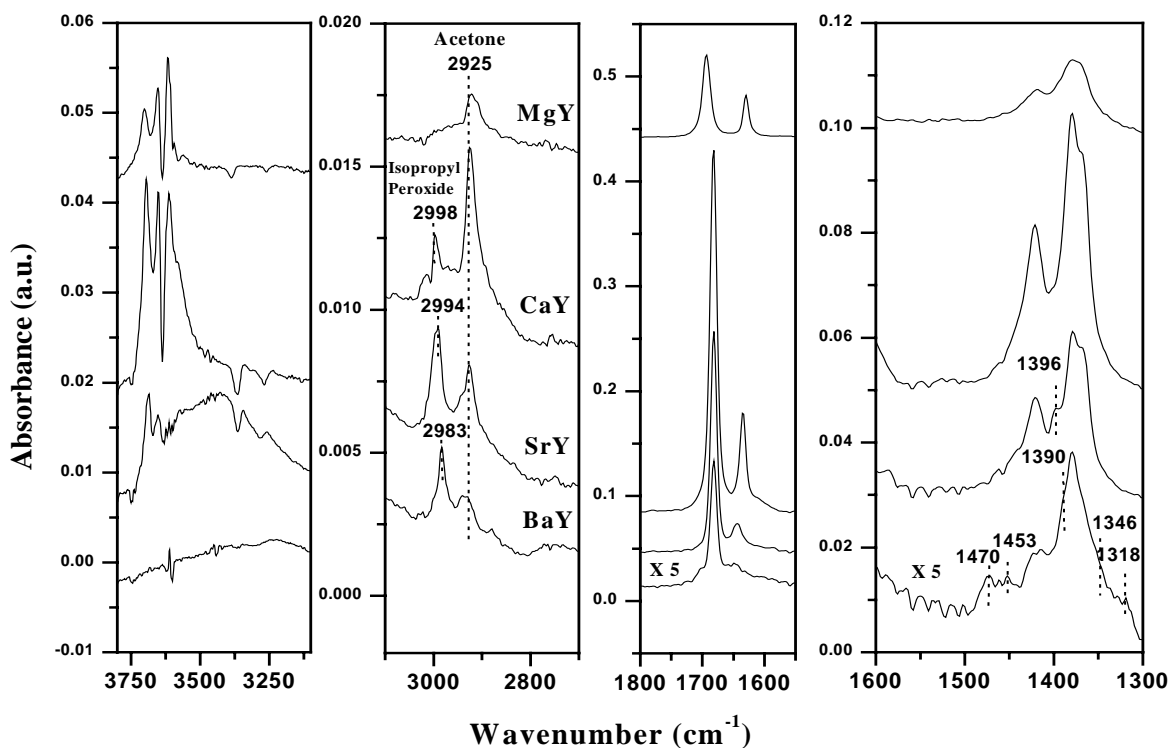


Figure 2-7. FTIR spectra after 20 hours propane oxidation, and subsequent 5 minutes evacuation.

zeolites was assigned to acetone CH<sub>3</sub> stretch after comparison of adsorbed acetone on activated zeolites. Evaluation of the acetone to isopropylhydroperoxide ratio showed increasing amounts of isopropylhydroperoxide relative to acetone with larger cation size.

**Table 2-2: Absorption Frequencies of propane oxidation products on different alkaline-earth exchanged Y zeolite (in cm<sup>-1</sup>)**

Reaction product				Assignment	Reference
MgY	CaY	SrY	BaY		
3700	3695	3686	3683	H <sub>2</sub> O	16; 18
		3430	3430	H <sub>2</sub> O	16; 18
1630	1634	1644	1650	H <sub>2</sub> O	8
3652	3652	3652		Brönsted Acid	16; 18
3611	3611	3611		Brönsted Acid	16; 18
			3245	Isopropyl hydroperoxide	8
	2998	2994	2983	Isopropyl hydroperoxide	10
			1470	Isopropyl hydroperoxide	8; 10
			1453	Isopropyl hydroperoxide	8; 10
		1396	1390	Isopropyl hydroperoxide	8; 10
			1346	Isopropyl hydroperoxide	8
			1318	Isopropyl hydroperoxide	8
3013	3013	3013		Acetone	AS <sup>(1)</sup>
2925	2925	2925	2925	Acetone	AS
1694	1682	1682	1682	Acetone	8; AS
1420	1420	1420	1420	Acetone	8; AS
1379	1379	1379	1379	Acetone	8; AS
1367	1367	1367	1367	Acetone	8; AS

Note: (1) AS: Authentic Sample

**Table 2-3: Zeolite, Calculated Intermediate Sanderson Electronegativity ( $S_{int}$ ), Calculated Average Charge on the Oxygen of the lattice ( $-\delta_O$ ) and Electrostatic Potential ( $e/r$ )**

	$S_{int}$	$-\delta_O$	$e/r(A^{-1})$
<b>MgY</b>	2.810	0.210	3.16
<b>CaY</b>	2.802	0.214	2.01
<b>SrY</b>	2.777	0.221	1.77
<b>BaY</b>	2.764	0.224	1.48

Intermediate Sanderson electronegativity  $S_{int}$  calculated from  $S_{int}=(S_p^p S_Q^q S_R^r S_T^t)^{1/(p+Q+r+t)}$  for compound  $P_p Q_q R_r T_t$ <sup>34</sup>, for electronegativity S of atom P, see Sanderson<sup>35</sup>. Calculated average charge charge  $-\delta_O$  on the oxygen of the lattice, using  $(S_{int}-S_o)/2.08S_o^{1/2}$ <sup>34</sup>. Electrostatic Potential ( $e/r$ ), see Word<sup>18</sup>.

## 2.4 Discussion

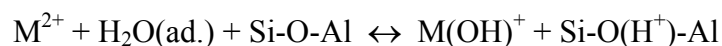
### 2.4.1 Effect of cation on propane adsorption and oxidation

Interaction of propane molecules with zeolites has been reported to be due to enhanced dispersion-force-interaction of non-polar molecules with framework oxygen<sup>22;24;25</sup>. When the framework negative charge is compensated by cations with low electronegativity, the charge on the oxygen atoms may be high enough to create basic properties. In most zeolite structures all oxygen atoms are accessible to adsorbates<sup>26</sup>. The calculated average charge of lattice oxygen ( $-\delta_O$ ) with different alkaline-earth exchanged zeolite is given in table 2-3. The basicity of framework oxygen increases with increasing the cation radius. Further, a lower degree of hydrolysis of water will lead to an increased amount of localized basic lattice oxygen<sup>14</sup>. Quantity of adsorbed propane at 1 mbar equilibrium pressure shows increasing amounts for MgY < CaY < SrY < BaY (Figure 2-2), which has the same order as increasing basicity of framework oxygen and decreasing hydrolysis level as deduced from the amount of Brönsted

acid sites (see below). The different adsorption spectra of propane also suggest that the adsorbed molecule can be influenced by nearby cations. There is no obvious relation between reaction rate and propane adsorption quantity with different alkaline-earth exchanged Y zeolite. However, the lower wavenumber band (from 2795 to 2849  $\text{cm}^{-1}$ ) of propane decreased in frequency with smaller cation radius. Additional experiments with deuterated propane will be performed to give more detailed information.

A cation effect has been demonstrated previously for NaY vs. BaY by Frei's group<sup>8;9;10;11</sup> and Vanoppen et al.<sup>12;27</sup> on their studies of photo and thermal oxidation of hydrocarbons in zeolites. The effect of type of cation on the oxidation activity of zeolites was attributed specifically to the electrostatic field of the cations. The present study shows that the acetone formation rate follows the order  $\text{CaY} > \text{SrY} > \text{MgY} > \text{BaY}$  (Figure 2-5a). With increasing electrostatic field, propane reaction rate increases in order  $\text{BaY} < \text{SrY} < \text{CaY}$ . These results are consistent with cyclohexane oxidation in alkali and alkaline-earth zeolite Y (NaY, BaY, SrY, CaY) in gas and liquid phase as reported by Vanoppen et al.<sup>12;27</sup>. However, MgY is less active than CaY and SrY, even though it has the smallest ion radius, having the highest electrostatic field<sup>18</sup>.

While the same ion-exchange procedure was carried out, elemental analysis in Table 2-1 indicated that CaY and SrY had higher cation concentration than MgY and BaY zeolite. Moreover, FTIR spectra of the activated zeolites showed that the hydrolysis degree (creating hydroxide and/or Brønsted acid sites) varies with exchanged cation according to  $\text{MgY} > \text{CaY} > \text{SrY} > \text{BaY}$ . One source of Brønsted acid sites for these cation-exchanged zeolites is now generally accepted to occur via:



This reaction is thought to occur during pretreatment or activation at elevated temperature. In the presence of low amounts of water,  $\text{M}^{2+}$  ions become localized and the associated electrostatic field may induce dissociation of coordinated water molecules to produce  $\text{M}(\text{OH})^+$  and  $\text{H}^+$ . The latter combine with lattice oxygen to give  $\text{Si-O}(\text{H})\text{-Al}$  groups similar to decationated samples<sup>14;16;28</sup>. The higher the electrostatic field, the easier the dissociation of water and the more stable the  $\text{M}(\text{OH})^+$  species is. In addition, the presence of a  $\text{Mg}(\text{OH})_x$  vibration the spectra suggests that in MgY most of the cations hydrolyzed into  $\text{Mg}(\text{OH})^+$ . Consequently, fewer  $\text{Mg}^{2+}$  are present in the zeolites, explaining the lower observed activity.

Interestingly, for BaY reaction occurred at room temperature in our experiment while a reaction temperature of 55°C was reported necessary by Frei's group<sup>8</sup>. This may be attributed to different water content due to different activation procedures. No water is present after activation in this paper, whereas

0.3 H<sub>2</sub>O molecules per super-cage remained after the activation procedure of Frei et al. Residual water in the zeolite shields the cation via coulombic interaction, resulting in a lower activity.

### 2.4.2 Product distribution

In order to probe product distribution, *ex-situ* proton NMR was applied to analyze the CDCl<sub>3</sub> extraction solution. Only water and acetone were found as products after oxidation of propane at room temperature. Nevertheless, isopropylhydroperoxide was reported as reaction intermediate of propane photo-oxidation reaction over BaY zeolite by Frei's group<sup>8</sup>. In the present study isopropylhydroperoxide was only observed after evacuation because its absorption peaks were masked by propane bands. Raising temperature or simply waiting in time leads to formation of acetone and water due to isopropylhydroperoxide decomposition. The fact that isopropylhydroperoxide was not detected by NMR may be due to either a too low concentration, or to possible decomposition during extraction, or to strong adsorption preventing desorption into the solvent.

The molar ratio of acetone and water from propane partial oxidation should be constant for all catalysts if a stoichiometric reaction between propane and oxygen takes place. Evaluation of IR data (Figure 2-5c), however, showed that the acetone/water ratio increases with increasing cation radius. It was reported that the products extinction coefficients are the same with different cation exchanged Y zeolite<sup>8</sup>. This suggests that water was lost during reaction. However, water desorption was excluded by on-line MS analysis. A possible explanation would be that produced water hydrolyzes into Brønsted acid sites and Ba(OH)<sup>+</sup> species. Unfortunately, the small changes in the OH-stretch region do not allow quantification at present. Interestingly, on BaY, the acetone/water ratio decreases with reaction time up to 20 hours, while the other catalysts have a constant ratio after 3 hours. Since BaY has mainly bare cations, produced water will be hydrolyzed, and consequently not be observed at 1650cm<sup>-1</sup>. Hydrolysis of water at room temperature has been reported when re-adsorbing water in dehydrated divalent cation exchanged Y zeolite<sup>14;15;18;28</sup>. This hydrolysis leads to *in-situ* generation of protons that are of importance for isopropylhydroperoxide decomposition as will be discussed below.

### 2.4.3 Product adsorption

It can be seen in Table 2-2 that the OH-stretch frequency shifted gradually from 3700cm<sup>-1</sup> for MgY to 3683cm<sup>-1</sup> for BaY, while the H<sub>2</sub>O bending mode frequency increased from 1630cm<sup>-1</sup> for MgY to 1650cm<sup>-1</sup> for BaY. Literature reporting on H<sub>2</sub>O direct bonding to cations showed a shift in wavenumber of isolated OH stretching from high frequency for LiX to low frequency for KX, while the H<sub>2</sub>O bending

mode shifted from low frequency for LiX to high frequency for KX<sup>30</sup>. The identical trends of water adsorption on the present alkaline-earth exchanged Y zeolites indicates that water is adsorbed on cation sites.

In addition, the methyl stretch vibrations for adsorbed isopropylhydroperoxide also shift in wavenumber from 2998cm<sup>-1</sup> on CaY to 2983cm<sup>-1</sup> on BaY, showing a similar trend as the OH stretch frequency of adsorbed water. Therefore, we conclude that adsorbed isopropylhydroperoxide is also related to the cation site.

For acetone the data showed the same C=O stretching wavenumber (1682cm<sup>-1</sup>) for CaY, SrY and BaY and a higher frequency (1694cm<sup>-1</sup>) for MgY. The methyl stretching and deformation vibrations were identical for all samples. Figure 2-8 shows the FTIR spectrum of acetone adsorbed at room temperature on CaY. Two  $\nu_{C=O}$  are visible at 1713 cm<sup>-1</sup> and 1701cm<sup>-1</sup>. The negative band at 3640 cm<sup>-1</sup> indicates interaction of acetone with Brönsted acid sites. Both C=O bands merged and shifted to 1683 cm<sup>-1</sup> when increasing temperature under vacuum, where it remained after cooling to room

temperature (Figure 2-8b). The total integrated intensity of C=O absorption remained the same. Further, methyl stretch and deformation bands showed no changes. Infrared spectroscopy has been used to study acetone adsorption on zeolite acid sites<sup>31;32</sup>. Bands at 1679~1682cm<sup>-1</sup> and 1690~1702cm<sup>-1</sup> were assigned to acetone C=O interaction with bridging Brönsted OH and with Lewis acid sites respectively. Moreover, the Brönsted acid site vibration is independent of the cation (Figure 2-1). Thus we conclude that acetone is adsorbed on or nearby Brönsted acid sites, resulting in identical adsorption frequencies for CaY, SrY and BaY, and a higher frequency for MgY which also contains Mg(OH)<sub>x</sub> species.

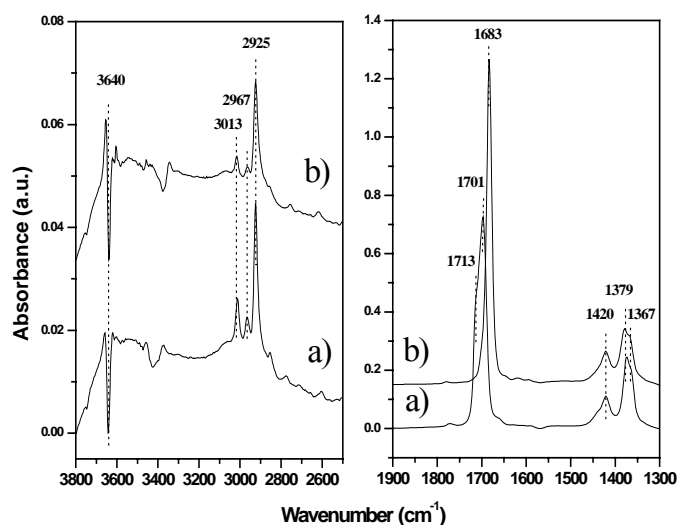


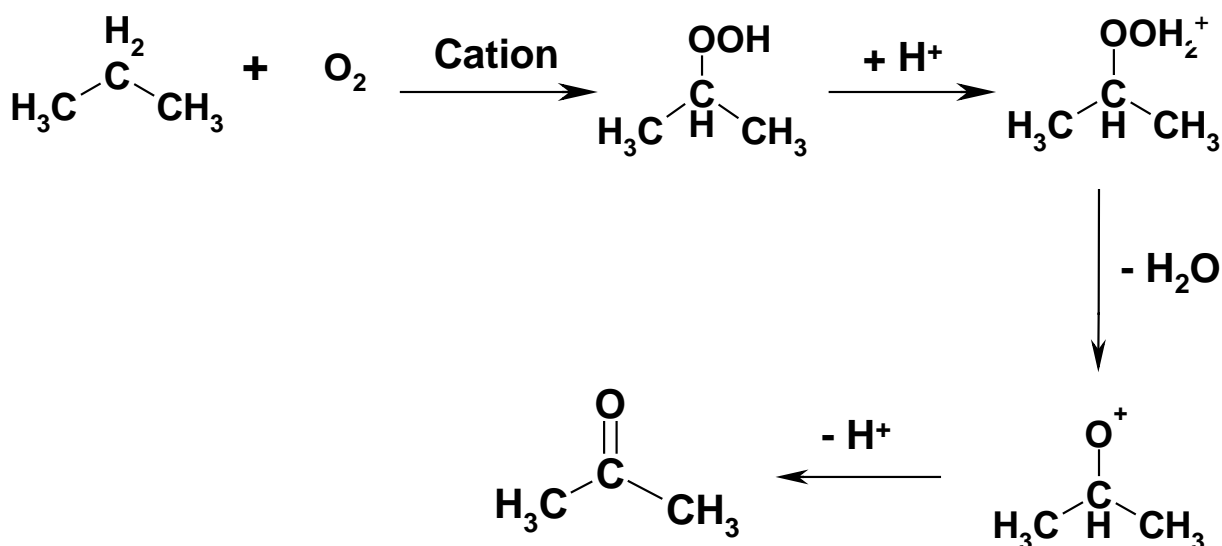
**Figure 2-8.** Adsorbed acetone (0.0005mbar) on CaY zeolite a) At room temperature; b) After 15 minutes heating at 300°C under vacuum, cooled to room temperature.

#### 2.4.4 Reaction mechanism

It has been proposed that the high mobility of alkane and oxygen in zeolites allows easy access to poorly shielded cation sites, resulting in spontaneously formation of an intermolecular charge-transfer complex, stabilized by parallel orientation to the electrostatic field, resulting in alkane radical cation and  $O_2^-$  formation<sup>6,7,11</sup>. After proton transfer from the hydrocarbon radical cation to the superoxide<sup>13</sup>, radical recombination is easily reached to form isopropylhydroperoxide, which is also observed as intermediate in our reaction. Thermal rearrangement of isopropylhydroperoxide to acetone and water is well-established<sup>8</sup> resulting in the overall reaction:



Hydroperoxide decomposition has been reported to be strongly accelerated in acid (HCl) treated NaY for cyclohexane photo-oxidation to cyclohexanone<sup>9</sup>. Also, thermal rearrangement of cyclohexylhydroperoxide to cyclohexanone and water is an established intramolecular heterolytic reaction in acidic solution<sup>33</sup>. In the present study, the relative ratio between isopropylhydroperoxide and acetone decreased according to BaY > SrY > CaY > MgY (Figure 2-7). On the other hand, the Brønsted acidity increasing for BaY < SrY < CaY < MgY (Figure 2-1). The different adsorption sites of isopropylhydroperoxide and acetone, as discussed above, suggest that the formation of hydroperoxide and its decomposition occurred at different active sites. The cation site directs the reaction to isopropylhydroperoxide while the Brønsted acid sites is involved in the decomposition into acetone and



*Scheme 1-1. Proposed mechanism for propane selective oxidation*

water (scheme 2-1). Additional evidence for this reaction scheme can be found in the acetone production curve of BaY (inset Figure 2-5a). The acetone production on BaY accelerated with reaction time, which might be attributed to creation of acid sites due to hydrolysis of produced water, in agreement with the high acetone to water ratio observed for BaY. Due to the very low concentration of produced water, quantification of hydrolysis level from the spectrum is difficult. It is not yet clear whether the cation and Brönsted acid sites act independently in the reaction or that a cooperation of both sites is needed, this is presently being investigated.

## 2.5 Conclusion

This study shows that propane can be oxidized to acetone, via isopropylhydroperoxide, at room temperature with increasing rates for BaY < MgY < SrY < CaY. The observed lower acetone growth rate for MgY, not expected based on its higher electrostatic field, can be explained by a higher hydrolysis degree of the cations, resulting in a lower amount of available Mg<sup>2+</sup> ions. Based on the FTIR data, water and isopropylhydroperoxide are adsorbed on or close to the cations in the zeolite, while acetone adsorbs on Brönsted acid sites, pointing to a two-step mechanism in which different active sites are involved. Moreover, surface reaction activity and selectivity (towards hydroperoxide or acetone) are determined by the presence of bare divalent cations as well as the number of Brönsted acid sites.

### Reference List

1. Centi, G.; Cavani, F.; Trifiro, F. *Selective oxidation by heterogeneous catalysis*, Kluwer Academic/Plenum Publishers: New York, 2000.
2. Centi, G.; Corberan, V. C.; Perathoner, S.; Ruiz, P. *Catalysis Today* **2000**, *61*, 1.
3. Centi, G.; Misono, M. *Catalysis Today* **1998**, *41*, 287-296.
4. Lyons, J. E.; Parshall, G. W. *Catalysis Today* **1994**, *22*, 313-333.
5. Dartt, C. B.; Davis, M. E. *Ind.Eng.Chem.Res.* **1994**, *33*, 2887.
6. Blatter, F.; Sun, H.; Vasenkov, S.; Frei, H. *Catalysis Today* **1998**, *41*, 297-309.
7. Frei, H. *3Rd World Congress on Oxidation Catalysis* **1997**, *110*, 1041-1050.
8. Sun, H.; Blatter, F.; Frei, H. *Catalysis Letters* **1997**, *44*, 247-253.
9. Sun, H.; Blatter, F.; Frei, H. *Journal of the American Chemical Society* **1996**, *118*, 6873-6879.
10. Blatter, F.; Sun, H.; Frei, H. *Chemistry-A European Journal* **1996**, *2*, 385-389.
11. Sun, H.; Blatter, F.; Frei, H. *Abstracts of Papers of the American Chemical Society* **1996**, *211*, 3-ORGN.



## Propane selective oxidation on alkaline earth exchanged Y zeolite at room temperature

12. Vanoppen, D. L.; DeVos, D. E.; Jacobs, P. A. *Progress in Zeolite and Microporous Materials, Pts A-C* **1997**, *105*, 1045-1051.
13. Larsen, R. G.; Saladino, A. C.; Hunt, T. A.; Mann, J. E.; Xu, M.; Grassian, V. H.; Larsen, S. C. *Journal of Catalysis* **2001**, *204*, 440-449.
14. Ward, J. W. *Journal of Physical Chemistry* **1968**, *72*, 4211-4223.
15. Donald W. Breck *Zeolite molecular sieves: structure, chemistry, and use*, Wiley: New York, 1974.
16. Uytterhoeven, J. B.; Schoonheydt, R. *Journal of Catalysis* **1969**, *13*, 425-434.
17. Ward, J. W. *Journal of Catalysis* **1967**, *9*, 225-236.
18. Ward, J. W. *Journal of Catalysis* **1968**, *10*, 34-46.
19. Sponer, J. E.; Sobalik, Z. *Journal of Physical Chemistry B* **2001**, *105*, 8285-8290.
20. Gough, K. M.; Murphy, W. F. *Journal of Physical Chemistry* **1987**, *87*, 3332-3340.
21. Geodokyan, K. T.; Kiselev, A. V. *Journal of Physical Chemistry* **1967**, *41*, 227,476.
22. H. van Bekkum *Introduction to zeolite science and practice*, Elsevier: Amsterdam, 2001.
23. Harald Guenther *NMR spectroscopy : basic principles, concepts, and applications in chemistry*, 2nd ed ed.; Chichester [etc.] : Wiley: 1995.
24. Smit, B. *Journal of Physical Chemistry* **1995**, *99*, 5597-5603.
25. Janchen, J.; Mortier, W. J. *Journal of Physical Chemistry* **1996**, *100*, 12489-12493.
26. Barthomeuf, D. *Catal.Rev.Sci-Eng.* **1996**, *38*, 521-613.
27. Vanoppen, D. L.; De Vos, D. E.; Jacobs, P. A. *Journal of Catalysis* **1998**, *177*, 22-28.
28. Subhash Bhatia *Zeolite catalysis : principles and applications*, CRC Press: Boca Raton, FA, 1990.
29. Kao, H. M.; Grey, C. P.; Ramamurthy, V. *Journal of Physical Chemistry* **1998**, *102*, 5627-5638.
30. Bertsch, L.; Habgood, H. W. *Journal of Physical Chemistry* **1963**, *67*, 1621.
31. Panov, A.; Fripiat, J. J. *Langmuir* **1998**, *14*, 3788-3796.
32. Panov, A.; Fripiat, J. J. *Journal of Catalysis* **1998**, *178*, 188-197.
33. Sheldon, R. A. *The chemistry of functional groups, peroxides*, Wiley: New York, 1983.
34. Mortier, W. J. *Journal of Catalysis* **1978**, *55*, 138-145.
35. Sanderson, R. T. *Journal of the American Chemical Society* **1983**, *105*, 2259-2261.

## Chapter 3

### **Desorption of Acetone From Alkaline-earth Exchanged Y Zeolite After Propane Selective Oxidation**

---

***Abstract:** The desorption of products from a series of alkaline-earth exchanged Y zeolites after room temperature propane selective oxidation was investigated by in-situ infrared and mass spectroscopy. The intermediate product, isopropylhydroperoxide(IHP), did not desorb during temperature-programmed-desorption experiments, but converted into acetone and water. Decomposition rate of IHP, produced from propane and oxygen at room temperature, into acetone increased in the order  $BaY < SrY < CaY (< MgY)$  which was attributed to the number of acid sites in the samples. TPD results on CaY zeolite point to two acetone adsorption sites, which are tentatively assigned to Brönsted acid sites and  $Ca(OH)_x$  species. Acetone mainly desorbs at higher temperatures ( $> 250$  °C) under dry conditions. Addition of water, however, results in gas phase acetone already at room temperature. From the results it can be concluded that water clearly facilitates acetone desorption, most likely via shielding of the electrostatic field and creation of additional sites.*

### 3.1 Introduction

Partial oxidation of small alkanes is increasingly important for application of natural gas and volatile petroleum fractions as new feedstock<sup>1-4</sup>. In most cases, molecular oxygen is the only economically viable oxidant. Unfortunately, direct oxidation by O<sub>2</sub> is very unselective for most small hydrocarbons. As a result, existing methods generate large amounts of unwanted products. Lack of selectivity is often caused by the free radical nature of the reaction, high exothermicity or further oxidation of the desired product. The free mobility of the radical intermediates results in indiscriminate attack on starting hydrocarbon and primary oxidation products. Moreover, under thermal conditions, in liquid or gas phase, oxygen attacks partially oxidized products more easily than starting hydrocarbons resulting in overoxidation. As products accumulate, the lack of control gets worse, which limits conversion to a few percent in most practical processes<sup>4-6</sup>.

Recently, Frei et al.<sup>7;8;9-12</sup>, Grassian et al.<sup>13</sup>, Vanoppen et al.<sup>14</sup> and our group<sup>15</sup> have demonstrated that (earth) alkali exchanged Y zeolite selectively oxidizes alkanes (ethane, propane, isobutene and cyclohexane) at room temperature. Reaction activity of gas phase cyclohexane and propane oxidation was found to increase in order NaY < BaY < SrY < CaY attributed to the increasing electrostatic field of the cations<sup>14;15</sup>. Complete selectivity was reported at conversions as high as about 35%<sup>9;10</sup>. The reaction mechanism proposed by Frei involved a charge transfer complex, [(C<sub>n</sub>H<sub>2n+2</sub>)<sup>+</sup>O<sub>2</sub><sup>-</sup>]. They hypothesized that the charge transfer complex is stabilized by the electrostatic field of exchanged cations in the zeolite and this stabilization allows access to the charge transfer state by visible light irradiation or by thermal activation<sup>7-12</sup>.

The selectivity of this partial oxidation by molecular oxygen is unprecedented. The high selectivity is attributed to the strong adsorption of polar carbonyl products inside the zeolite pores, preventing overoxidation. Nevertheless, to turn this type of selective oxidation into a practical process, the barrier for product desorption has to be overcome. At present, release of small oxygenated hydrocarbons from zeolite Y is only achieved by extraction with polar organic solvents<sup>16</sup>. A solvent free method would be environmentally and economically preferable. So the critical problem is to achieve continuous desorption of products from the zeolite. Use of a carrier gas and modestly elevated temperature have been proposed to give chance to desorb polar products at acceptable rates<sup>9</sup>. However, desorption data are still absent for those reactions. Moreover, selectivity will face a challenge due to over-oxidation of oxygenates by increasing temperature.

The present paper reports on temperature-programmed-desorption (TPD) of propane partial oxidation products using *in situ* FTIR and MS. The effect of additional water on the desorption patterns was investigated as well.

## 3.2 Experimental

### 3.2.1 Materials

Alkaline-earth cation (Mg, Ca, Sr, and Ba) exchanged Y-zeolites were prepared from NaY (Akzo Nobel, sample code: 1122-207) with Si/Al ratio of 2.5. The parent zeolite was exchanged three times with 0.1M solution of respectively magnesium chloride, calcium chloride, strontium nitrate, or barium chloride (Merck) for 20 hours at 90 °C under stirring. The resulting alkaline-earth exchanged Y zeolite was washed three times with distilled water, filtered and dried at 100 °C overnight. The chemical composition of catalysts was analyzed by X-ray fluorescence. The  $M^{2+}$  ( $Mg^{2+}$ ,  $Ca^{2+}$ ,  $Sr^{2+}$  and  $Ba^{2+}$ )/Al ratio was 0.34, 0.43, 0.45 and 0.35 for MgY, CaY, SrY and BaY respectively. Powder X-ray diffraction gave no indication for collapse of zeolite structure, even not after calcination at 650 °C.

### 3.2.2 Infrared Spectroscopy

The zeolite powder was pressed into a self-supporting wafer and analyzed *in-situ* during reaction and desorption by means of transmission FTIR spectroscopy using a Bruker Vector22 FTIR spectrometer with a MCT detector. A miniature cell, equipped with  $CaF_2$  transparent windows, which can be evacuated to pressure below  $10^{-7}$  mbar was used for the *in-situ* experiments. The temperature is variable from room temperature to 500 °C. Each spectrum consists of 32 scans taken at  $4\text{ cm}^{-1}$  resolution. The spectra were corrected for absorption of the activated zeolite (for details see Ref. 15).

### 3.2.3 Temperature Programmed Desorption (TPD)

The infrared cell was used as a batch reactor for propane oxidation at 1mbar propane and 40mbar oxygen pressure. After 20 hours reaction, followed by evacuation for 1 hour, the remaining adsorbed molecules were removed by temperature programmed desorption (rate  $10\text{ °C/minute}$ , up to 500 °C). Infrared spectra were taken simultaneously with on-line mass spectroscopy for detection of gas phase species.

## 3.3 Results

### 3.3.1 Surface species after propane oxidation

Figure 3-1 shows the FTIR spectra after 20 hours reaction of propane and oxygen followed by 1 hour evacuation for different exchanged Y-zeolites. The observed vibrations can be attributed to acetone (2925, 1694, 1682, 1420, 1379,  $1367\text{cm}^{-1}$ ), water (3700, 3695, 3686, 3683, 3430, 1650, 1644, 1634,

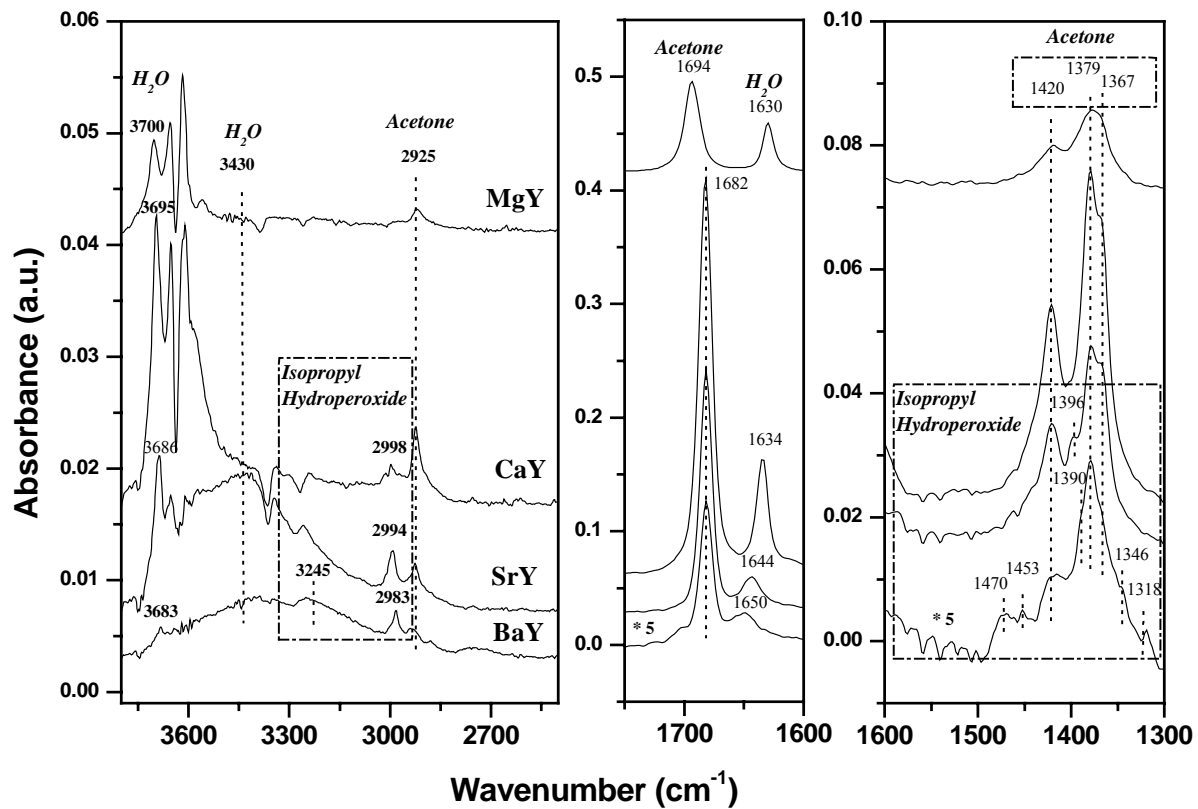


**Figure 3-1.** Different FTIR spectra after 20 hours propane oxidation, followed by one hour evacuation

1630  $\text{cm}^{-1}$ ) and isopropylhydroperoxide (IHP) (3245, 2998, 2994, 2983, 1470, 1453, 1396, 1390, 1346, 1318  $\text{cm}^{-1}$ )<sup>7,8,15</sup>. On MgY only acetone and water were observed.

Figure 3-2 reports the change in band intensity for IHP and acetone to illustrate the effect of evacuation at room temperature. About 4%, 7% and 25% of IHP converted into acetone and water on BaY, SrY and CaY respectively after one hour evacuation. No products could be detected in the gas phase by on-line MS spectroscopy during

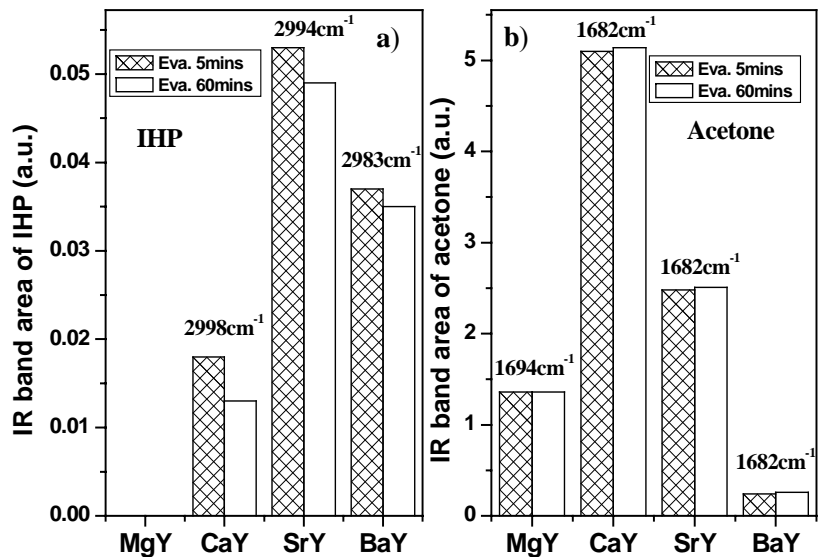


**Figure 3-2.** Infrared intensity change of IHP and acetone before and after one hour at room temperature under vacuum

evacuation at room temperature.

### 3.3.2 Infrared study of desorbing species

The TPD-profiles of IHP, acetone and water as observed in the infrared spectra for SrY are compiled in Figure 3-3. The band intensity of IHP (band at  $2994\text{cm}^{-1}$ , Figure 3-3a) decreased with raising temperature. A dramatic decrease of intensity occurred from  $80\text{ }^{\circ}\text{C}$ . The IHP band totally disappeared at  $170\text{ }^{\circ}\text{C}$ . Concurrently, the acetone ( $\nu_{\text{C=O}}$  at  $1682\text{cm}^{-1}$ ) and water ( $\delta_{\text{H}_2\text{O}}$  at  $1644\text{cm}^{-1}$ ) intensities also varied. For acetone (Figure 3-3b), the C=O stretch intensity increased until temperature reached about  $170\text{ }^{\circ}\text{C}$ . Then it was constant up to  $400\text{ }^{\circ}\text{C}$ . Subsequently, decreasing acetone intensity was found if temperature increased further. Similar behavior of water, the water signal ( $\delta_{\text{H}_2\text{O}}$ , Figure 3-3c) first increased when temperature was raised. Maximum intensity was observed at  $140\text{ }^{\circ}\text{C}$ , from where it reduced and totally disappeared at  $320\text{ }^{\circ}\text{C}$ .

The IHP decomposition profile in the infrared spectra during TPD for alkaline earth exchanged Y zeolite is given in Figure 3-4. It was found that IHP decomposition on BaY was slower than on CaY and SrY. Figure 3-5 displays the difference in infrared intensity for acetone ( $\nu_{\text{C=O}}$ , integrated area) before TPD and at  $230\text{ }^{\circ}\text{C}$  during TPD. As indicated above, with raising temperature, IHP decomposition was observed, and simultaneously acetone and water (not shown) amounts increased on CaY, SrY and BaY. The ratio of converted IHP (integrated area at  $2998\text{cm}^{-1}$  for CaY,  $2994\text{cm}^{-1}$  for SrY and  $2983\text{cm}^{-1}$  for BaY in Figure 3-1) and produced acetone ( $\nu_{\text{C=O}}$ , integrated area, in Figure 3-5) was  $0.06 \pm 0.03$ ,  $0.09 \pm$

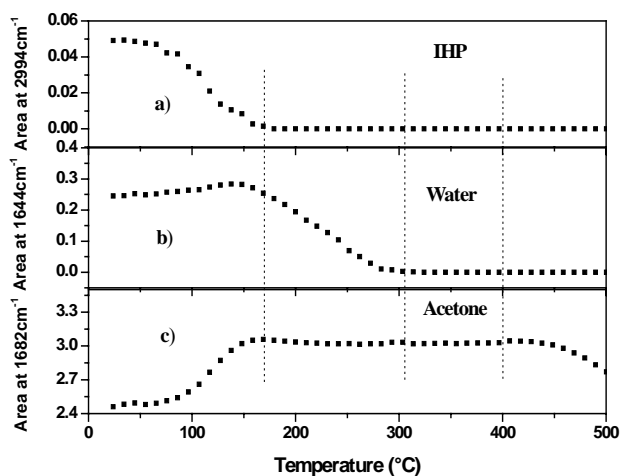


**Figure 3-3.** Change of FTIR band intensity (integrated area) of products on SrY zeolite during TPD

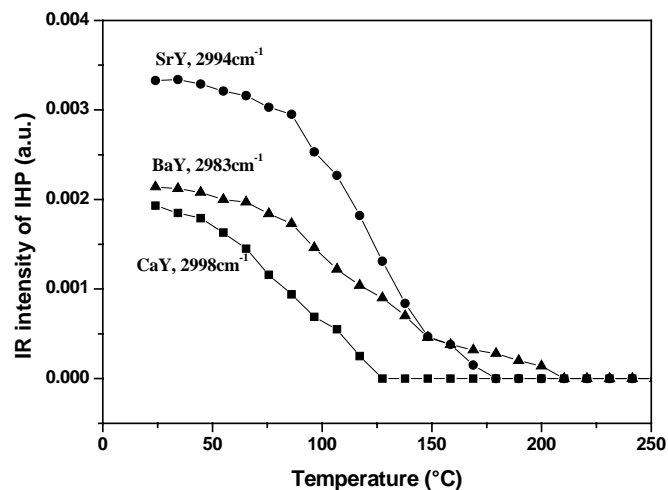


**Figure3- 4.** Change of FTIR band intensity of IHP on alkaline-earth exchanged Y zeolites during TPD

0.01 and  $0.09 \pm 0.01$  for CaY, SrY and BaY respectively. The large error for CaY is caused by the very small amount of IHP for which, in addition, the vibrations overlap with acetone, that is present in large amount. For SrY and BaY there clearly is less acetone and more IHP, resulting in a smaller error. At 230 °C, IHP fully decomposed for all catalysts, but no acetone desorbed yet. Temperatures at which water totally desorbed were 280 °C for BaY, 320 °C for SrY and 400 °C for both CaY and MgY.

Figure 3-6 shows the infrared spectra of adsorbed species on SrY before TPD (Fig. 3-6a), at 500 °C during TPD (Fig. 3-6b), and after TPD, dwell 30 minutes at 500 °C, and subsequent cooling to room temperature (Fig 3-6c). Based on the spectra, water and only part of acetone desorbed. No other oxidation or dimerization products (e.g. mesityl oxide) were found in the infrared spectra for the zeolites studied.

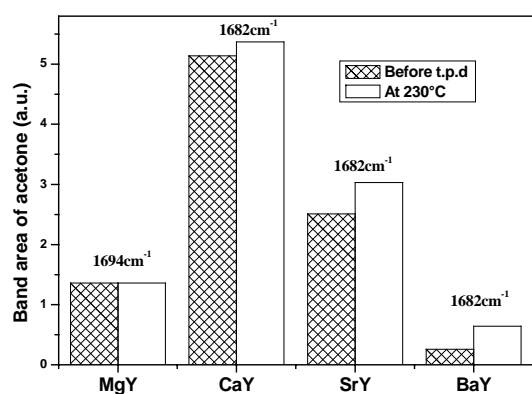


**Figure 3-5.** Infrared intensity of acetone before TPD and at temperature 230°C during TPD

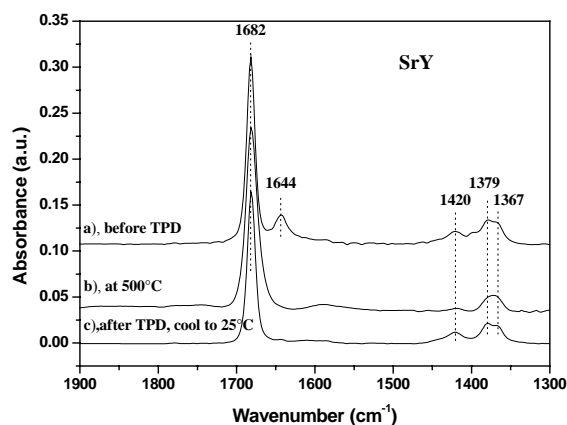


**Figure 3-6.** Infrared spectra of adsorbed species on SrY at conditions: a) after 20 hours propane oxidation, followed 1 hours evacuation; b) TPD experiment at temperature 500°C; c) after TPD, dwell 30 minutes, followed cooling to 25°C

Interestingly, it was found that most of the acetone was still on the surface of MgY, CaY and SrY, but from BaY completely desorbed after temperature-programmed-desorption, subsequent evacuation at 500 °C for 30 minutes and cooling to room temperature under vacuum (Figure 3-7). About 10% acetone for both MgY and CaY, about 25% acetone from SrY and 100% acetone from BaY desorbed during this experiment.

### 3.3.3 Mass spectroscopy study of desorbing species

Simultaneously with infrared data, mass spectra were taken to detect gas phase compounds during TPD (Figures 3-8a and b). It was observed that water desorption started at 60 °C with BaY, 80 °C with SrY, 110 °C with CaY and 140 °C with MgY.

Acetone desorption initiated in the same order, namely at 230 °C, 300 °C, 300 °C and 350 °C for BaY, SrY, CaY and MgY respectively. Desorption did not reach a maximum at 500 °C (max. temperature for FTIR cell) on these catalysts except for BaY, where the acetone maximum intensity occurred at around 425 °C.

With mass spectrometry also no other oxidation or dimerization products could be detected.

### 3.3.4 Effect of water on acetone desorption

After 25 hours reaction of propane and oxygen on CaY, the reaction system was evacuated for 10 minutes (Figure 3-9a). Subsequently, 0.5mbar water was introduced into the infrared cell and kept for 30 minutes, after which the system was evacuated for one hour (Figure 3-9b). After adding water to CaY, the water bending mode was appreciably broader and several bands were observed (1634, 1644, 1622  $\text{cm}^{-1}$ ).

Influenced by the adsorbed water, acetone C=O stretch vibration shifted from 1682 $\text{cm}^{-1}$  to 1689 $\text{cm}^{-1}$ , but acetone  $\text{CH}_3$  deformations (1420, 1379, 1367 $\text{cm}^{-1}$ ) did not change.

Very surprisingly, acetone was observed in the gas phase during evacuation at room temperature, while for the dry zeolite no acetone could be detected (Figure 3-10, part A).

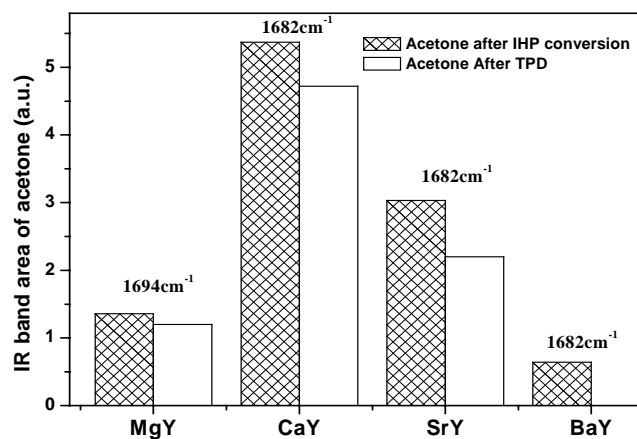


**Figure 3-7.** Change of acetone after TPD, followed 500 °C half hour heating under vacuum on alkaline-earth exchanged Y zeolites.

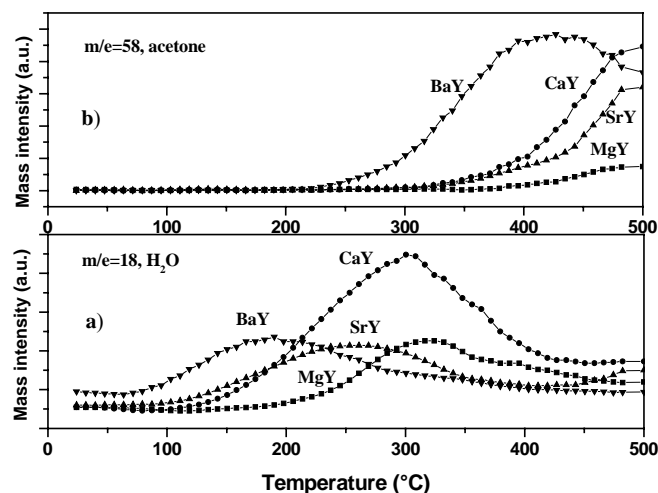


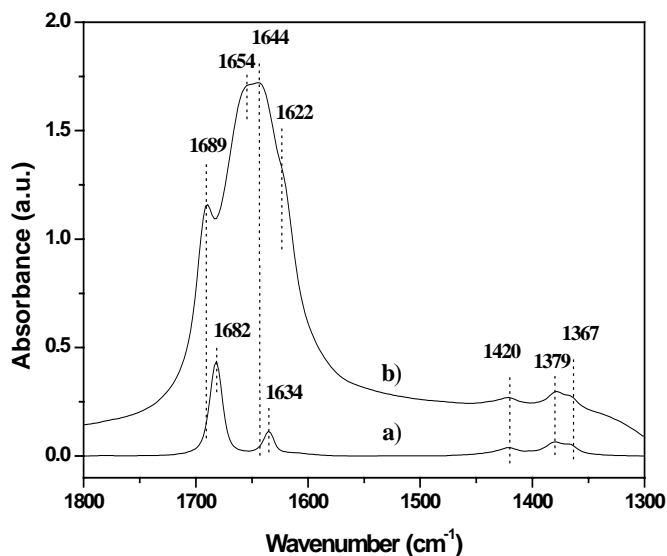
**Figure 3-8.** TPD-MS of products desorption after propane oxidation on alkaline-earth exchanged Y zeolites.



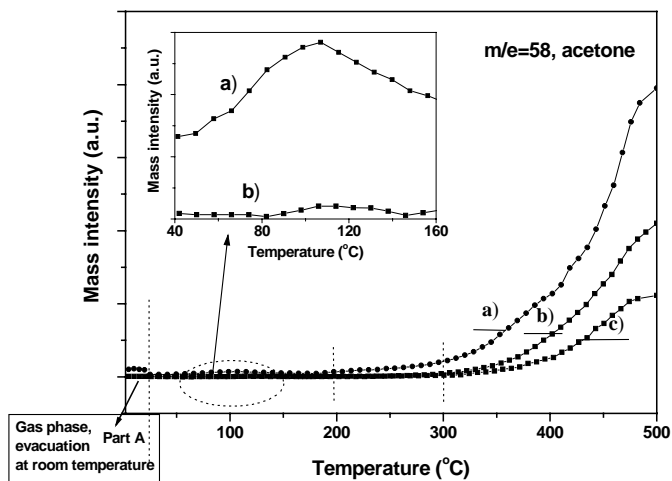
After evacuation, TPD experiments were performed (Figure 3-10a). A small amount of acetone was detected in the gas phase for temperatures from 50 °C to 160 °C (see insert Figure 3-10). The onset of a second desorbing acetone species was 200 °C, about 100 °C lower than in experiments without pre-adsorbed water (Figure 3-10b and c). In addition, mass spectroscopy showed large amounts of water present in the gas phase when acetone was desorbing. Moreover, without added water, mainly at one temperature desorbing acetone species was observed, and only a very small amount was detected around 120 °C.

Figure 3-11 displays the relative amount of desorbed acetone for experiments with and without pre-adsorbed water prior to TPD. After TPD and subsequent half an hour isothermal heating at 500 °C, about 20% of the total amount of acetone had desorbed when water was added compared to 10% of acetone from dry zeolite, irrespective of the acetone coverage. Additional experiments (not shown) have indicated that higher quantities of water increase the amount of desorbed acetone.

Since acetone desorbed from CaY zeolite is enhanced by water, additional experiments were carried out in a glass batch reactor with 0.15bar propane, 1.5bar oxygen and 80mg activated MgY, CaY, SrY and BaY zeolites respectively. After 20



**Figure 3-9.** FTIR spectra of a) after 25 hours propane oxidation, followed by ten minutes evacuation; b) after adding 0.5mbar water, 30 minutes dwell and evacuation for one hour, all at room temperature



**Figure 3-10.** TPD acetone desorption on CaY at conditions: a) after 25 hours reaction, evacuated 10 minutes, followed adding 0.5mbar water; b) after 35 hours reaction; c) after 20 hours reaction

hours reaction at room temperature in the dark, no acetone was detected in the gas phase by mass spectrometry in all cases. After 15 minutes evacuation, followed by injection of 0.5ml of water, a significant concentration of acetone was detected in the gas phase above each of the four catalysts, in agreement with the low-pressure experiment in the infrared cell on CaY zeolite. After these experiments, the samples were taken out and infrared spectra were recorded; no acetone could be observed anymore in each of zeolite samples.

### 3.4 Discussion

During evacuation at room temperature under dry conditions, no products were observed in the gas phase. Only slight decomposition of isopropylhydroperoxide (IHP) into acetone and water was found (Figure 3-2). With increasing temperature, IHP intensity decreased and disappeared before temperature reached 230 °C for CaY, SrY and BaY as observed in the infrared spectra (Figure 3-4). Simultaneously acetone intensity increased in similar ratios to the original amount of IHP on the catalyst surface. The low value of the IHP to acetone ratio is caused by the fact that the absolute intensity decrease for IHP is much lower than the absolute growth of acetone, due to the different extinction coefficients for IHP (C-H) and acetone (C=O) vibrations. The intensity of acetone was constant above 230 °C until desorption temperature was reached (Figure 3-3c). For MgY the amount of acetone was constant from the start of TPD up to desorption temperature, since no IHP was present to be converted.

These results support the two-step reaction path for propane selective oxidation to acetone and water over alkaline earth exchanged zeolite as proposed in our previous paper <sup>15</sup>:



Additionally, on BaY clearly more IHP than acetone was present after 20 hours reaction, since conversion of IHP results in a total amount of acetone that is over twice (2.4 times) the original amount of acetone produced from propane and oxygen (Figure 3-5a). Consequently, total propane conversion

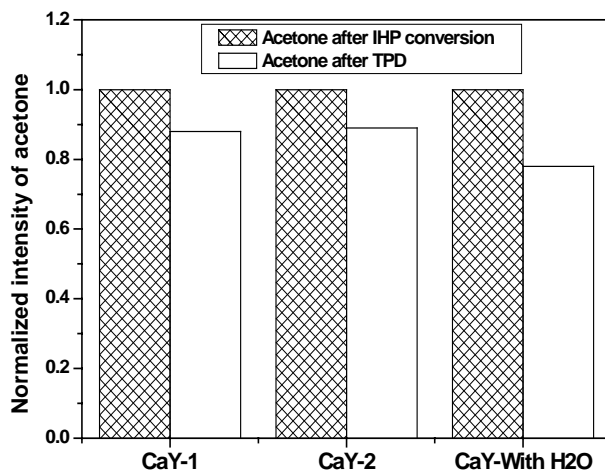


**Figure 3-11.** Change of acetone ( $\nu_{\text{C=O}}$ , normalized) intensity after TPD, and evacuation at 500°C for half an hour for CaY zeolite with and without adding water after reaction. (CaY-1, 20 hours reaction; CaY-2, 35 hours reaction; CaY-with H<sub>2</sub>O, 25 hours reaction, evacuated for 10 minutes at room temperature, followed by adding 0.5mbar H<sub>2</sub>O).

over BaY at room temperature is 2.4 times higher than previously reported, that was based on the amount of acetone observed<sup>15</sup>. IHP converted much slower into acetone over BaY than for CaY and SrY (Figure 3-4).

Based on the IR band positions of adsorbed IHP and acetone on the zeolite, we proposed that IHP formation and decomposition into acetone occur at different active sites<sup>15</sup>. The cation site directs the reaction from propane into IHP while Brönsted acid sites seem to be involved in the decomposition of IHP into acetone. The present observation that the relative higher amount of IHP after 20 hours reaction (Figure 3-5) and its slower conversion over BaY, that hardly has any Brönsted sites (Figure 3-4), supports our previous finding of the importance of Brönsted acid sites for the IHP decomposition. We reported previously that the Brönsted acidity increases in the order BaY < SrY < CaY < MgY based on direct observations on the intensity of the OH vibrations<sup>15</sup>. Moreover, the present results suggest that the exceptional acetone desorption behavior of BaY can also be attributed to the lower acidity of this sample. Acetone desorption initiated at 230 °C, 300 °C, 300 °C and 350 °C on BaY, SrY, CaY and MgY respectively. Acetone adsorption obviously is so strong that it only partially desorbed from MgY, CaY and SrY, even after isothermal heating at 500 °C for half hour (Figure 3-7). Completely desorption of acetone under the above condition was only achieved for BaY. No obvious relation was found between acetone desorption temperature or quantity and its C=O stretch frequency (Figure 3-1), indicating that the C=O stretch vibration cannot be used as a measure for the acetone binding strength in the studied zeolite.

Starting temperature of water desorption observed in the infrared spectra for SrY was 140 °C (Figure 3-3), while mass spectroscopy already detected water desorption at 80 °C (Figure 3-8). This can be easily explained, since during a TPD experiment two reactions simultaneously take place:



If the IHP decomposition rate is higher than the water desorption rate, the infrared intensity of water will increase while simultaneously desorbed water will be detected in gas phase.

The strong adsorption of partially oxidized hydrocarbons was proposed to be responsible for the high selectivity towards oxygenates<sup>10,13</sup>. However, it is also causing the desorption problem in this type of samples. Interestingly, the present study clearly shows that acetone can be desorbed in the gas phase even at room temperature by simple addition of water to the sample (Figure 3-10 and 3-12). Upon addition of water to CaY zeolite, the onset of the high temperature acetone desorption was found to decrease with 100 °C. Further, an additional low temperature acetone desorption peak was observed at about 100 °C (Figure 3-10). Finally, the relative amount of desorbed acetone after addition of water is

significantly higher than the amount from a dry zeolite (note: the amount of water is much more than the number of cations present). As no other oxidation or dimerization products (e.g. mesityl oxide) were found in the infrared spectra and mass spectra during reaction and TPD, hydrolysis of such compounds can be excluded to contribute to the increased amounts of desorbed acetone. Moreover, acetone coverage did not affect the onset of desorption or the relative desorbed amount of acetone (Figures 3-10 and 3-11). Addition of water resulted in two clear acetone desorption peaks during TPD, one around 100 °C and one starting around 200 °C. Importantly, during acetone desorption also large amounts of water vapor were observed. For the dry zeolite only a very small amount of acetone was found to desorb around 120 °C. At present we assume this is likely caused by desorption of the small amount of water present in the zeolite after propane oxidation. Apparently, the water partial pressure is too low to facilitate acetone desorption for dry CaY, causing higher desorption temperatures and smaller desorbing quantities.

The two acetone desorption peaks suggest that acetone is adsorbed on two different sites on CaY zeolite. In addition to Brønsted acid sites, as we proposed before, small amounts of acetone may be adsorbed onto Lewis acid sites or  $\text{Ca}(\text{OH})_x$  species. In principle, different adsorption sites are expected to result in different frequencies for acetone vibrations. However, since the site contributing to the low temperature peak only covers a minor part of the total acetone amount, different acetone frequencies could not be observed.

The influence of the water in the zeolite can be explained by various interactions. Firstly, water can shield the electrostatic field within the zeolite cages through coordination to the cations<sup>8</sup>. Secondly, adsorbed water on cations or protons changes the Brønsted and Lewis acidity of the zeolite<sup>17;17-19;19</sup>. Normally, addition of water to dry CaY creates more Brønsted acid sites and  $\text{Ca}(\text{OH})_x$  species, while Lewis acid sites are converted into Brønsted sites. At present we cannot exclude one of these effects. The observed shift in C=O stretch frequency upon addition of water (Figure 3-9) could be due to creation of new adsorption sites in addition to superposition of this peak on the large water signal. After TPD, the remaining C=O stretch vibration appeared at its original frequency in the infrared spectra. As expected, an increase of the Brønsted acid sites and  $\text{Ca}(\text{OH})_x$  signals was found after TPD.

It is clear that the presence of water on CaY zeolite resulted in two effects: more acetone was desorbed for both desorption peaks and the temperature onset of both desorption peaks was decreased (Figure 3-10). The lower desorption temperatures indicate that the abundant presence of water weakens the acetone adsorption strength. Moreover, the increased intensity of the low-temperature peak points to creation of extra sites of this particular type after addition of water. This supports the possibility that  $\text{Ca}(\text{OH})_x$  species might be responsible for the low-temperature desorption peak. Moreover, increasing

the amount of water added to the zeolite after reaction from 0.015 mol/g<sub>zeolite</sub> (in the infrared experiment) to 0.35 mol/g<sub>zeolite</sub> (in the glass batch experiment), the amount of acetone desorbed was increased from 20% to almost 100%.

Although addition of water to the feed of propane and oxygen rapidly deactivates the zeolite due to the high hydrophilicity of Y zeolite<sup>17</sup>, our results convincingly show that desorption of acetone at room temperature is possible by simply adding water after reaction. Since regeneration of wet zeolites can be done at much lower temperatures than for acetone-saturated zeolites, the water-assisted desorption of acetone possibly opens up a route for application of these samples to produce acetone in large amounts. Although detailed studies on the effect of water on desorption of acetone have been performed only for CaY, it is evident that the observation that desorption is assisted by water holds for all each alkaline earth modified Y zeolites.

Presently, experiments are performed to determine the delicate balance between good activity, selectivity and desorption of products by tuning zeolite properties and feed composition.

### 3.5 Conclusion

Decomposition rate of IHP, produced from propane and oxygen at room temperature, into acetone increases in the order BaY < SrY < CaY (< MgY) which is attributed to the number of acid sites in the samples. TPD results on CaY zeolite point to two acetone adsorption sites, which we tentatively assign to Brønsted acid sites and Ca(OH)<sub>x</sub> species. Acetone mainly desorbs at higher temperatures (> 250 °C) under dry conditions, only a minor amount is observed around 120 °C. Addition of water, however, results in gas phase acetone already at room temperature. Further, upon addition of water, both desorption peaks are shifted to lower temperature and show increased intensities. It can be concluded that water clearly facilitates acetone desorption, most likely via shielding of the electrostatic field and creation of additional sites. To reach practical application of this type of samples for partial oxidation of small alkanes, a balance has to be found between cations, acid sites, and the amount of water in the zeolites or reactants.

#### Reference List

1. Centi, G.; Misono, M. *Catalysis Today* **1998**, *41*, 287-296.
2. Centi, G.; Perathoner, S. *Current Opinion in Solid State & Materials Science* **1999**, *4*, 74-79.
3. Centi, G.; Corberan, V. C.; Perathoner, S.; Ruiz, P. *Catalysis Today* **2000**, *61*, 1.

4. Centi, G.; Cavani, F.; Trifiro, F. *Selective oxidation by heterogeneous catalysis*, Kluwer Academic/Plenum Publishers: New York, 2000.
5. Dartt, C. B.; Davis, M. E. *Ind.Eng.Chem.Res.* **1994**, *33*, 2887.
6. Hodnett, B. K. *Heterogeneous catalytic oxidation*, Jone Wiley & Sons Ltd, Chichester: 2000.
7. Sun, H.; Blatter, F.; Frei, H. *Journal of the American Chemical Society* **1996**, *118*, 6873-6879.
8. Sun, H.; Blatter, F.; Frei, H. *Catalysis Letters* **1997**, *44*, 247-253.
9. Frei, H. *3Rd World Congress on Oxidation Catalysis* **1997**, *110*, 1041-1050.
10. Blatter, F.; Sun, H.; Vasenkov, S.; Frei, H. *Catalysis Today* **1998**, *41*, 297-309.
11. Blatter, F.; Sun, H.; Frei, H. *Chemistry-A European Journal* **1996**, *2*, 385-389.
12. Sun, H.; Blatter, F.; Frei, H. *Abstracts of Papers of the American Chemical Society* **1996**, *211*, 3-ORGN.
13. Larsen, R. G.; Saladino, A. C.; Hunt, T. A.; Mann, J. E.; Xu, M.; Grassian, V. H.; Larsen, S. C. *Journal of Catalysis* **2001**, *204*, 440-449.
14. Vanoppen, D. L.; DeVos, D. E.; Jacobs, P. A. *Progress in Zeolite and Microporous Materials, Pts A-C* **1997**, *105*, 1045-1051.
15. Xu, J.; mojet, B. L.; Ommen, J. G. v.; Lefferts, L. *Phys.Chem.Chem.Phys.* **2003**, *5*, 4407-4413.
16. H.van Bekkum *Introduction to zeolite science and practice*, Elsevier: Amsterdam, 2001.
17. Donald W.Breck *Zeolite molecular sieves: structure, chemistry, and use*, Wiley: New York, 1974.
18. Uytterhoeven, J. B.; Schoonheydt, R. *Journal of Catalysis* **1969**, *13*, 425-434.
19. Ward, J. W. *Journal of Catalysis* **1968**, *10*, 34-46.

## Chapter 4

### **The Effect of $\text{Ca}^{2+}$ Position in Zeolite Y on Selective Oxidation of Propane at Room Temperature**

---

***Abstract:** The activity of CaNaY zeolites in selective oxidation of propane with increasing  $\text{Ca}^{2+}$  content at room temperature was studied with infrared spectroscopy and ammonia temperature programmed desorption. Increasing  $\text{Ca}^{2+}$  exchange level in CaNaY zeolites resulted in a variety of altered properties: the amount of Brønsted and Lewis acid sites increased, the adsorption of propane increased, the initial acetone formation rate increased and the desorption of acetone retarded. Moreover, all these properties showed a sudden change with  $\text{Ca}^{2+}$  content above 50%  $\text{Na}^+$  exchange level, which can be fully attributed to the location of  $\text{Ca}^{2+}$  in the Y-zeolite framework. It is convincingly shown that only  $\text{Ca}^{2+}$  ions located in the supercage contribute to the formation of Brønsted and Lewis acidity as well as propane oxidation activity at room temperature.*

#### 4.1 Introduction

Zeolites belong to a large family of (alumino)silicates constituted by corner-linked  $\text{TO}_4$  tetrahedra (T represents for either Al or Si) that adopt a remarkable variety of crystalline structures containing channels and/or cavities with different dimensions<sup>1-4</sup>. Aluminum containing zeolites have a negatively charged framework which results from  $\text{AlO}_2^-$  units replacing neutral  $\text{SiO}_2$  units. The negative charge is balanced by an equivalent number of extra-framework cations, often alkali or alkaline-earth metal cations. Zeolite Y is the synthetic form of faujasite and has a Si/Al ratio between 2 – 5. Its framework has two main cages: the large supercage results from an assembly of the basic units, the sodalite cages (Figure 4-1). The spherical supercages are approximately 1.3nm in diameter. Access to supercages is afforded by four 12-membered ring windows about 0.84nm in diameter, which are tetrahedrally distributed around the center of the supercages. The supercages thus form a three-dimensional network with each supercage connected to four other supercages through a 12 membered ring window.

The unit cell of Y zeolite consists of eight supercages. Charge compensating cations can occupy three positions in Y zeolite (see Figure 4-1). The first type, site I and I' is located on the hexagonal prism faces between the sodalite units. The second type, site II' and II is located in the open hexagonal faces. The third type, site III is located on the walls of the supercage. In a dry zeolite, site I', II', II and III cations are shielded on one side only, the other side, exposed to the center of sodalite-cage or supercage, remains unshielded. This leads to a partial shielding of the anionic framework of the zeolite as well, as a consequence

electrostatic field gradients are generated extending into the supercage.

Recently, a new approach of selective oxidation of alkanes (ethane, propane, isobutane and cyclohexane) on cation exchanged Y zeolite was presented by Frei et al.<sup>5-8</sup>, Grassian et al.<sup>9</sup>, Vanoppen et al.<sup>10</sup> and our group<sup>11</sup>. The proposed explanation for the selective oxidation, either thermally or photochemically activated, is the confinement of the reactants in a restricted environment (supercage) that exhibits a strong electrostatic field. Complete selectivity was reported due to (1) the diffusional

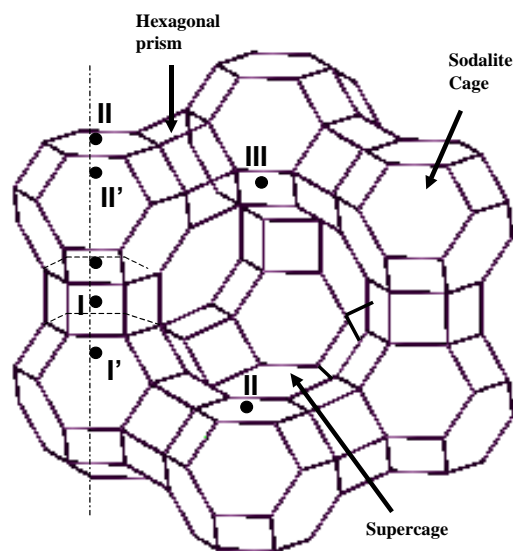


**Figure 4-1.** Structure of zeolite Y, where the location of cation site I, I', II, II', and III are shown.



constraints to avoid radical coupling reactions and (2) strong adsorption of partially oxidized products to avoid over-oxidation<sup>9;12-14</sup>. Activity was reported to increase in the order NaY < BaY < SrY < CaY caused by the increasing cation electrostatic field<sup>10;11</sup>. It needs to be stressed that the catalytic cycle has not yet been closed because the oxygenates formed are left adsorbed strongly in the zeolite.

Our recent results indicated that propane adsorbed *via* interaction with framework oxygen. Propane adsorption increased with higher basicity of the zeolite lattice oxygen in a series of alkaline-earth exchanged Y zeolites (i.e. BaY > SrY > CaY > MgY)<sup>11</sup>. Moreover, the rate of propane oxidation into acetone was not only influenced by the type of metal cations in the zeolite, but also by the Brønsted acidity of the zeolite<sup>11</sup>.

For alkaline-earth exchanged Y zeolites, Ca-Y was observed to have the highest propane and cyclohexane oxidation activity<sup>10;11</sup>. Until now experiments have been performed exclusively with fully exchanged zeolites. However, sites I, I' and II' in cation exchanged Y zeolite are inaccessible to most organic molecules and even for small molecules such as CO (minimum kinetic diameter is 0.37nm) and N<sub>2</sub> (minimum kinetic diameter is 0.36nm), because of the inability to penetrate through a six-membered ring from the supercage into the sodalite cavities<sup>15</sup>. Only cations located on site II and III are expected to be readily accessible for organic molecules adsorbed within a supercage<sup>2;16</sup>.

On the other hand, cations in the sodalite cages have an effect on the total electrostatic field in the zeolite. Furthermore, the number of Brønsted acid sites varies with cation type; while zeolite NaY can be prepared free of acid sites this is difficult for fully exchanged CaY zeolite<sup>11;17</sup>. To better understand the role of cations and Brønsted acid sites on the thermal selective oxidation of propane, we investigated the effect of the amount of Ca<sup>2+</sup> cations on (1) zeolite acidity, (2) propane adsorption, (3) propane selective oxidation and (4) acetone desorption properties for a series of CaNaY zeolites.

## 4.2 Experimental

### 4.2.1 Materials

The parent material used for this study was a NaY zeolite (Akzo Nobel, sample code: 1122-207) with Si/Al ratio of 2.5. The CaNaY zeolites were prepared by aqueous ion-exchange of NaY with calcium nitrate solutions of varying concentration (Table 4-1) under stirring for 6 hours at 90°C. Subsequently, the samples were washed three times with distilled water, filtered and dried at 100°C overnight. The chemical composition of the zeolites was analyzed by X-ray fluorescence (XRF) (Table 4-1). Powder X-ray diffraction gave no indication for collapse of the zeolite structure after activation. <sup>27</sup>Al MAS NMR showed no indication for the formation of extra-framework aluminum after activation at 500°C.

Samples are designated CaNaY(xx), with xx representing the Na<sup>+</sup> exchange level as determined from elemental analysis, e.g. for CaNaY(70), 70% of Na<sup>+</sup> was exchanged by Ca<sup>2+</sup>.

**Table 4-1. Chemical analysis of zeolite samples used in this study (Determined by XRF)**

Zeolite	Base material	Exchanged with	Chemical composition (wt%)				Molar ratio		<sup>(1)</sup> Exchanged (%)
			Al <sub>2</sub> O <sub>3</sub>	SiO <sub>2</sub>	Na <sub>2</sub> O	CaO	Na/Al	Ca/Al	
NaY	NaY	-	21.47	66.03	12.50		0.96		-
CaNaY16	NaY	300ml 0.005M Ca(NO <sub>3</sub> ) <sub>2</sub>	21.58	66.17	10.58	1.67	0.81	0.07	16
CaNaY32	NaY	300ml 0.01M Ca(NO <sub>3</sub> ) <sub>2</sub>	21.65	66.42	8.41	3.51	0.64	0.15	32
CaNaY45	NaY	300ml 0.015M Ca(NO <sub>3</sub> ) <sub>2</sub>	21.61	66.13	6.96	5.31	0.53	0.22	45
CaNaY58	NaY	300ml 0.02M Ca(NO <sub>3</sub> ) <sub>2</sub>	21.67	66.25	5.37	6.71	0.41	0.28	58
CaNaY73	NaY	300ml 0.05M Ca(NO <sub>3</sub> ) <sub>2</sub>	21.78	66.22	3.44	8.56	0.26	0.36	73
CaNaY90	NaY	300ml 0.05M Ca(NO <sub>3</sub> ) <sub>2</sub> repeated 3 times	21.93	65.83	1.30	10.94	0.1	0.45	90

(1) Exchanged (%) was calculated from the Na content related to the Na content of NaY zeolite

#### 4.2.2 Infrared Spectroscopy

The zeolite powder was pressed into a self-supporting wafer and analyzed *in-situ* during adsorption and reaction by means of transmission FTIR spectroscopy using a Bruker Vector22 FTIR spectrometer with a MCT detector. A miniature cell, equipped with CaF<sub>2</sub> transparent windows, which can be evacuated to pressure below 10<sup>-7</sup> mbar, was used for the *in-situ* experiments. The temperature can be varied from room temperature to 500°C. Each spectrum consists of 32 scans taken at 4cm<sup>-1</sup> resolution.

The samples were activated at 500°C (ramp 10°C/min, dwell 2 hrs) in vacuum ( $<10^{-7}$  mbar), and subsequently cooled down to 100°C and 300°C for ammonia adsorption. Gas phase ammonia was introduced into the infrared cell until equilibrium was reached at 1 mbar. Then the system was evacuated and spectra were recorded. The FTIR spectra were corrected for absorption by the background spectrum.

For propane adsorption and selective oxidation study, the samples were activated in vacuum ( $<10^{-7}$  mbar) at 500°C (ramp 10°C/min) for 2 hours, subsequently cooled down to 200°C (dwell 10 hours), and cooled to room temperature. Loading of reactants (propane and oxygen) was controlled *via* the partial pressure. Propane was introduced into the IR cell until equilibrium was reached at 1 mbar in the gas phase, followed by addition of 40 mbar of oxygen. A calibration curve was made by adsorption of known amounts of acetone at room temperature in order to determine the quantity of produced acetone from propane and oxygen. The amount of produced isopropylhydroxide (IHP) was determined by the increase in acetone quantity after thermal conversion of IHP into acetone and water, using an acetone/IHP ratio of 1. The FTIR spectra in propane adsorption and reaction studies were corrected for absorption by the activated zeolite.

### 4.2.3 Ammonia Temperature Programmed Desorption Studies (NH<sub>3</sub>-TPD)

A home-made temperature programmed desorption (TPD) setup connected to a UHV chamber equipped with a mass spectrometer (Balzers QMG 420) was used for dedicated desorption experiments. After activation at  $10^{-3}$  mbar at 500°C for 2 hours, 60mg of a sample was exposed to 10mbar of gas phase ammonia at 100°C (to avoid physisorbed NH<sub>3</sub>). When the adsorption equilibrium was reached, the sample was evacuated for 1.5 hours at  $10^{-3}$  mbar. Then TPD with an increment of 10°C/min up to 700°C was started.

## 4.3 Results

### 4.3.1 Catalyst characterization

Transmission FTIR spectra of the activated CaNaY zeolites with different Ca<sup>2+</sup> content are presented in Figure 4-2. The spectra were calibrated on the amount

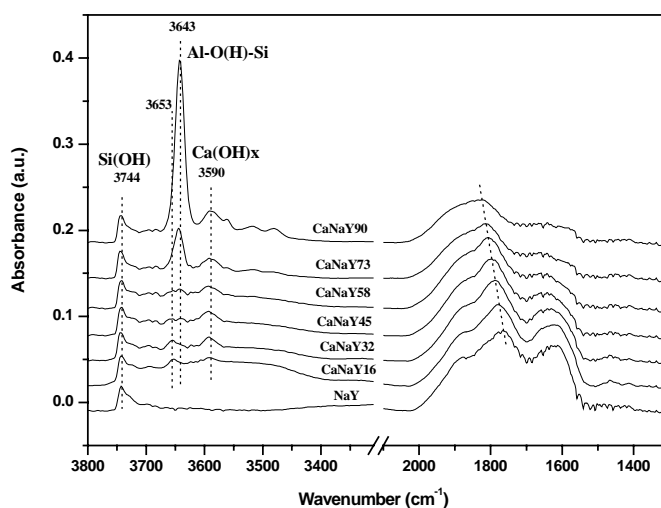


**Figure 4-2.** Infrared spectra of activated CaNaY zeolite.

of sample. All samples exhibited an identical isolated silanol peak at 3744cm<sup>-1</sup>, which can be attributed to the outer surface of zeolite crystals or silica impurities<sup>2;17;18</sup>. The absorption band at 3653~3643cm<sup>-1</sup> indicated the presence of Brönsted acid sites<sup>2;17-19</sup>. The Brönsted acidity hardly changed with rising calcium content, until sample CaNaY73 from which a clear new band at 3643cm<sup>-1</sup> was detected which increased in intensity for CaNaY90. The broad band at 3590cm<sup>-1</sup> can be attributed to the Ca(OH)<sub>x</sub> species<sup>11;18;20</sup>, and its intensity increased with increasing calcium content. Further, the T-O-T overtone vibrations in the 1700-1900cm<sup>-1</sup> region showed a clear shift to higher wavenumber with increasing calcium exchange level, in agreement with literature<sup>11;21</sup>.

NH<sub>3</sub>-TPD was used to differentiate between the number and strength of acid sites in the samples. Figure 4-3a shows the corresponding TPD profiles on the CaNaY zeolites. For the parent NaY a small peak at 200°C was observed, which was previously attributed to aluminum in lattice defect sites<sup>2</sup>. With increasing Ca-content it can be seen from Figure 3a that NH<sub>3</sub> desorbed from at least two types of sites. One type desorbed at low temperature between 150 and 300°C (LT-NH<sub>3</sub>), whereas desorption at higher temperature took place between 250 and 450°C (HT-NH<sub>3</sub>). To evaluate the relative amounts of the LT- and HT-NH<sub>3</sub> peaks deconvolution was carried out (Figure 4-3b). High quality fits were obtained by fitting with only two Gaussian peaks ( $r^2 > 0.998$ ). For both sites, the amount of desorbed ammonia steadily increased until 58% Na<sup>+</sup> was replaced by Ca<sup>2+</sup>, then a large increase for both sites was observed on CaNaY73 and CaNaY90. Furthermore, the temperature of the maximum of the desorption peaks also gradually shifted to higher values with increasing calcium content.

Although NH<sub>3</sub>-TPD clearly showed two desorption sites, these sites cannot automatically be assigned to Brönsted and/or Lewis acid sites, based on TPD only. For this reason, additional infrared experiments on ammonia desorption were carried out. Figure 4-4b shows the infrared spectra of CaNaY90 after adsorption of ammonia at 100°C, followed by evacuation for 5 hours. In comparison with the infrared

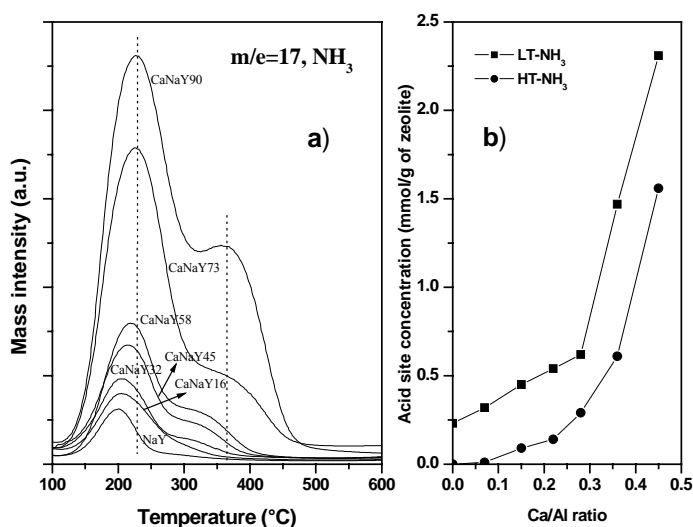


**Figure 4-3.** a) NH<sub>3</sub>-TPD profiles of series CaNaY zeolite; b) adsorbed ammonia concentration of Ca-exchanged Y zeolite as a function of Ca loading.

spectra of the activated sample (Figure 4-4a), the band at  $3644\text{cm}^{-1}$  (Brönsted acid sites) disappeared and concurrently new bands at  $3400$ ,  $3375$ ,  $3347$ ,  $3280$ ,  $1610$  and  $1464\text{cm}^{-1}$  appeared. Adsorption of ammonia at  $300^\circ\text{C}$ , followed by evacuation for 1 hour at  $300^\circ\text{C}$  (Figure 4-4c), resulted in almost complete recovery of the band intensity at  $3644\text{cm}^{-1}$  and bands at  $3375$ ,  $3280$  and  $1610\text{cm}^{-1}$  decreased but remained. In literature, the  $1464\text{cm}^{-1}$  peak is normally assigned to ammonium cations arising from the protonation of ammonia on Brönsted acid sites, while the band at  $1610\text{cm}^{-1}$  is attributed to ammonia bonded to Lewis acid sites<sup>22;23</sup>.

The infrared spectra in figure 4-4 clearly show that ammonia adsorbed on both Brönsted and Lewis acid sites at  $100^\circ\text{C}$ , while only adsorption on Lewis acid sites occurred at  $300^\circ\text{C}$ . Further, from comparison of the infrared spectra in Figure 4-4 follows that the bands at  $3400$  and  $3347\text{cm}^{-1}$  are due to N-H stretch vibrations of  $\text{NH}_4^+$ , since they appear together with the band at  $1464\text{cm}^{-1}$  and they are not present when the O-H stretch vibration of the Brönsted acid sites is observed at  $300^\circ\text{C}$  (Figure 4-4c). The peaks at  $3375$  and  $3280\text{cm}^{-1}$  belong to N-H stretch vibration of  $\text{NH}_3$  adsorbed at Lewis acid site, since they appear together with the band at  $1610\text{cm}^{-1}$ , even at  $300^\circ\text{C}$ . Since no change in intensity at  $3744\text{cm}^{-1}$  and

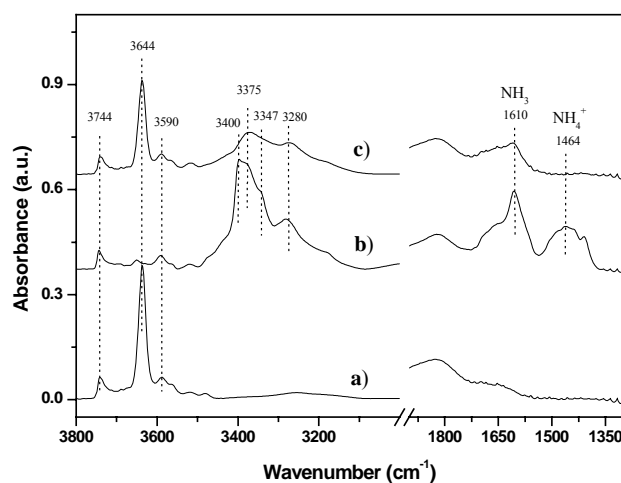


**Figure 4-4.** Infrared spectra of a) activated CaNaY90 zeolite; b) 1 bar ammonia adsorbed on CaNaY90 zeolite at  $100^\circ\text{C}$  followed evacuation 5 hours; c) 1 bar ammonia adsorbed on CaNaY90 zeolite at  $300^\circ\text{C}$  followed evacuation 1 hour.

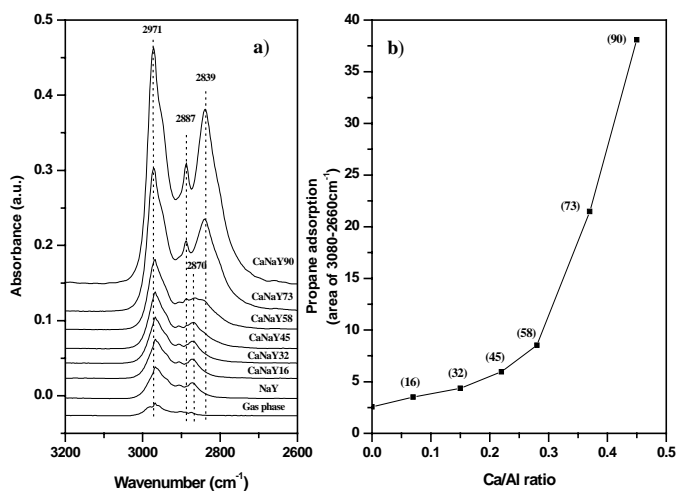


**Figure 4-5.** a) Infrared spectra of 1 bar propane adsorption on series of CaNaY zeolite; and b) propane adsorption quantity as function of the degree of  $\text{Ca}^{2+}$  content

$3590\text{cm}^{-1}$  was found after adsorbed ammonia, it can be concluded that ammonia did not adsorb on Si-OH or  $\text{Ca}(\text{OH})_x$  species.

### 4.3.2 Propane adsorption on CaNaY

Figure 4-5a presents the FTIR spectra of adsorbed propane at 1mbar pressure of propane on CaNaY at room temperature. The band at  $2971\text{cm}^{-1}$  steadily increased with higher calcium content. Interestingly, from CaNaY58 new bands at  $2839\text{cm}^{-1}$  and  $2887\text{cm}^{-1}$  appeared, which intensities increased with increasing calcium exchange. Figure 4-5b displays the propane uptake (interpreted as integrated area between  $3080\text{cm}^{-1}$  and  $2660\text{cm}^{-1}$ ) as function of the degree of  $\text{Ca}^{2+}$  content. A small increase in the propane adsorption was found below 58% of  $\text{Na}^+$  exchange, while a considerable increase in the amount of adsorbed propane was observed for higher calcium contents.

### 4.3.3 Propane oxidation on CaNaY zeolites.

After loading 1 mbar propane and 40 mbar oxygen on activated CaNaY73 zeolite, infrared spectra showed reactant depletion and product formation as a function of time (Figure 4-6a). The developing absorptions can be completely attributed to acetone ( $1682, 1421, 1379, 1367\text{cm}^{-1}$ ), and water ( $1634\text{cm}^{-1}$ )<sup>5;11</sup>.

The initial acetone formation rate (calculated from data of first 2 hours reaction) as a function of the degree of  $\text{Ca}^{2+}$  content is displayed in Figure 4-6b. As expected, the reaction rate increased when increasing the zeolite  $\text{Ca}^{2+}$  content. However, a dramatic increase in the reaction rate was observed from CaNaY58 up to CaNaY90.

Figure 4-7a shows the acetone formation rate as a function of time, based on the integrated area

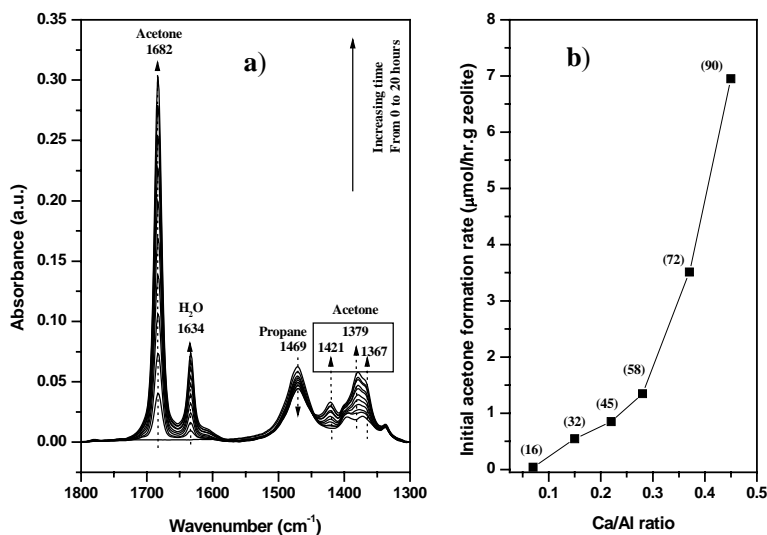


**Figure 4-6.** a) Infrared spectra of CaNaY73 zeolite after loading 1mbar propane and 40mbar oxygen at room temperature as function of time; b) Initial acetone formation rate of propane oxidation as function of degree of  $\text{Ca}^{2+}$  content (initial rate was calculated from data of first 2 hours of reaction)

of the acetone  $\nu_{C=O}$  infrared absorption peak. While for CaNaY73 and CaNaY90 the rate is observed to decrease in time, the samples with lower calcium content clearly show a maximum in activity. Figure 4-7b displays the fluctuation of the acetone to water ratio as a function of time. It was found that the ratio of acetone to water decreased with increasing  $Ca^{2+}$  content until 73% of  $Na^+$  was replaced. For CaNaY16 no significant water signal was observed in the infrared spectrum after 20 hours reaction.

After 20 hours reaction and removal of adsorbed propane via evacuation, bands at  $2998\text{cm}^{-1}$  and  $2925\text{cm}^{-1}$  were detected that previously were masked by propane (Figure 4-8), which were attributed to isopropylhydroperoxide (IHP) and acetone respectively <sup>7,11</sup>. Decomposition of IHP at  $200^\circ\text{C}$  has been reported to form acetone and water exclusively <sup>14</sup>. Therefore, all evacuated samples were further heated at  $200^\circ\text{C}$  and followed with FTIR (not shown). It was found that about 7% for CaNaY90, 9% for CaNaY73, 14% for CaNaY58 and 11% for CaNaY45 of additional acetone was produced from the converted IHP compared to the acetone amount at the beginning of these experiments. No acetone was formed on CaNaY32 and CaNaY16 when heating the samples, which

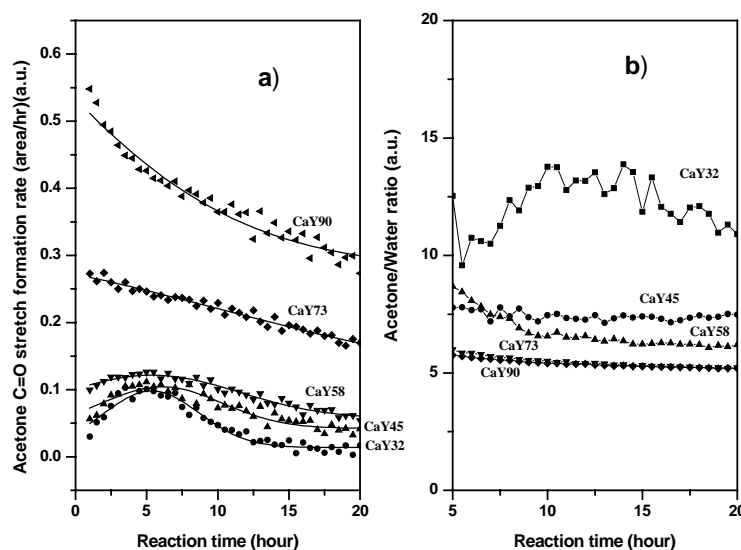


**Figure 4-7.** a) Acetone C=O stretch formation rate as function of time for propane oxidation on CaNaY zeolite; b) Acetone/water ratio as function of time for propane oxidation on series CaNaY zeolites.

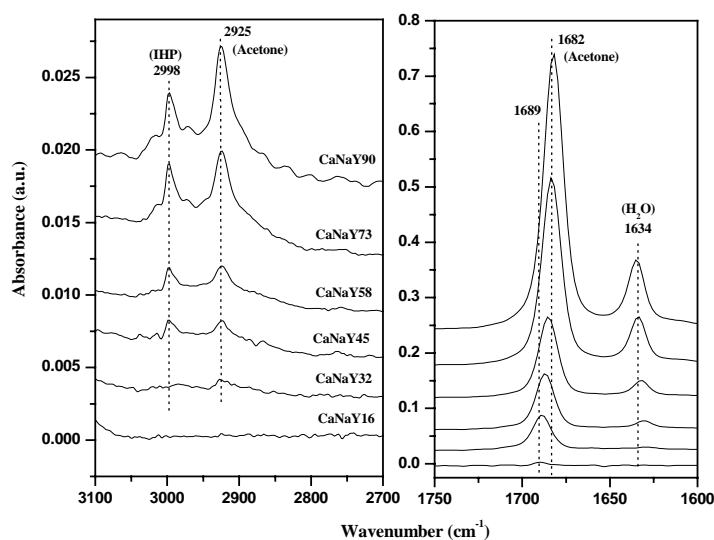


**Figure 4-8.** Infrared spectra after 20 hours reaction, followed 5 minutes evacuation.

agrees with the fact that no IHP was detected after propane oxidation (Figure 4-8). Further, a clear shift in the acetone C=O stretch frequency was observed from 1689cm<sup>-1</sup> for CaNaY16 to 1682cm<sup>-1</sup> for CaNaY90. In addition, the water-bending mode shows a small shift to higher wavenumber with increasing calcium content. Both observations have been explained by a difference in adsorption sites: water adsorbs close to the Ca<sup>2+</sup> cations, while acetone is associated with the Brønsted sites in the samples<sup>11;14</sup>, which will be discussed in the following section.

It has been discussed in our previous paper<sup>11;14</sup> that propane partial oxidation to acetone on alkaline-earth exchanged Y zeolite proceeds via isopropylhydroperoxide(IHP) as a reaction intermediate, which results in the overall reaction:



The present and previous results showed that the molar ratio of [IHP]/[acetone] was in the range of 0.07 and 0.14 after 20 hours reaction for all CaNaY zeolites studied.<sup>14</sup> Consequently, it can be concluded that the IHP decomposition into acetone is considerably faster than the IHP formation on CaNaY zeolite. Therefore, the rate of acetone formation can reasonably be assumed to reflect the propane conversion rate in this work.

#### 4.3.4 Acetone desorption from CaNaY zeolites

After 20 hours reaction and subsequent 1 hour evacuation, no desorbed products were detected by on-line mass spectrometry. For this reason, temperature-programmed-desorption (TPD) was applied to attempt to remove the remaining adsorbed molecules (rate 10°C/minute, up to 500°C, dwell half hour). At the end of the TPD experiment, the samples were cooled to room temperature and infrared data were taken. Figure 4-9 displays the acetone desorption quantity for the series of CaNaY zeolites based on the acetone C=O band intensity at 1689~1682cm<sup>-1</sup> before and after the TPD<sup>14</sup>. It can be clearly seen that the relative amount of desorbed acetone increased with decreasing Ca<sup>2+</sup> content. No new bands were observed in the infrared spectra during

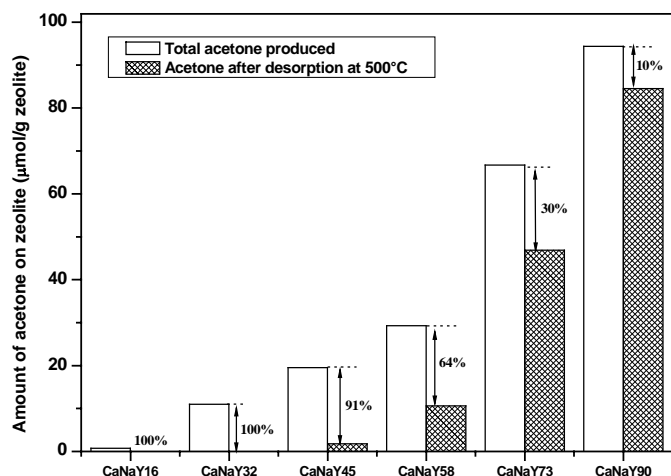


**Figure 4-9.** Desorption of acetone after TPD experiment.



desorption, thus excluding the conversion of acetone into other products. During TPD also mass spectra were taken to detect gas phase compounds. Acetone and water were detected exclusively and no other oxidation or dimerization products could be detected.

#### 4.4 Discussion

Several characteristics of the CaNaY zeolite samples changed in parallel with increasing the  $\text{Ca}^{2+}$ -exchange level: (1) FTIR intensity of Brönsted acid sites and  $\text{Ca}(\text{OH})_x$  species increased (Figure 4-2), (2) amount of desorbed ammonia (Figure 4-3) from Brönsted and Lewis acid sites increased, (3) the adsorbed propane quantity increased (Figure 4-5), (4) the initial acetone formation rate increased (Figure 4-6) and (5) the amount of desorbed acetone after TPD decreased (Figure 4-9).

Furthermore, all these properties show a sudden change from CaNaY58 to higher  $\text{Ca}^{2+}$  amounts, which can be explained by the location of  $\text{Ca}^{2+}$  in the supercage of the Y-zeolite framework as will be explained below. In a typical fully dehydrated NaY zeolite, the distribution of  $\text{Na}^+$  ions in each unit cell is 30 ions located in site I, 20 ions located in site I' and 8 ions located in site II (see Figure 1) <sup>24</sup>. After a full exchange with  $\text{Ca}^{2+}$ , single crystal X-ray analysis showed that the  $\text{Ca}^{2+}$  ions in a completely dehydrated Y-zeolite are distributed according to 14 ions in site I, 4 in site I' and 11 ions in site II per unit cell <sup>25</sup>. This would suggest that roughly 40% of the  $\text{Ca}^{2+}$  ions are located in the supercages, in case of complete exchange.

A marked change in the adsorption of CO and  $\text{CO}_2$  on CaNaY zeolite has been reported when the degree of calcium exchange exceeds about 50% and 46% respectively <sup>19;27</sup>. This agrees well with the observations in this study (Figure 4-3 and Figure 4-5). The results with CO and  $\text{CO}_2$  have been explained based on the location of  $\text{Ca}^{2+}$  in the supercage, since the CO and  $\text{CO}_2$  molecules can not pass the six membered ring to reach the sodalite cages, like propane in this study. The slight inconsistency between the single crystal X-ray study, suggesting about 40% of the  $\text{Ca}^{2+}$  ions in the supercage, with the interpretation of the adsorption studies, suggesting 50% of the  $\text{Ca}^{2+}$  ions in the supercage, might be due to differences in the activation temperature <sup>26</sup> or to changes in the  $\text{Ca}^{2+}$  siting induced by the adsorption of molecules like CO,  $\text{CO}_2$  and propane.

At lower exchange levels the  $\text{Ca}^{2+}$  cations occupy preferably the energetically most favorable sites, i.e. site I in the hexagonal prisms <sup>27</sup>. In this site the cations are fully surrounded by lattice oxygen, causing maximal screening of the positive charge. When the exchange level is increased, the additional cations are located in sites I' and II, somewhat displaced from the centers of the two types of six-numbered rings in the sodalite unit. These cations are shielded by lattice oxygen at one side only, while at the other side the cation is exposed to the center of sodalite cage or supercage respectively <sup>25</sup>. These

partially shielded charge centers generate an electrostatic field extending into the zeolite cages. The shielding is especially limited for cations facing a supercage. Therefore, site I positions are occupied first by Ca<sup>2+</sup> ions; however, Jacobs et al. concluded that a small fraction of the Ca<sup>2+</sup> ions start to occupy supercage positions before the hexagonal prisms are completely occupied<sup>19</sup>.

### 4.4.1 Brönsted and Lewis acidity

It is generally accepted that in divalent-cation exchanged Y-zeolites, the strong electrostatic field of M<sup>2+</sup> cations on water molecules can result in a dissociation of these molecules according to<sup>17;20</sup>:  $\text{Ca}^{2+} + \text{H}_2\text{O}(\text{ad}) \rightarrow \text{Ca}(\text{OH})^+ + \text{H}^+$ . The protons are fixed to lattice oxygen atoms and account for the hydroxyl vibration at 3653 - 3643cm<sup>-1</sup>. The hydroxyl vibration at 3590cm<sup>-1</sup> results from the Ca(OH)<sub>x</sub> species (Figure 4-2). The higher electrostatic field of supercage Ca<sup>2+</sup> ions results in a sharp increase in Brönsted acidity as observed in the FTIR spectra (Figure 4-2).

Combination of the infrared results in Figure 4-4 with the TPD results in Figure 4-3 leads to the conclusion that the HT-NH<sub>3</sub> peak can be attributed to ammonia desorbing from Lewis acid sites. The LT-NH<sub>3</sub> peak should be assigned to both Brönsted acid sites and Lewis acid sites, since NH<sub>3</sub> adsorption at 100°C results in IR signals (Figure 4-4) attributed to ammonia on both types of sites. Most likely, for all samples also a small amount could be adsorbed on aluminum defect sites as was observed for the parent NaY, however this peak could obviously not be separated from the LT-NH<sub>3</sub> peak in Figure 4-3.

Three different sources for Lewis acid sites in CaNaY zeolites might contribute: (1) structural defects in the framework, (2) extra-framework aluminum, (3) bare Ca<sup>2+</sup> ions. <sup>27</sup>Al MAS NMR, however, showed no extra-framework aluminum. Moreover, for USY zeolites it was shown that NH<sub>3</sub> desorbed at lower temperatures from aluminum Lewis acid sites than from Brönsted acid site, i.e. below 200°C<sup>22</sup>. Consequently, the high temperature desorption peak arises from bare Ca<sup>2+</sup> cations. For Ca<sup>2+</sup> and Sr<sup>2+</sup> exchanged X-zeolites it was observed by X-ray diffraction that ammonia adsorbed exclusively on Ca<sup>2+</sup> and Sr<sup>2+</sup> located in the sodalite and supercage<sup>30;31</sup>. In fully exchanged CaY zeolite, only a very small fraction of Ca<sup>2+</sup> (4 of in total 29 cations) is located in the sodalite cage (site I')<sup>26</sup>. For this reason we conclude that the HT-NH<sub>3</sub> peak mainly is originating from supercage Ca<sup>2+</sup> ions.

The bare metal cations in Y zeolite play an essential role in selective oxidation of alkanes<sup>11;14</sup>. It is not yet clear how many Ca<sup>2+</sup> ions in the supercage position are converted to Ca(OH)<sub>x</sub> species. This is currently under investigation.

### 4.4.2 Propane adsorption

Figure 4-10a shows the amount of adsorbed propane normalized to the total number of  $\text{Ca}^{2+}$  ions in the zeolites. It clearly demonstrates that propane adsorption per  $\text{Ca}^{2+}$  decreased with increasing  $\text{Ca}^{2+}$

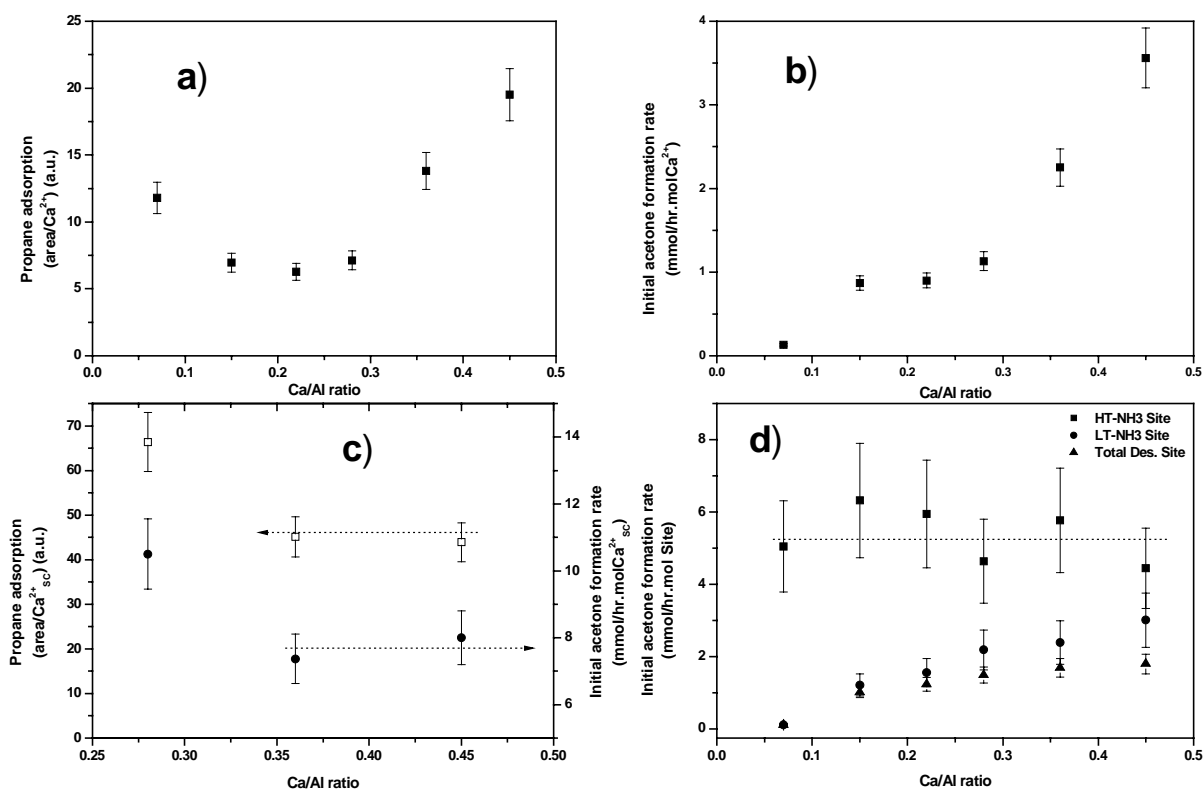


**Figure 4-10.** a) Propane adsorption (FTIR band area between  $3100\text{cm}^{-1}$  and  $2700\text{cm}^{-1}$ ) per  $\text{Ca}^{2+}$  as function of  $\text{Ca}^{2+}$  content; and b) Initial rate of formation of acetone per  $\text{Ca}^{2+}$  during propane oxidation as function of  $\text{Ca}^{2+}$  content; c) Propane adsorption and initial acetone formation rate per  $\text{Ca}^{2+}$  in the supercage (SC) as function of  $\text{Ca}^{2+}$  content; and d) Initial acetone formation rate per ammonia desorption site as function of  $\text{Ca}^{2+}$  content.

content until 50% of  $\text{Na}^+$  was replaced by  $\text{Ca}^{2+}$ , subsequently the propane adsorption per  $\text{Ca}^{2+}$  increased rapidly. The largest contribution to the total integrated area of propane  $\nu_{\text{C-H}}$  vibrations originates from the peak at  $2839\text{cm}^{-1}$ , which was only visible from CaNaY58 to CaNaY90 (Figure 4-5a). Hydrocarbon adsorption in zeolites has been reported to be due to enhanced interaction with framework oxygen, however the bonding of alkanes in zeolites is known to be influenced as well by polarization of saturated hydrocarbons at cations. Normally, the latter contribution is smaller than the enhanced interaction from the close fit of the adsorbate molecules within zeolite cages or channels<sup>3;28;29</sup>. The C-H vibration at  $2839\text{cm}^{-1}$  on CaNaY58 -73 and -90 (Figure 4-5a) indicates a significant interaction between propane and the zeolite. Further, it is also well established that molecules such as propane (minimum

kinetic diameter 0.43nm) are too big to penetrate the six membered rings (about 0.25nm in diameter) to enter the sodalite cages and the hexagonal prisms<sup>2</sup>; propane thus adsorbs in the supercages exclusively. The sudden and linear increase in the amount of adsorbed propane per Ca<sup>2+</sup> from CaNaY58 up to CaNaY90 strongly suggests this is due to Ca<sup>2+</sup> cations in the supercages, which induce both a cation-dipole interaction and an increasing basicity of nearby lattice oxygen ions, since supercage Ca<sup>2+</sup> cations cannot shield lattice charges equally well as monovalent Na<sup>+</sup> ions.

### 4.4.3 Propane oxidation

For CaNaY32, CaNaY45 and CaNaY58, activation was observed in the first hours of reaction, accompanied by a high acetone to water ratio compared to CaNaY73 and CaNaY90 (Figure 4-7). In a previous paper, we explained these phenomena by the hydrolysis of produced water on zeolites with low initial Brönsted acidity<sup>11</sup>. Hydrolysis leads to higher acidity, which favors decomposition of isopropylhydroperoxide (IHP) into acetone, resulting in a higher acetone to water ratio. Further, the presence of water in the zeolite will inevitably reduce the electrostatic field resulting in deactivation as observed for all samples. The fact that no activation curve was observed for CaNaY73 and CaNaY90 suggests that the rate of deactivation is higher than the rate of activation, which is probably due to the larger amounts of water formed in the initial stage. Moreover, these samples already have significant Brönsted acidity, which limits the possibility for additional hydrolysis of produced water. Therefore the acetone to water ratio is smaller.

Figure 4-10b shows the normalized initial acetone formation rate per Ca<sup>2+</sup> cation in the zeolites. Clearly, a sudden linear increase is observed with calcium levels above 50% exchange, similar to the amount of adsorbed propane (Figure 4-10a). Assuming that from 50% exchange level up, the cations fill up sites in the supercages, the adsorbed propane quantity and initial oxidation rate per supercage-Ca<sup>2+</sup> was calculated for CaNaY58, CaNaY73 and CaNaY90 (Figure 4-10c). A constant propane quantity and oxidation rate per supercage-Ca<sup>2+</sup> ion was found within experimental error for CaNaY73 and CaNaY90. For CaNaY58 the calculated numbers are slightly higher (1.15 times) compared to CaNaY73 and CaNaY90. Since the CaNaY58 sample is just above the 50% exchange level only a minority of Ca<sup>2+</sup>-cations would be in the supercage based on the assumption. The result here indicates that approximately 15% more Ca<sup>2+</sup> ions are located in the supercage. This is also in agreement with the observation that both CaNaY32 and CaNaY45 show some propane oxidation activity. Since propane cannot enter the sodalite cages or hexagonal prisms, this activity is likely to be due to a few cations located in the supercages. Our observations agreement with the conclusion of Jacobs et al.<sup>19</sup> that, although

preferential filling of site I positions by  $\text{Ca}^{2+}$  takes place, some  $\text{Ca}^{2+}$  ions occupy supercage position before the hexagonal prisms are completely occupied.

To test our assumption, the initial acetone formation rate per Lewis acid site, as obtained from the  $\text{NH}_3$ -TPD experiments, was calculated (Figure 4-10d). For comparison also the normalized activity per Brönsted acid site and total number of acid sites is given in Figure 4-10d. Clearly, only for the Lewis acid sites a similar activity per site was found for all CaNaY zeolites. Since the Lewis sites were identified as bare  $\text{Ca}^{2+}$  supercage cations (see above), this confirms that only  $\text{Ca}^{2+}$  cations in the supercage contribute almost exclusively to propane oxidation activity at room temperature.

#### 4.4.4 Acetone desorption

Finally, Figure 4-9 shows that the relative amount of desorbed acetone decreases with higher  $\text{Ca}^{2+}$  exchange level, even though the acetone coverage was higher. Furthermore, the shifts to lower wavenumber in the infrared spectra for both the Brönsted OH frequency as well as the C=O stretch frequency of acetone with increasing calcium content are similar (Figure 4-2 and 4-8), which suggests that acetone is adsorbed on the Brönsted acid sites. The present results are in agreement with previous observations on different alkali-earth exchanged Y zeolites, that the relative amount of desorbed acetone decreased with increasing Brönsted acidity<sup>14</sup>. Obviously, acetone is well stabilized in zeolites with high contents of  $\text{Ca}^{2+}$  and Brönsted acid sites. At present, it is not yet clear whether Brönsted acid sites also affect the IHP formation or whether  $\text{Ca}^{2+}$  cations influence the acetone adsorption state; this is currently under investigation.

#### 4.5 Conclusion

Increasing the  $\text{Ca}^{2+}$  exchange level in CaNaY zeolites results in altered properties for the zeolites: the amount of Brönsted and Lewis acid sites increased, the adsorbed propane quantity increased, the initial acetone formation rate increased and the amount of desorbed acetone decreased. Moreover, all these properties showed a sudden change above 50%  $\text{Na}^+$  exchange levels with  $\text{Ca}^{2+}$ , which can be fully attributed to the location of  $\text{Ca}^{2+}$  in the Y-zeolite framework. Clearly, only  $\text{Ca}^{2+}$  ions located in the supercage contribute to the formation of Brönsted and Lewis acidity as well as propane oxidation activity at room temperature.

#### Reference List

1. Barthomeuf, D. *Catal.Rev.Sci-Eng.* **1996**, 38, 521-613.
2. Donald W.Breck, *Zeolite molecular sieves: structure, chemistry, and use*, Wiley: New York, 1974.

3. H.van Bekkum, *Introduction to zeolite science and practice*, Elsevier: Amsterdam, 2001.
4. Subhash Bhatia, *Zeolite catalysis : principles and applications*, CRC Press: Boca Raton, FA, 1990.
5. Sun, H.; Blatter, F.; Frei, H. *Catalysis Letters* **1997**, *44*, 247-253.
6. Sun, H.; Blatter, F.; Frei, H. *Journal of the American Chemical Society* **1996**, *118*, 6873-6879.
7. Blatter, F.; Sun, H.; Frei, H. *Chemistry-A European Journal* **1996**, *2*, 385-389.
8. Sun, H.; Blatter, F.; Frei, H. *Abstracts of Papers of the American Chemical Society* **1996**, *211*, 3-ORGN.
9. Larsen, R. G.; Saladino, A. C.; Hunt, T. A.; Mann, J. E.; Xu, M.; Grassian, V. H.; Larsen, S. C. *Journal of Catalysis* **2001**, *204*, 440-449.
10. Vanoppen, D. L.; DeVos, D. E.; Jacobs, P. A. *Progress in Zeolite and Microporous Materials, Pts A-C* **1997**, *105*, 1045-1051.
11. Xu, J.; mojet, B. L.; Ommen, J. G. v.; Lefferts, L. *Phys.Chem.Chem.Phys.* **2003**, *5*, 4407-4413.
12. Blatter, F.; Sun, H.; Vasenkov, S.; Frei, H. *Catalysis Today* **1998**, *41*, 297-309.
13. Frei, H. *3Rd World Congress on Oxidation Catalysis* **1997**, *110*, 1041-1050.
14. Xu, J.; mojet, B. L.; Ommen, J. G. v.; Lefferts, L. *Journal of Physical Chemistry B* **2004**, *108*, 218-223.
15. Bordiga, S.; Scarano, D.; Spoto, G.; Zecchina, A.; Lamberti, C.; Otero Arean, C. *Vib.Spectrosc.* **1993**, *5*, 69.
16. Ramamurthy, V.; Lakshminarasimhan, P.; Grey, C. P.; Johnston, L. J. *Chem.Commun.* **1998**, 2411-2424.
17. Ward, J. W. *Journal of Physical Chemistry* **1968**, *72*, 4211-4223.
18. Ward, J. W. *Journal of Catalysis* **1968**, *10*, 34-46.
19. Jacobs, P. A.; Cauwelaert, F. H.; Uytterhoeven, J. B. *J.C.S.Faraday I* **1972**, *68*, 1056-1068.
20. Uytterhoeven, J. B.; Schoonheydt, R. *Journal of Catalysis* **1969**, *13*, 425-434.
21. Sponer, J. E.; Sobalik, Z. *Journal of Physical Chemistry B* **2001**, *105*, 8285-8290.
22. H.Miessner; H.Kosslick; U.Lohse; B.Parlitz; Vu-Anh Tuan. *Journal of Physical Chemistry* **1993**, *97*, 9741-9748.
23. Nakamoto, K. *Infrared spectra of Inorganic and Coordination compounds*, Wiley-Interscience: New York: 1986.
24. Eulenberger, G. R.; Shoemaker, D. P.; Keil, J. G. *Journal of Physical Chemistry* **1967**, *71*, 1812-1819.
25. Bennett, J. M.; Smith, J. V. *Zeolites* **1968**, *3*, 633-642.
26. Costenoble, M. L.; Mortier, W. J.; Uytterhoven, J. B. *J.C.S.Faraday I* **1977**, *73*, 466-476.
27. Egerton, T. A.; Stone, F. S. *Trans. Faraday Soc.* **1970**, *66*, 2364-2377.
28. Janchen, J.; Mortier, W. J. *Journal of Physical Chemistry* **1996**, *100*, 12489-12493.
29. Smit, B. *Journal of Physical Chemistry* **1995**, *99*, 5597-5603.
30. Se Bok Jang; Mi Suk Jeong; Yang Kim; Seong Hwan Song; Karl Seff. *Microporous and Mesoporous Materials* **1999**, *28*, 173-183.
31. Se Bok Jang; Mi Suk Jeong; Yang Kim; Seong Hwan Song; Karl Seff. *Microporous and Mesoporous Materials* **1999**, *30*, 233-241.

## Chapter 5

### **The Effects of Brönsted Acidity in the Mechanism of Selective Oxidation of Propane to Acetone on CaY Zeolite at Room Temperature**

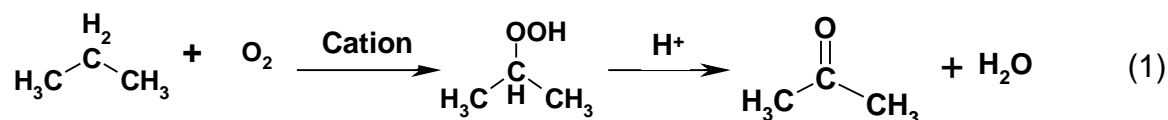
---

***Abstract:** The importance of Brönsted acid sites for propane partial oxidation to acetone in CaY was investigated using in-situ FTIR spectroscopy. With increasing concentration of Brönsted acid sites on calcium exchanged Y zeolite, Volcano type of plots were observed for: (1) amount of adsorbed propane; (2) initial acetone formation rate; (3) total amount of acetone produced after 20 hours of reaction; (4) acetone selectivity. The results clearly show that Brönsted acidity increases the isopropylhydroperoxide (IHP) formation rate, most likely via a catalytic  $H^+$ -abstraction as well as the IHP decomposition into acetone and water. Moreover, with increasing IHP concentration 2-propanol was found in addition to acetone. The decomposition of produced isopropylhydroperoxide (IHP) was found to be second order in IHP on CaY and HCaY zeolites. Since the number of Brönsted acid sites also affects the number of  $Ca^{2+}$  cations in the zeolites on optimum in  $H^+/Ca^{2+}$  ratio was observed for both activity and selectivity.*

## 5.1 Introduction

The direct selective oxidation of light alkanes into valuable products is one of most challenging subjects of catalytic chemistry, since the global abundance of low alkanes and the huge economic incentives<sup>1</sup>. The main disadvantage of partial oxidation is that light alkanes are usually less reactive than the desired products, and further oxidation to CO<sub>x</sub> is thermodynamically favored. Recent efforts towards improvement of the selectivity of light alkane oxidation are mainly based on catalysis over metals, metal oxides<sup>2-4</sup> or zeolite supported metal oxides<sup>5;6</sup>. Although selectivity is much improved, all these methods still generate substantial amounts of carbon oxides or other carbon fragmentation products, some even at low hydrocarbon conversion.

The inefficiency associated with low conversion has motivated the search for solid catalysts that are active and selective for the oxidation of light alkanes. Recently, a new approach of selective oxidation of alkanes (ethane, propane, isobutane and cyclohexane)<sup>7-11</sup> on cation exchanged Y zeolite was presented under photo or thermal conditions. The concept is that the hydrocarbon and oxygen are confined in a restricted environment (Zeolite cages), followed by the formation of charge transfer complex, [(C<sub>n</sub>H<sub>2n+2</sub>)<sup>+</sup>O<sub>2</sub><sup>-</sup>]. The complex could stabilize in the presence of a strong electrostatic field due to cation ions. The alkyl hydroperoxide was observed as reaction intermediate. Complete selectivity was reported at conversions as high as 22%, by in situ FTIR measurements of propane oxidation to acetone for BaY zeolite. However, the catalytic reaction cycle was not yet closed, since no product desorption could be observed at such condition. Based on the cation dependent, the reaction activity was reported to increase in order NaY < BaY < SrY < CaY with increasing the electrostatic field of the cation for the gas phase reactions of cyclohexane to cyclohexanone<sup>7;12</sup> and propane to acetone<sup>11</sup>. In contrast, Larsen et. al indicated that proton abstraction from the hydrocarbon radical cation to O<sub>2</sub><sup>-</sup> is the rate determining step for the conversion of cyclohexane to cyclohexanone on BaY and NaY zeolites, because of the observation of a pronounced deuterium kinetic isotope effect<sup>8</sup>. Further, recent results in our group showed that the rate of propane oxidation to acetone is, moreover, influenced by the type of earth-alkali cations, the Brønsted acidity of the zeolite and the position of cation in the zeolite<sup>11;13;14</sup>. Cations in the supercage of zeolite Y are exclusively responsible for the propane oxidation reaction. A two-step mechanism with two different active sites was proposed: conversion of propane into isopropylhydroperoxide (IHP) takes place on earth-alkali cations, while the decomposition into acetone and water occurs by Brønsted acid sites, as follows:





However, a systematic variation of concentration of Brönsted acid sites while keeping the earth-alkali cations the same is needed to prove a relationship between Brönsted acidity and IHP conversion. Moreover, it is not yet clear whether the cation and Brönsted acid sites act independently in this reaction or that a cooperation of both sites is needed. Further, increasing Brönsted acidity by introducing  $\text{NH}_4^+$ , followed decomposition in cation exchanged Y zeolite will lead to decrease the electrostatic field of cations, because the total amount of positive charge (Brönsted acid or cation) that compensate to the negative zeolite framework should be the same. In other words, the cation and Brönsted acid sites can't be varied independently.

A loss of product selectivity has been reported by increasing the Brönsted acidity as a result of photooxidation of 1-alkenes, toluene and *p*-xylene in cation exchanged zeolites, leading to polymerization and condensation reactions<sup>15,16</sup>. Further, in liquid phase oxidation of cyclohexane on alkali or alkaline-earth exchanged Y zeolite, it has been shown that the Brönsted acidity plays rather as inhibitor than as catalyst<sup>17</sup>. In liquid phase, the typical radical reaction path *via* homolytic peroxide decomposition has been proposed. Although the restricted environment (zeolite cage) limited the diffusion of free radical to follow the chain propagation at low temperature gas phase reaction, nevertheless, a contribution of free radical chemistry can't be excluded.

In order to answer the above-mentioned questions, we investigated the details of propane selective oxidation reaction on a series of CaY zeolite with varying proton concentration by using infrared spectrometry. The target is to gain insight into the reaction mechanism and the reaction path exerted by cation and acid property of catalyst.

## 5.2 Experimental

### 5.2.1 Materials

The base material used for this study was a NaY (Akzo Nobel, sample code: 1122-207) with Si/Al ratio of 2.5. The CaY zeolite was prepared by three times repeated aqueous exchange of the base NaY zeolite with 0.05M calcium nitrate solutions followed by washing three times with distilled water, filtered and dried at 100°C overnight.

The series of HCaY zeolites were prepared by exchange of CaY zeolite with  $\text{NH}_4\text{NO}_3$  solutions. The  $\text{NH}_4^+$  loading of the zeolite was controlled by the concentration of  $\text{NH}_4^+$  in the aqueous solution. All zeolites followed the same procedure of washing and drying as described above. The final HCaY zeolites were obtained by decomposition at 500°C under vacuum. After decomposition, the source of Brönsted acid sites can be contributed from both decomposition of  $\text{NH}_4^+$  ions and hydrolysis of water at  $\text{Ca}^{2+}$  sites. The chemical composition of catalysts (determined by X-ray fluorescence (XRF)),  $\text{Ca}^{2+}/\text{Al}$

and  $\text{NH}_4^+/\text{Al}$  ratio, as well as sample names is listed in Table 5-1. It showed that  $\text{Ca}^{2+}$  was gradually replaced by  $\text{NH}_4^+$ ; whereas the sodium content, which remains in CaY zeolite, only slightly decreased, and almost kept constant for the series of HCaY zeolites.

**Table 4-1 Chemical analysis of zeolite samples used in this study (Determined by XRF)**

Zeolite	<u>Chemical composition (wt%)</u>				Molar ratio		
	$\text{Al}_2\text{O}_3$	$\text{SiO}_2$	$\text{Na}_2\text{O}$	$\text{CaO}$	$\text{Na}^+/\text{Al}$	$\text{Ca}^{2+}/\text{Al}$	$\text{NH}_4^+/\text{Al}^{(1)}$
CaY	21.93	65.83	1.30	10.94	0.10	0.45	-
H(4)CaY	21.93	65.45	1.09	10.54	0.08	0.44	0.04
H(7)CaY	22.00	66.50	1.26	10.25	0.09	0.42	0.07
H(13)CaY	22.19	67.09	1.21	9.51	0.09	0.39	0.13
H(26)CaY	22.58	68.12	1.03	8.27	0.08	0.33	0.26
Ca-NaY73	21.78	66.22	3.44	8.56	0.26	0.36	-
Na-CaY71	21.77	65.97	3.67	8.59	0.28	0.36	-

(1)  $\text{NH}_4^+$  content was calculated based on the charge balance; Iron content <0.02wt%;

Nevertheless, the  $\text{NH}_4^+$  and  $\text{Ca}^{2+}$  cation cannot be varied independently, because the total amount of positive charge should keep constant. Thus, another two samples were prepared in order to vary the concentration of Brønsted acid sites, while keeping the calcium content constant. A partial sodium back-exchanged CaY zeolite was prepared by ion exchanging CaY with a  $\text{NaNO}_3$  solution, in order to remove the protons formed by the hydrolysis of calcium complex (sample indicated as Na-CaY71). During back-exchanged, it inevitably exchanges part of calcium cation as well. Thus, a partially exchanged CaNaY was prepared with NaY and controlled concentration of calcium nitrate solution (sample indicated as Ca-NaY73), in order to make two catalysts having an identical calcium content with different Brønsted acid sites. After ion exchange, both samples were washed and dried following the procedure described above. The catalyst chemical composition (determined by X-ray fluorescence (XRF)) in Table 5-1 showed the same  $\text{Ca}^{2+}/\text{Al}$  ratio was obtained. However, higher  $\text{Na}^+/\text{Al}$  ratio for Na-CaY71 than for Ca-NaY73 was found. In addition, 27Al MAS NMR showed no extra-framework aluminum for the studied samples, even not after activation at 500°C.

### 5.2.2 Infrared Spectroscopy

The zeolite powder (30mg) was pressed into a self-supported wafer and analyzed *in-situ* during adsorption and reaction by means of transmission FTIR spectroscopy using a Bruker Vector22 FTIR spectrometer with a MCT detector. A miniature cell, equipped with CaF<sub>2</sub> transparent windows, which can be evacuated to pressure below 10<sup>-7</sup> mbar was used for the *in-situ* experiments. The temperature is variable from room temperature to 500°C. Each spectrum consists of 32 scans taken at 4cm<sup>-1</sup> resolutions.

Zeolite samples were activated at 500°C (ramp 10°C/min) for 2 hours in vacuum (<10<sup>-7</sup> mbar), subsequently cooled down to 100°C for ammonia adsorption. Ammonia was introduced into the infrared cell and until equilibrium was reached at 1mbar. Then the system was evacuated and spectra were recorded. The FTIR spectra of activated zeolite structure and ammonia adsorption were corrected for absorption by the background spectrum.

For propane selective oxidation study, samples were activated in vacuum (<10<sup>-7</sup>mbar) at 500°C (ramp 10°C/min) for 2 hours, subsequently cooled down to 200°C (dwell 10 hours), and cooled to room temperature. Loading of reactants (propane and oxygen) was controlled by gas pressure. Propane was introduced into the IR cell until equilibrium was reached at 1 mbar in the gas phase, followed by addition of 40 mbar of oxygen. Calibration curves were made by adsorption of known amounts of acetone and 2-propanol at room temperature in order to determine the quantity of produced acetone from propane and oxygen. The amount of produced isopropylhydroxide (IHP) was determined by the increase in acetone quantity as a result of thermal conversion of IHP into acetone and water. The FTIR spectra in propane adsorption and reaction studies were corrected for absorption by the activated zeolite.

### 5.2.3 Ammonia Temperature Programmed Desorption Studies (NH<sub>3</sub>-TPD).

A home-made temperature programmed desorption (TPD) setup connected to a UHV chamber equipped with a mass spectrometer (Balzers QMG 420) was used for dedicated desorption experiments. After activation at 10<sup>-3</sup> mbar at 500°C for 2 hours, 60mg of a sample was exposed to 10mbar of gas phase ammonia at 100°C (to avoid physisorbed NH<sub>3</sub>). When the adsorption equilibrium was reached, the sample was evacuated for 1.5 hours at 10<sup>-3</sup> mbar. Then TPD with an increment of 10°C/min up to 700°C was started.

## 5.3 Results and discussion

### 5.3.1 Catalyst characterization.

Calibrated transmission FTIR spectra of the activated CaY and series HCaY zeolites samples are given in Figure 5-1a. All samples showed an isolated silanol peak at  $3744\text{cm}^{-1}$ , which is either on the outer surface terminating the zeolite crystals or on silica impurities<sup>18-20</sup>. The intensity of this band is constant for all zeolites.

SiOHAl groups, Brønsted type acid sites, which were produced by hydrolysis of water at a cation or occurred from deammoniation gave rise to two IR absorption bands. The band at  $3644\text{cm}^{-1}$  (high-frequency

(HF) band) was attributed to O-H groups within the large supercage. The low-frequency (LF) band at  $3555\text{cm}^{-1}$  appearing on H(13)CaY and H(26)CaY was assigned to hydroxyl groups hidden within the sodalite cages of the zeolite structure<sup>20</sup>. Further, the O-H vibration at  $3590\text{cm}^{-1}$  originates from  $\text{Ca}(\text{OH})_x$  species<sup>11;14</sup> and steeply decreased and finally disappeared with increasing ammonia exchange level. The T-O-T overtone vibrations between  $1700$  and  $1900\text{cm}^{-1}$  showed a slightly red shift with increasing ammonia exchange level, in agreement with literature<sup>11;21</sup>.

Figure 5-1b shows the infrared spectra of activated Ca-NaY73 and Na-CaY71 samples having the same calcium content. A clear decrease of the band at  $3644\text{cm}^{-1}$  was observed for Na-CaY71 sample compared to both CaY and Ca-NaY73, which indicates that most of the protons were exchanged by sodium ions. Na-CaY71 and Ca-NaY73 showed similar intensities for the O-H vibration from both isolated silanol ( $3744\text{cm}^{-1}$ ) and  $\text{Ca}(\text{OH})_x$  species ( $3590\text{cm}^{-1}$ ).

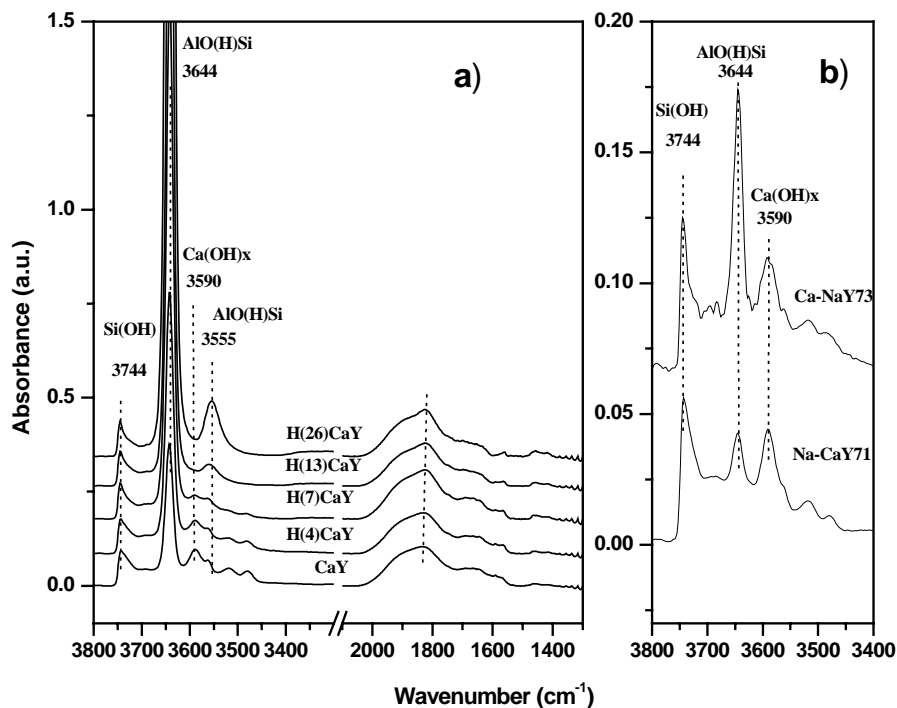


**Figure 5-1.** Infrared spectra of a) activated CaY and series HCaY zeolites; b) activated Ca-NaY73 and Na-CaY71 zeolites

The source of Brønsted acid sites of CaY zeolite is now generally accepted to occur during pretreatment or activation of a divalent cation exchanged zeolite at elevated temperature *via* the reaction:  $\text{Ca}^{2+} + \text{H}_2\text{O}(\text{ad}) + \text{Si-O-Al} \rightarrow \text{Ca}(\text{OH})^+ + \text{Si-O}(\text{H}^+)-\text{Al}$

During the  $\text{Na}^+$  back-exchange process, protons were replaced, based on the FTIR spectra and elemental analysis (Table 1):  $\text{Si-O}(\text{H}^+)-\text{Al} + \text{Na}^+(\text{Solution}) \rightarrow \text{Si-O}(\text{Na}^+)-\text{Al} + \text{H}^+(\text{Solution})$

Recently, we showed that  $\text{NH}_3$ -TPD is a suitable technique to differentiate between the number and type of acid sites in the calcium exchanged Y zeolite samples<sup>14</sup>. Ammonia desorbing at low temperature (between 150 and 300°C, LT- $\text{NH}_3$ ) was identified to desorb mainly from Brønsted acid sites, whereas desorption at higher temperature (between 300 and 450°C, HT- $\text{NH}_3$ ) was attributed to originate from calcium cation sites in the zeolite supercage<sup>14;22</sup>. Comparison of the  $\text{NH}_3$ -TPD profiles of Ca-NaY73 and Na-CaY71 (not-shown) confirmed a low amount of protons on Na-CaY71 while the amount of supercage  $\text{Ca}^{2+}$ -ions was comparable to Ca-NaY73.

Further, ammonia adsorption was studied with FTIR spectroscopy to differentiate between Lewis and Brønsted acid sites. Figure 5-2 shows, as a typical example, the IR spectra for CaY and H(13)CaY after adsorption of 1mbar  $\text{NH}_3$  at 100°C and subsequent evacuation (to remove physisorbed  $\text{NH}_3$ ). Compared to the spectra in Figure 1, the intensity of the hydroxyl stretch vibrations at 3644 $\text{cm}^{-1}$  and 3555 $\text{cm}^{-1}$  clearly decreased. The hydroxyl groups at 3744 $\text{cm}^{-1}$  and 3590 $\text{cm}^{-1}$  were not affected by ammonia adsorption, indicating a very weak acidity of silanol groups and  $\text{Ca}(\text{OH})_x$  species. Well-resolved absorbances appeared in the range of N-H deformation modes below 1700 $\text{cm}^{-1}$ , which could be assigned to ammonia species adsorbed on different acid sites. The band at 1610 $\text{cm}^{-1}$  was assigned to ammonia bound to Lewis sites<sup>14;21-23</sup>. Because no extra-framework aluminum was found by NMR for the studied samples, this species was attributed to ammonia coordinated to calcium cations. The bands at 1674 $\text{cm}^{-1}$  and between 1484 $\text{cm}^{-1}$

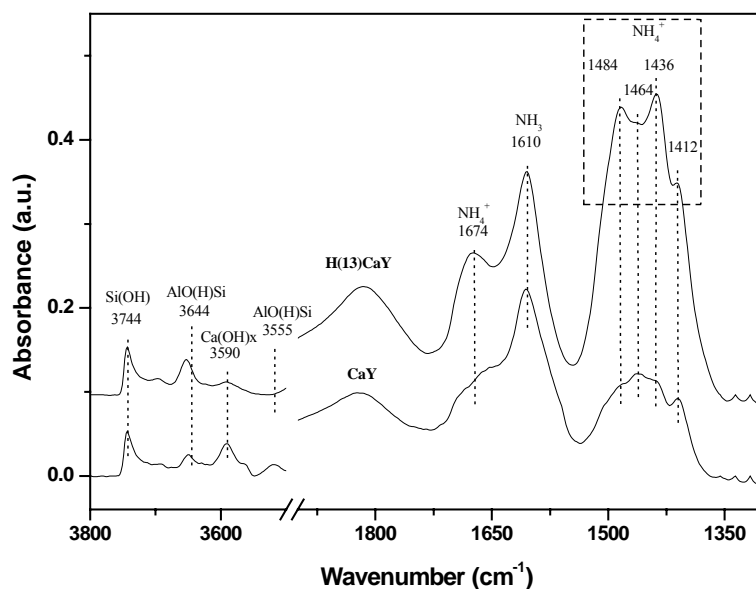


**Figure 5-2.** Infrared spectra of ammonia adsorption on CaY and H(13)CaY zeolite

and  $1412\text{cm}^{-1}$  were assigned to ammonium ions arising from the protonation of ammonia on Brönsted acid sites<sup>14;21-23</sup>. A high amount of Brönsted acid sites was observed on H(13)CaY sample compared to CaY.

In conclusion, of the infrared spectra, ammonia adsorption and  $\text{NH}_3$ -TPD are in good agreement with the results of the zeolite chemical composition analysis (Table 1) and the expected changes in acidity were confirmed.

### 5.3.2 Propane adsorption

Figure 5-3 displays the propane uptake at 1mbar pressure (interpreted as integrated FTIR band area between  $3080\text{cm}^{-1}$  and  $2660\text{cm}^{-1}$ , details of spectra in ref. 10, 13) by the different zeolites at room temperature. With increasing proton content, first (from CaY to H(7)CaY) a slight increase (15%) in propane uptake was found. However, from H(7)CaY to H(26)CaY, the propane amount decreased largely by about 50%. Interestingly, about 30% less propane was found on Na-CaY71 zeolite (low Brönsted acidity) compared to Ca-NaY73 zeolite (high Brönsted acid sites).

Propane adsorption in alkaline-earth exchanged Y zeolites has been reported to be due to enhanced interaction with framework oxygen and polarization at cation sites<sup>11;14;24;25</sup>. It also has been reported that propane could be adsorbed via hydrogen bonds to the Brönsted acid sites of acid Y zeolite<sup>26</sup>. To investigate the effect of  $\text{Ca}^{2+}$ -cations and Brönsted acid sites on the propane adsorption capacity of these samples, ammonia adsorption was used to poison possible propane adsorption sites. It has been previously shown that at  $100^\circ\text{C}$  ammonia adsorbs on both  $\text{Ca}^{2+}$  and Brönsted acid sites, while at  $300^\circ\text{C}$  ammonia preferentially blocks  $\text{Ca}^{2+}$  cations<sup>14</sup>.

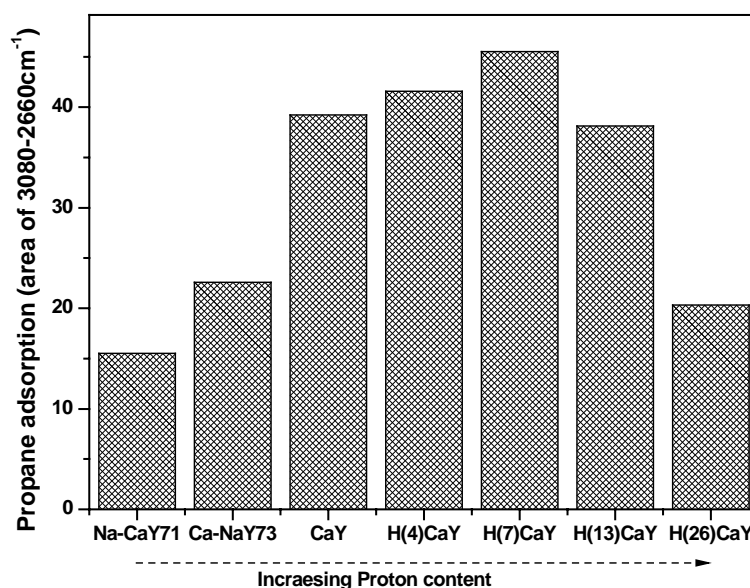


**Figure 5-3.** Propane adsorption quantity as 1mbar propane adsorption on Ca-NaY73, Na-CaY71 and series HCaY zeolites

Thus, one CaY sample was prepared by ammonia adsorption at 100°C, and subsequent evacuation (sample indicated as CaY-100) and one was prepared by ammonia adsorption at 300°C, followed by evacuation (sample indicated as CaY-300). Subsequently, both samples were cooled to room temperature and 1mbar propane was adsorbed. Figure 5-4 show the infrared spectra of the hydroxyl vibration and C-H vibrations after these

treatments in comparison with the adsorption of propane on un-treated CaY. The infrared spectrum of the pre-treated sample before exposure to propane was taken as a background. First, for CaY-100 infrared bands of propane at 2838 and 2887 $\text{cm}^{-1}$  present after propane adsorption on CaY, disappeared, while these two bands are still visible on CaY-300. Since the infrared band at 2838 and 2887 $\text{cm}^{-1}$  only appeared when bare  $\text{Ca}^{2+}$  cation were present in the supercage<sup>11;14</sup>, we concluded that these two bands originated from propane adsorbed on or close to supercage  $\text{Ca}^{2+}$  cations. Obviously, these sites are not accessible anymore in CaY-100, while only partly available in CaY-300.

Second, compared to CaY much less propane adsorbed (integrated area between 3080 $\text{cm}^{-1}$  and 2660 $\text{cm}^{-1}$ ) on CaY-300 (50%) and CaY-100 (10%). Third, no changes in the hydroxyl region could be observed for CaY-100 upon propane adsorption, which is in agreement with the fact that the pre-adsorbed ammonia blocks all the Brönsted sites. For CaY-300 a decrease of the O-H band at 3640  $\text{cm}^{-1}$  can be seen, but this is only about 10% of the original intensity of this band (Figure 5-1). It has been reported that the contribution of Brönsted acid sites to the heat adsorption of propane is 6kJ/mol compared to 31 kJ/mol of total heat adsorption of propane adsorbed on HY zeolite<sup>20;26</sup>. Further, the cation polarization of propane increases with increasing cation charge or decreasing cation radius. Adsorption of n-hexane on HY and NaY revealed as such a higher induction of polarity by protons than sodium cations<sup>20;26</sup>. The results of this study are in good agreement, since the quantity of adsorbed

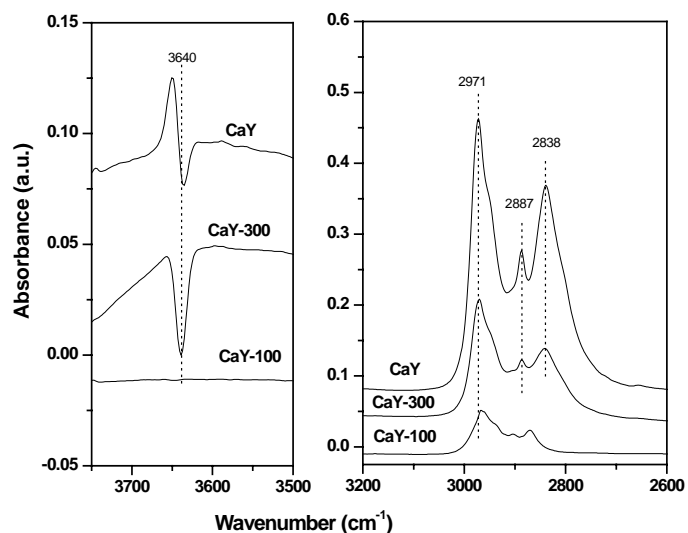


**Figure 5-4.** Infrared spectra of 1mbar propane adsorption on CaY with different pre-treatment conditions (CaY-100: adsorb  $\text{NH}_3$  at 100°C, followed 5 hours evacuation at 100°C; CaY-300: adsorb  $\text{NH}_3$  at 300°C, followed 1hour evacuation)

propane is increasing for Ca-NaY73 > Na-CaY71 (Figure 5-3), while both have the same calcium content but less protons on Na-CaY71 compared to Ca-NaY73.

Comparing the polarization capability of  $\text{Ca}^{2+}$  and  $\text{H}^+$  is more complicated, since from  $\text{H}^+$  to  $\text{Ca}^{2+}$  both the charge (higher polarization) and cation radius (lower polarization) increases. Moreover, also the mobility of  $\text{H}^+$  in the zeolite will determine its final effective electrostatic field. In addition, the FTIR data show that increasing exchange of calcium with proton the signal of  $\text{Ca}(\text{OH})_x$  species ( $3590\text{ cm}^{-1}$ ) diminished. Combination of this result with the Ca-content (Table 5-1) points to the conclusion that first  $\text{Ca}(\text{OH})_x$  species are exchanged by ammonium ions, followed by exchange of bare  $\text{Ca}^{2+}$  ions at higher proton exchange levels. As such the Ca-content as determined by elemental analysis is gradually lowered with increased proton content. The change in amount of adsorbed propane (Figure 5-3) can also be explained by the subsequent exchange of  $\text{Ca}(\text{OH})_x$  and  $\text{Ca}^{2+}$  ions. It was shown here (Figure 5-4) and in previous studies that  $\text{Ca}(\text{OH})_x$  hardly contribute to quantity of adsorbed propane<sup>11</sup>. Comparison of CaY to H(7)CaY shows that the Ca-content decreased while proton content increased, and simultaneously propane adsorption increased due to the affinity of propane for protons. Further decrease of the calcium content by exchanging with protons leads to removal of  $\text{Ca}^{2+}$  ions, that have a much higher propane affinity than protons and consequently the amount of adsorbed propane drops significantly from H(7)CaY to H(26)CaY.

### 5.3.3 Propane oxidation: activity

Previously, we showed that infrared spectroscopy is a suitable tool to study the selective propane oxidation at low pressures to be able to unravel the reaction mechanism. In the infrared spectra depletion of propane (between  $3080\text{cm}^{-1}$  and  $2660\text{cm}^{-1}$ ) and production of acetone (at  $1682$ ,  $1421$ ,  $1379$ ,  $1367\text{cm}^{-1}$ ) and water (infrared band at  $3695$ ,  $1634\text{cm}^{-1}$ ) was followed [details in refs 10, 13].

#### 5.3.3.1 HCaY series

Upon loading 1 mbar of propane and 40 mbar of oxygen on the activated HCaY zeolites, thermal reaction was noted at room temperature just minutes after introducing the gases into the cell. All absorptions that were observed could be attributed to acetone and water<sup>10;11;14</sup>.



Figure 5-5a shows the acetone formation rate for the HCaY zeolites as function of time, based on the amount of formation of adsorbed acetone. The same trends were observed for the consumption rate of adsorbed propane (interpreted as decreasing area of infrared band between  $3080\text{cm}^{-1}$  and  $2660\text{cm}^{-1}$ , not shown). CaY, H(4)CaY and H(7)CaY showed a decreasing rate in time, while for H(13)CaY and H(26)CaY the rate first increased and after 10 hours started to decrease. The highest initial acetone formation rate was observed for H(7)CaY, while H(13)CaY reached the same activity after about 10 hours. Although the initial activities do not show a linear relationship with the amount of protons, it can be seen that the deactivation rate after 10 hrs of reaction steadily increased with higher proton amounts.

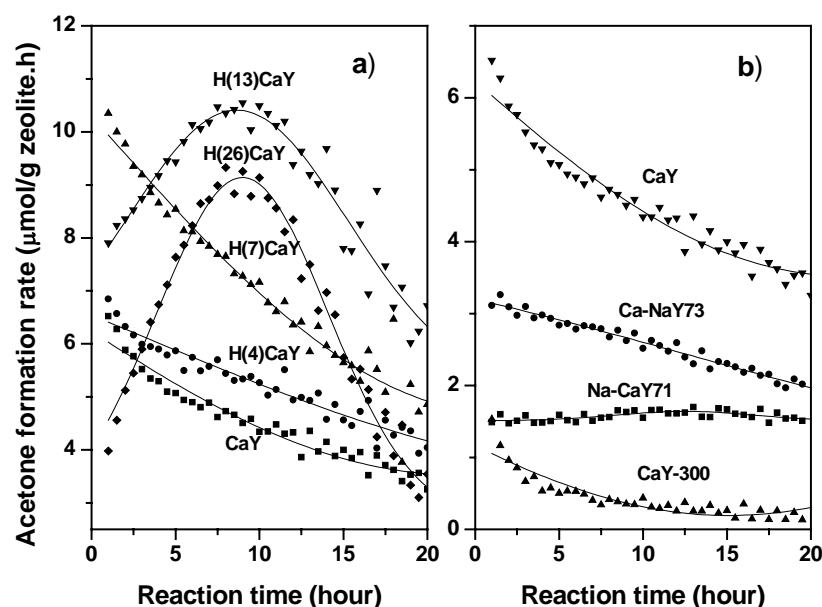


**Figure 5-5.** Acetone formation rate as function of reaction time a) on CaY and series HCaY zeolite; b) on Ca-NaY73, Na-CaY71, and CaY-300 (ammonia pre-adsorption at  $300^\circ\text{C}$ )

### 5.3.3.2 Ca-NaY73 and Na-CaY71

Room temperature propane partial oxidation was further studied on Ca-NaY73 and Na-CaY71 zeolites, which contain the same calcium amount but have different Brønsted acidity. Figure 5-5b reports the acetone formation rate as function of reaction time, the activity of CaY was added as a reference. The initial acetone formation rate of Ca-NaY73 is approximately half of CaY, while for Na-CaY71 the rate again was half of that of Ca-NaY73. Further, Ca-NaY73 showed a continuous decrease of the acetone formation rate while Na-CaY71 showed a slight increase for the first 12 hours of reaction.

### 5.3.3.3 Ammonia pretreated samples

After loading 1mbar and 40mbar oxygen into the ammonia pre-treated zeolites the formation of acetone and water was followed (Figure 5-5b). CaY-100 did not show any activity at room temperature

(not shown), while CaY-300 exhibited a ten times lower activity than the untreated CaY zeolite. Clearly, in addition to the propane adsorption capacity, the presence of supercage  $\text{Ca}^{2+}$  ions is also essential for the selective oxidation of propane, as these  $\text{Ca}^{2+}$  supercage ions are selectively occupied with  $\text{NH}_3$  at  $300^\circ\text{C}$ , as discussed before.

### 5.3.4 Propane oxidation: selectivity.

To investigate the selectivity of the reaction, adsorbed propane was removed by 5 min evacuation after 20 hrs of reaction (Figure 5-6a). Only propane was detected by on-line MS analysis during evacuation. Bands at  $3014\text{cm}^{-1}$ ,  $2998\text{cm}^{-1}$ ,  $2989\text{cm}^{-1}$  and  $2925\text{cm}^{-1}$  were observed that were initially masked by propane. These bands could be attributed to isopropylhydroperoxide (IHP,  $2998\text{cm}^{-1}$ ) and acetone ( $3014$  and  $2925\text{cm}^{-1}$ )<sup>11;13;14</sup>, while the band at  $2989\text{cm}^{-1}$  was assigned to 2-propanol as confirmed by comparison with the IR spectrum after adsorption of 2-propanol in CaY. The O-H stretch vibration of 2-propanol could not be observed because it overlaps with the water O-H stretch vibrations. Complete selectivity to acetone was observed on CaY, in agreement with previous results<sup>11;13;14</sup>. However, acetone selectivity decreased for the proton-exchanged zeolites since 2-propanol was formed. Further, the IHP amount reduced with increasing Brønsted acidity. Surprisingly, for Na-CaY73 which has a low amount of protons, both a large quantity of IHP and 2-propanol were observed (Figure 5-6a, bottom line). Also, a higher molar ratio of IHP to acetone was found for Na-CaY71 compared to Ca-NaY73.

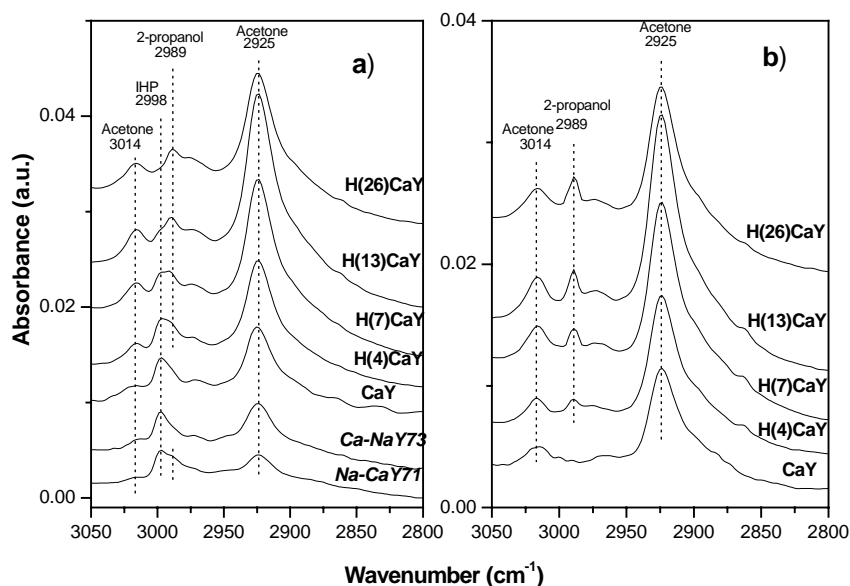


**Figure 5-6.** IR spectra of a) After 20 hours reaction, followed 5 minutes evacuation; b) Heating of a) at  $200^\circ\text{C}$  10 minutes, cool to room temperature on CaY and series of HCaY zeolites

IHP amount reduced with increasing Brønsted acidity. Surprisingly, for Na-CaY73 which has a low amount of protons, both a large quantity of IHP and 2-propanol were observed (Figure 5-6a, bottom line). Also, a higher molar ratio of IHP to acetone was found for Na-CaY71 compared to Ca-NaY73.

Previously it was shown that at  $200^\circ\text{C}$  IHP can be easily decomposed into acetone and water without desorption of acetone<sup>12</sup>. Thus, the system was further heated to  $200^\circ\text{C}$  ( $10^\circ\text{C}/\text{minute}$ ), kept for 10

minutes at 200°C, and cooled to room temperature, after which FTIR spectra were taken (Figure 5-6b). Clearly, the band at 2998cm<sup>-1</sup> (IHP) disappeared, with a concurrent growth of the acetone C=O band, while the band at 2989cm<sup>-1</sup> (2-propanol) still showed on the spectra. Except for water, no desorption of other product molecules were detected by infrared spectroscopy and on-line MS analysis during IHP conversion.

To better understand 2-propanol and acetone formation, two typical samples (CaY and H(13)CaY) were selected to investigate selectivity at different reaction times (Figure 5-7).

The amounts of IHP and acetone formed at different reaction times are listed in Table 5-2. For CaY, the IHP concentration slightly decreased from 5 to 20 hours of reaction, while for H(13)CaY, the IHP concentration increased from 5 to 10 hours of reaction, and dramatically decreased after 20 hours reaction.

Further, the concentrations of both IHP and acetone were higher for H(13)CaY compared to CaY at both 5 hours and 10 hours reactions, while a lower IHP concentration for H(13)CaY was found after 20 hours reaction compared to CaY. In addition, after decomposition of IHP, acetone and water were formed exclusively on CaY and H(13)CaY after 5 hours, while, small amounts of 2-propanol (band at 2989cm<sup>-1</sup>) were observed additionally, on H(13)CaY after 10 and 20 hours reaction. For H(13)CaY a significant higher amount of 2-propanol was observed for 20 hours reaction compared to 10 hours reaction.

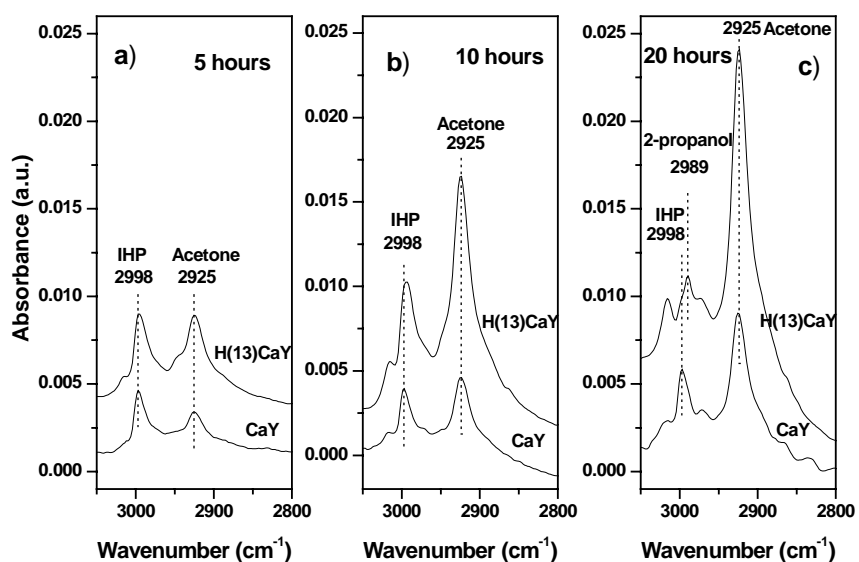


**Figure 5-7.** Infrared spectra of 1mbar propane and 40mbar propane reaction on CaY and H(13)CaY a) 5hrs, followed 5 minutes evacuation; b) 10hours, followed 5 minutes evacuation; c) 20 hours, followed 5 minutes evacuation

CaY at both 5 hours and 10 hours reactions, while a lower IHP concentration for H(13)CaY was found after 20 hours reaction compared to CaY. In addition, after decomposition of IHP, acetone and water were formed exclusively on CaY and H(13)CaY after 5 hours, while, small amounts of 2-propanol (band at 2989cm<sup>-1</sup>) were observed additionally, on H(13)CaY after 10 and 20 hours reaction. For H(13)CaY a significant higher amount of 2-propanol was observed for 20 hours reaction compared to 10 hours reaction.

**Table 5-2 IHP and acetone concentration of propane oxidation at different reaction time**

	<i>CaY</i>		<i>H(13)CaY</i>	
	IHP ( $\mu\text{mol/g}$ )	Acetone ( $\mu\text{mol/g}$ )	IHP ( $\mu\text{mol/g}$ )	Acetone ( $\mu\text{mol/g}$ )
<b>5 hours</b>	6.7	30	7.7	46
<b>10 hours</b>	6.0	53	14.9	97
<b>20 hours</b>	6.0	92	3.6	178

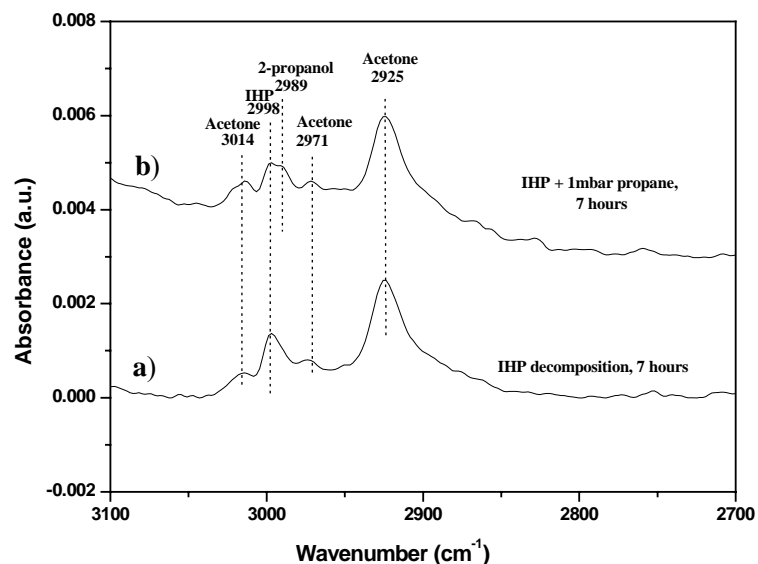


**Figure 5-8.** a) Infrared spectra of 5 hours 1mbar propane and 40mbar oxygen reaction on *CaY* zeolite at room temperature, followed 7 hours evacuation; b) Infrared spectra of 5 hours 1mbar propane and 40mbar oxygen reaction on *CaY* zeolite at room temperature, followed 5 minutes evacuation, then loaded 1mbar propane and stayed 7 hours, subsequently 5 minutes evacuation

It has been proposed that a possible reaction path for production of alcohol is the reaction between a hydroperoxide and a hydrocarbon to form two molecules of alcohol<sup>8</sup>. To test this suggested reaction path, two parallel experiments were carried out. Since IHP cannot be loaded into the zeolites, first 5 hours of reaction were performed for two batches of *CaY* using 1mbar of propane and 40mbar oxygen, followed by 5 minutes evacuation. In the first experiment, the system was continuously evacuated for 7

hours. In the second experiment, 1mbar of propane was reloaded and kept for 7 hours, followed by 5 minutes evacuation. The infrared spectra after those two treatments are given in Figure 5-8.

Decomposition of IHP solely leads to acetone and water only (Figure 5-8a, experiment 1). Still some IHP was left after 7 hours since the reaction was done at room temperature. In the presence of propane, however, 2-propanol was produced in addition to acetone and water (Figure 5-8b, experiment 2). Also

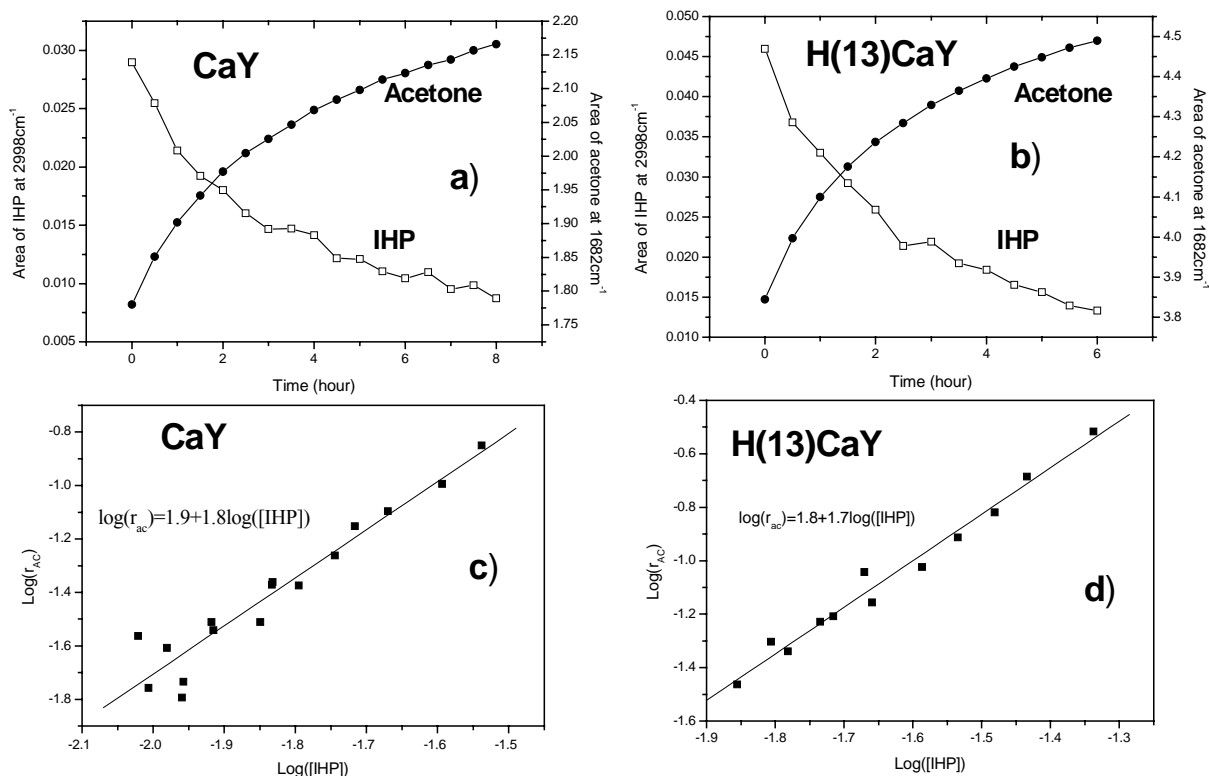


**Figure 5-9.** Acetone and IHP concentration as function of time during IHP decomposition at room temperature a) on CaY zeolite; b) on H(13)CaY zeolite. Kinetic analysis of room temperature IHP decomposition c) on CaY zeolite; d) on H(13)CaY zeolite

less acetone was produced, indicating that part of the IHP converted into 2-propanol instead of acetone and water.

### 5.3.5 Kinetics of IHP decomposition

Finally, the kinetics of IHP decomposition in the absence of propane was studied. For CaY and H(13)CaY, after 5 hours of reaction at room temperature with 1mbar propane and 40mbar oxygen, the system was evacuated. Subsequently, IHP decomposition and acetone formation were monitored by

infrared spectroscopy at room temperature (Figures 5-9a and 5-9b). For both samples a decrease in IHP and a concurrent increase in acetone were observed. On-line mass spectroscopy revealed no products in the gas phase. From the results in Figures 5-9a and 5-9b, the rate of IHP decomposition into acetone was analyzed (Figures 5-9c and 5-9d). Clearly, plotting  $\log[r_{AC}]$  versus  $\log[IHP]$  ( $r_{AC}$ : rate of acetone formation,  $\text{area}(\text{band at } 1682\text{cm}^{-1})/\text{hr}$ ;  $IHP$ :  $\text{area}(\text{band at } 2998\text{cm}^{-1})$ ) results in a straight line from which the order in IHP was determined: respectively 1.8 and 1.7 for CaY and H(13)CaY.

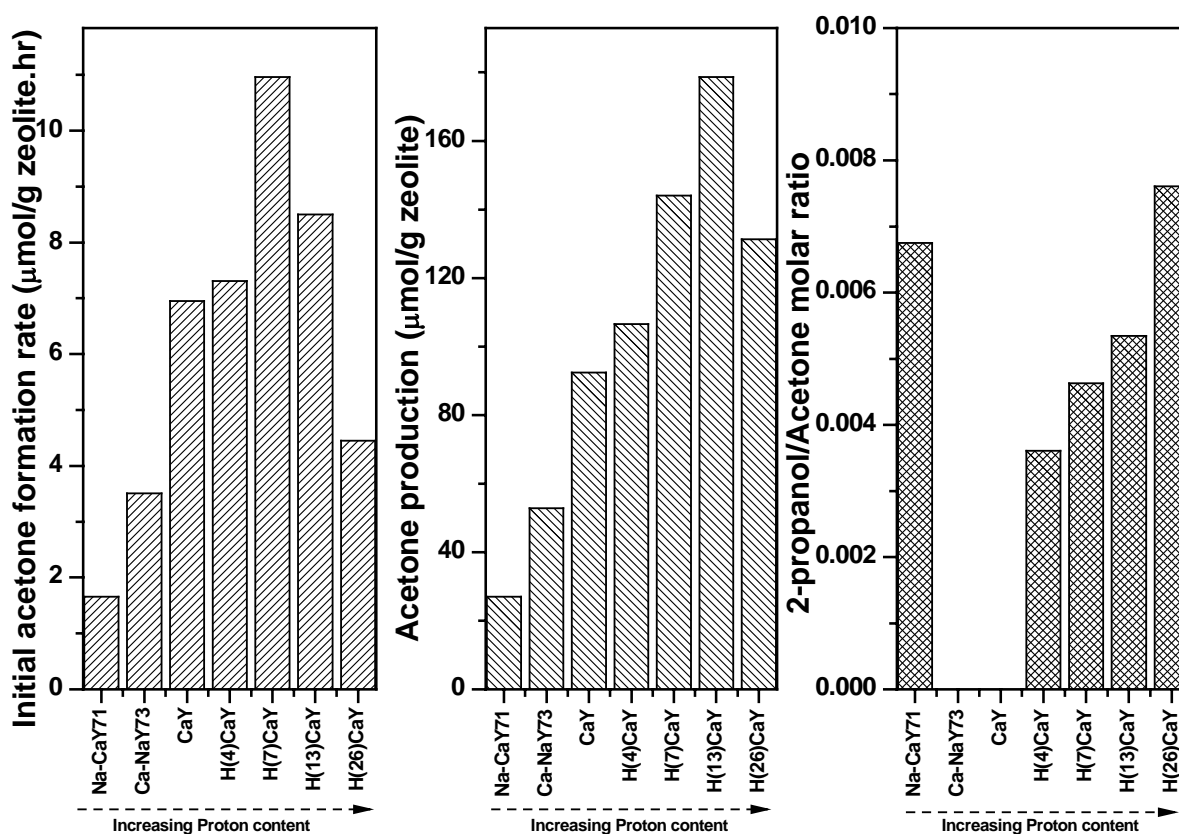


**Figure 5-10.** a) Initial acetone formation rate; b) Acetone formation after 20 hours reaction; c) 2-propanol to acetone ratio on series calcium exchange Y zeolite

### 5.3.6 General discussion

This study shows that with increasing of number of protons in the series Na-CaY71 > Ca-NaY73 > CaY > H(4)CaY > H(7)CaY > H(13)CaY > H(26)CaY, Volcano type of plots are observed for:

- amount of adsorbed propane (Figure 5-3)
- initial acetone formation rate (Figure 5-10a)
- total amount of acetone produced after 20 hours of reaction (Figure 5-10b)

- acetone selectivity (Figure 5-10c)

Interestingly, the maximum of the Volcano plots for amount of adsorbed propane, initial acetone activity and total amount of acetone produced varies between H(7)CaY and H(13)CaY. Figure 5-11 shows initial acetone formation rates as a function of propane adsorption. Although, in general, a linear trend is observed between the amount of adsorbed propane and the initial acetone formation rate, the scattering of the points is beyond the experimental error. Therefore, the amount of adsorbed propane cannot fully account for the observed differences in activity as a function of catalyst composition.

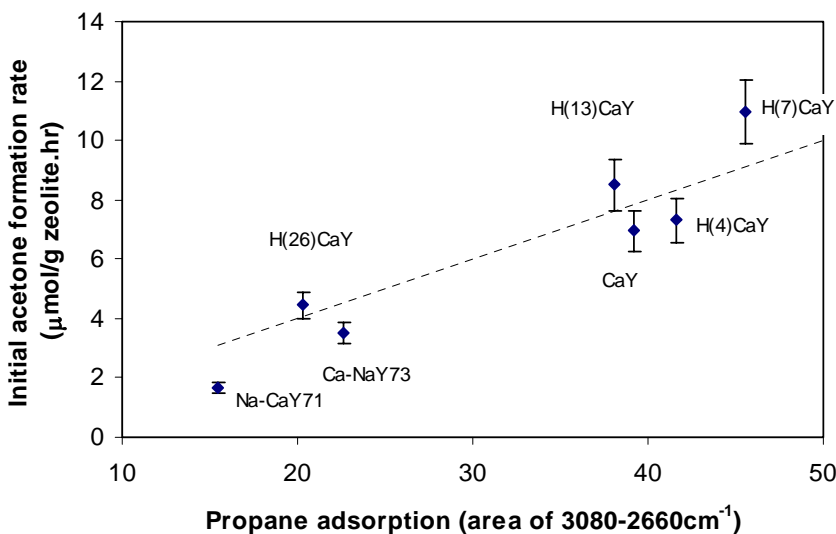
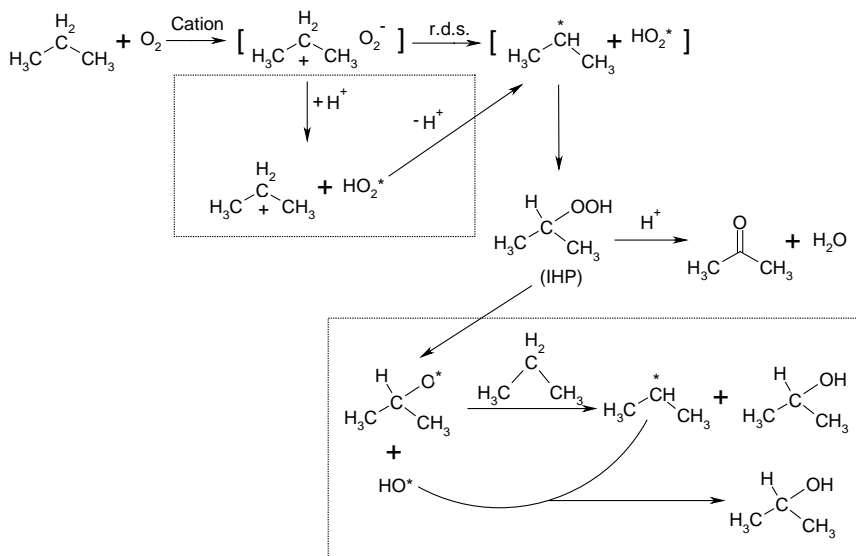


**Figure 5-11.** Initial acetone formation rate as function propane adsorption on series calcium exchanged Y zeolite

At present, in literature it is proposed that the active site for the activation of propane in this reaction is a bare  $\text{Ca}^{2+}$  cation, located in the supercage<sup>14</sup>. The electrostatic field of the cation is thought to be capable of stabilizing charge-transfer states between propane and oxygen [ $\text{C}_3\text{H}_8^+ \text{O}_2^-$ ] by Coulombic interaction<sup>11;12;27</sup>. Subsequent abstraction of a proton from the acidic hydrocarbon cation to the basic superoxygen ion should result in the formation of  $\text{C}_3\text{H}_7^*$  and  $\text{HO}_2^*$  radicals. Recombination of these radicals into isopropylhydroperoxide (IHP) is possible, or, at elevated temperature, they may start a radical chain reaction. However, in the restricted zeolite cages and at relatively low temperature, the radical recombination reaction is faster than the radical chain reaction<sup>27</sup>. Finally, it was shown that if a zeolite contains Brønsted acid sites in addition to earth-alkali cations, IHP can be decomposed into acetone and water<sup>11</sup>. Scheme 5-1 summarized these reactions. In the following discussion we will extend this mechanism with additional reactions (dashed boxes in Scheme 5-1) based on the finding in the present chapter.

### **5.3.6.1 Catalytic effect of protons on IHP formation**

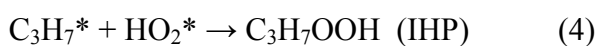
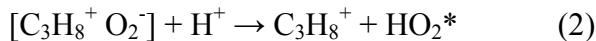
The importance of supercage  $\text{Ca}^{2+}$  cations for propane oxidation reaction, as reported earlier<sup>14</sup> was confirmed in this study by propane adsorption and oxidation after pre-adsorption of ammonia (Figure 5-4). Blocking of all supercage  $\text{Ca}^{2+}$  cations and Brønsted acid sites by adsorbed ammonia caused a significant change in propane adsorption and a total inhibition of oxidation activity (Figure 5-4). Releasing part of the ammonia from calcium cation sites and recovering all Brønsted acid sites (CaY-300), still a large decrease in propane oxidation activity was found compared to CaY without pre-adsorption of ammonia (Figure 5-5b).



**Scheme 5-1.** Proposed mechanism for propane oxidation over proton modified CaY zeolite. The reactions in the dashed boxes are based on the findings in the present paper

However, the data on the concentrations of IHP and acetone in CaY and H(13)CaY after 5 and 10 hours (Figure 5-7, Table 5-2) contradict with the model that  $\text{Ca}^{2+}$  ions are exclusively responsible for the formation of IHP. Although less propane adsorption was observed on H(13)CaY (Figure 5-3), and H(13)CaY contains only about 70% of the number of supercage  $\text{Ca}^{2+}$  ions as compared to CaY (Table 5-1), after 5 hours of reaction the amount of IHP formed on H(13)CaY is already 1.1 times higher than found for CaY, while after 10 hours it is about 2.5 times higher than for CaY (Table 5-2). Additionally, more acetone was produced on H(13)CaY compared to CaY for both 5 and 10 hours of reaction.

As said above, the critical point of formation of IHP is thought to be a charge-transfer complex  $[\text{C}_3\text{H}_8^+ \text{O}_2^-]$ , followed by the rate-determining step of proton abstraction from the acidic hydrocarbon cation ( $\text{C}_3\text{H}_8^+$ ) to basic superoxygen ( $\text{O}_2^-$ ), to form  $\text{C}_3\text{H}_7^*$  and  $\text{HO}_2^*$  radicals, which then rapidly recombine into IHP (1). The observed influence of protons on the enhancement of IHP formation can be explained by a catalytic effect of the protons of the zeolite in the proton-abstraction step:





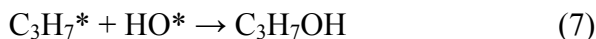
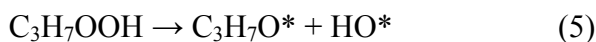
Since the proton abstraction of the charge-transfer complex was found to be rate determining<sup>8</sup>, the catalytic effect of protons on the IHP formation rate can be explained by opening up an alternative, faster route to IHP via reactions (2) to (4).

This would indeed result in a Volcano type of behavior as a function of proton content, since with increasing  $[H^+]$  concurrently the amount of supercage  $Ca^{2+}$  decreased (Table 5-1) and thus the amount of formed charge-transfer complexes decreased. Combination of these two phenomena leads to an optimum for  $Ca^{2+}$  and  $H^+$  concentration on the oxidation activity as was observed (Figure 5-10).

For HCaY13 and HCaY26 a significant increase in acetone formation rate was observed in the first 10 hours of reaction, while the other zeolites only showed a deactivation as a function of time. Again, two phenomena take place at the same time. First, the amount of IHP increases with higher proton content according to the reactions (2) to (4), as discussed above. Since the conversion of IHP into acetone is a second order reaction (Figure 5-9), higher IHP concentrations will increase the acetone formation rate because the IHP concentration increases in time (Table 5-2). Especially, for H(13)CaY and H(26)CaY the very high Brønsted acidity in the samples (Figure 1) will strongly enhance catalytic pathway (2) to (4), resulting in increased amount of IHP in the first 10 hours, as observed in Figure 5-7. The observation also strongly implied that with increasing proton concentration, the rates of proton abstraction and IHP decomposition are getting competitive. At the same time, the production of acetone and water deactivates the samples since the product molecules adsorb onto the active cations and protons<sup>11</sup>. The formation rate of the charge-transfer complex would decrease faster when more water is produced and less supercage  $Ca^{2+}$  ions are present. This indeed agrees with the increasing deactivation rate with increasing proton content and decreasing  $Ca^{2+}$  amount (Figure 5-5).

### **5.3.6.2 2-propanol production**

Similar to the activity, also the selectivity to acetone shows a Volcano type of behavior as a function of  $H^+/Ca^{2+}$  ratio (Figure 5-10c). However, in this case the optimum selectivity is found at much lower proton content, namely for CaNaY73 and CaY (100%). With both increasing and decreasing Brønsted acidity, 2-propanol was found as a by-product. Inspired by the work of Vanoppen et. al. for liquid phase oxidation of cyclohexane<sup>17</sup>, it may be suggested that ion-exchanged Y zeolite are also capable of catalyzing homolytic IHP decomposition. Figure 5-8 showed that addition of propane to IHP in the absence of oxygen on CaY led to the formation propanol. Since infrared spectra have revealed that adsorbed IHP adsorbed close to the cation sites<sup>11</sup>, the calcium cation could activate the peroxide bond in IHP which results in the formation of  $C_3H_7O^*$  and  $HO^*$  radicals. Subsequently, an alkyloxy radical reacts with propane, followed by radical recombination into 2 molecules of 2-propanol:



The contribution of reactions (5) to (7) demonstrate that the zeolite cages cannot be considered to be completely isolated as propane added later is involved. Because only small amounts of 2-propanol were found throughout the series, reactions (5) to (7) must be slower than the decomposition of IHP into acetone and water. Decreasing Brönsted acid sites slow down IHP decomposition into acetone and water, thus favoring the competing route via IHP homolytic cleavage, which explains the increased 2-propanol formation as was found for Na-CaY71. In addition, for H(13)CaY much more 2-propanol was formed after 20 hours than after 10 hours of reaction (Figure 5-7), while the concentration of IHP (Table 5-2) and the acetone formation rate (Figure 5-5) dramatically decreased in this time span. Again, IHP decomposition into acetone is slowed down, which favors the homolytic splitting to result 2-propanol. As such, the balance between IHP catalytic decomposition into acetone and IHP homolysis to produce 2-propanol is influenced by the  $\text{H}^+/\text{Ca}^{2+}$  ratio of the sample.

#### 5.4 Conclusion

The importance of Brönsted acid sites for propane partial oxidation to acetone in CaY was investigated using *in-situ* FTIR spectroscopy. With increasing concentration of Brönsted acid sites on calcium exchanged Y zeolite, Volcano type of plots were observed for: (1) amount of adsorbed propane; (2) initial acetone formation rate; (3) total amount of acetone produced after 20 hours of reaction; (4) acetone selectivity. The results clearly show that Brönsted acidity increases the IHP formation rate, most likely via a catalytic  $\text{H}^+$ -abstraction as well as the IHP decomposition into acetone and water. Formation of a minor amount of 2-propanol was observed when decreasing or increasing Brönsted acidity compared to fully Ca-exchanged sample. This was attributed to a parallel reaction pathway of IHP homolytic decomposition in addition to IHP decomposition into acetone and water. This study convincingly shows that the activity and selectivity of Ca-exchanged Y-zeolites is determined by a subtle balance between the number of supercage  $\text{Ca}^{2+}$  ions and Brönsted acid sites.

#### Reference List

1. Centi, G.; Cavani, F.; Trifiro, F. *Selective oxidation by heterogeneous catalysis*, Kluwer Academic/Plenum Publishers: New York, 2000.
2. Ai, M. *Catalysis Today* **1998**, *42*, 297-301.

3. Centi, G.; Corberan, V. C.; Perathoner, S.; Ruiz, P. *Catalysis Today* **2000**, *61*, 1.
4. Chaar, M. A.; Patel, C.; Kung, H. H. *Journal of Catalysis* **1988**, *109*, 463-467.
5. Lin Luo; Jay A. Labinger; Mark E. Davis. *Journal of Catalysis* **2001**, *200*, 222-231.
6. Centi, G.; Trifiro, F. *Appl. Catal. A-Gen.* **1996**, *143*, 3-16.
7. Blatter, F.; Sun, H.; Frei, H. *Chemistry-A European Journal* **1996**, *2*, 385-389.
8. Larsen, R. G.; Saladino, A. C.; Hunt, T. A.; Mann, J. E.; Xu, M.; Grassian, V. H.; Larsen, S. C. *Journal of Catalysis* **2001**, *204*, 440-449.
9. Sun, H.; Blatter, F.; Frei, H. *Journal of the American Chemical Society* **1996**, *118*, 6873-6879.
10. Sun, H.; Blatter, F.; Frei, H. *Catalysis Letters* **1997**, *44*, 247-253.
11. Xu, J.; mojet, B. L.; Ommen, J. G. v.; Lefferts, L. *Phys. Chem. Chem. Phys.* **2003**, *5*, 4407-4413.
12. Vanoppen, D. L.; DeVos, D. E.; Jacobs, P. A. *Progress in Zeolite and Microporous Materials, Pts A-C* **1997**, *105*, 1045-1051.
13. Xu, J.; mojet, B. L.; Ommen, J. G. v.; Lefferts, L. *Journal of Physical Chemistry B* **2004**, *108*, 218-223.
14. Xu, J.; mojet, B. L.; Ommen, J. G. v.; Lefferts, L. *Journal of Physical Chemistry B* **2004**, *108*, 15728-15734.
15. Panov, A. G.; Larsen, R. G.; Totah, N. I.; Larsen, S. C.; Grassian, V. H. *Journal of Physical Chemistry B* **2000**, *104*, 5706-5714.
16. Xiang, Y.; Larsen, S. C.; Grassian, V. H. *Journal of the American Chemical Society* **1999**, *121*, 5063-5072.
17. Vanoppen, D. L.; De Vos, D. E.; Jacobs, P. A. *Journal of Catalysis* **1998**, *177*, 22-28.
18. Ward, J. W. *Journal of Physical Chemistry* **1968**, *72*, 4211-4223.
19. Ward, J. W. *Journal of Catalysis* **1968**, *10*, 34-46.
20. Donald W. Breck *Zeolite molecular sieves: structure, chemistry, and use*, Wiley: New York, 1974.
21. Sponer, J. E.; Sobalik, Z. *Journal of Physical Chemistry B* **2001**, *105*, 8285-8290.
22. H. Miessner; H. Kosslick; U. Lohse; B. Parltitz; Vu-Anh Tuan. *Journal of Physical Chemistry* **1993**, *97*, 9741-9748.
23. Nakamoto, K. *Infrared spectra of Inorganic and Coordination compounds*, Wiley-Interscience: New York: 1986.
24. H. van Bekkum *Introduction to zeolite science and practice*, Elsevier: Amsterdam, 2001.
25. Smit, B. *Journal of Physical Chemistry* **1995**, *99*, 5597-5603.
26. Florian Eder. PhD thesis; Thermodynamics and siting of alkane sorption in molecular sieves. University of Twente, 1996.
27. Frei, H. *3rd World Congress on Oxidation Catalysis* **1997**, *110*, 1041-1050.

## Chapter 6

### **Formation of $M^{2+}(O_2)(C_3H_8)$ Species in Alkaline-earth Exchanged Y Zeolite during Propane Selective Oxidation**

---

**Abstract:** *The adsorption of oxygen and  $d_2$ -propane on a series of alkaline-earth exchanged Y zeolite at room temperature was studied with in situ infrared spectroscopy. Surprisingly at room temperature, oxygen adsorption led to the formation of supercage  $M^{2+}(O_2)$  species. Further, at low propane coverage, propane was found to adsorb linearly on  $Mg^{2+}$  cations, but a square adsorption structure was observed for propane adsorbing on  $Ca^{2+}$ ,  $Sr^{2+}$  and  $Ba^{2+}$  cations. It is demonstrated that  $O_2$  and propane can simultaneously attach to one active center ( $M^{2+}$ ) to form a  $M^{2+}(O_2)(C_3H_8)$  species which is proposed to be the precursor in propane selective oxidation. Selectivity to acetone in the propane oxidation reaction decreases with increasing temperature and cation size, due to the formation of 2-propanol and carboxylate ions. An extended reaction scheme for the selective oxidation of propane over alkaline earth exchanged Y-zeolites is proposed.*

## 6.1 Introduction

Partial oxidation of alkanes with high selectivity at higher conversion is almost always impossible because of the fact that the product molecules are easier activated than the alkane reactants<sup>1,2</sup>. As a result, production costs of partial oxidized hydrocarbons increase significantly because of inefficient use of feedstock, high demands for heat transfer caused by deep oxidation, and cost associated with product separation. High selectivity can generally be obtained at very low conversion, but then a heavy penalty is caused by cost for separation and recycling. The inefficiency associated with low conversion has motivated the search for solid catalysts that are active and selective for the oxidation of alkanes.

One of the essential functions of a catalyst in catalytic oxidation reactions is the activation of oxygen. The high bond energy in  $O_2$  is one of the reasons that the activation energy of uncatalyzed oxidation reaction is high and at moderate temperatures a catalyst must be used<sup>3</sup>. Generally, selective oxidation processes using gaseous oxygen as oxidizing agent can be classified in two groups. In the first type, oxygen activation occurs by its adsorption and incorporation into an oxide catalyst and its reactivity can be explained by a Mars-van Krevelen type mechanism<sup>2</sup>. In this mechanism, lattice oxygen is the active oxygen species for oxidation reactions, while gaseous oxygen re-oxidizes the catalyst to close the catalytic cycle. The second group usually involves a radical type mechanism with oxygen activated by a homogeneous catalyst such as  $Co^{2+}$  salts or through hydrocarbon auto-oxidation process<sup>4</sup>. The similarity in the two groups is the redox mechanism involved. Recently, a new approach in selective oxidation of alkanes<sup>5-13</sup> on alkali or alkaline-earth exchanged Y zeolite was presented. Alkali and alkaline-earth cations in zeolites do not show any redox properties. Therefore, activation of oxygen in those cation-exchanged zeolites is different from the traditional processes.

It has been proposed that the photon-induced reaction involves the formation of an activated charge-transfer ion pair of  $A^+O_2^-$  through electron transfer from the alkane A to the  $O_2$  molecule. The electrostatic field induced by alkali or alkaline-earth ions in the zeolite is thought to play a key role in stabilizing this ion pair. An alkane radical cation  $A^+$  is known to be highly acidic and therefore has a very strong tendency for proton transfer to the basic superoxide anion  $O_2^-$ . Subsequent radical recombination results in alkylhydroperoxide as reaction intermediate. Finally, heterolytic elimination of water from the alkylhydroperoxide results in the formation of a carbonyl-containing product. Complete selectivity was reported at conversions as high as about 22%, by in situ FTIR measurements of propane oxidation to acetone for BaY zeolite<sup>9</sup>. Similar results have been obtained for the thermally induced selective oxidation reaction, although the observed conversion levels were lower<sup>12</sup>. Until now a similar reaction pathway has been assumed for the thermal oxidation as for the photochemical reaction. In this paper we limit ourselves to the thermal reaction.

So far, alkali or alkaline earth ions are only responsible in the proposed mechanism for the electrostatic field. However, the details of those active sites for reactant activation need to be further clarified in order to develop this new class of catalysts for selective oxidations.

Transmission infrared spectroscopy has been used to study the oxygen adsorbed on zeolites (e.g. NaA, CaA, NaY, BaY, LiX) to investigate the electrostatic properties of the cations in the zeolite<sup>14-16</sup>. So far, this adsorbed oxygen species was only observed by transmission FTIR at low temperature (below 273K). At room temperature and in DRIFT mode, an extremely weak IR band of O<sub>2</sub> adsorbed on cation-exchanged low-silica X-zeolites was observed<sup>16</sup>. In addition, infrared adsorption studies showed that propane can adsorb on alkaline-earth exchanged Y zeolite and polarizes at the supercage cation site<sup>12;13</sup>. However, the exact adsorption geometry and interaction between oxygen and propane in Y-zeolite are not yet identified. For this reason, we have investigated oxygen and propane adsorption in earth-alkali exchanged Y-zeolite in more detail using deuterated propane. In addition, the thermal reactions using both normal and deuterated propane have been compared.

## 6.2 Experimental

### 6.2.1 Materials

Alkaline-earth cation (Mg, Ca, Sr, and Ba) exchanged Y-zeolites were prepared from NaY (Akzo Nobel, sample code: 1122-207) with Si/Al ratio of 2.5. The parent zeolite was exchanged three times with 0.1M solution of respectively magnesium chloride, calcium nitrate, strontium nitrate, or barium chloride (Merck) for 20 hours at 90°C under stirring. The resulting alkaline-earth exchanged Y zeolite was washed three times with distilled water, filtered and dried at 100°C overnight. The chemical composition of catalysts was analyzed by X-ray fluorescence. The M<sup>2+</sup>(Mg<sup>2+</sup>, Ca<sup>2+</sup>, Sr<sup>2+</sup> and Ba<sup>2+</sup>)/Al ratio was 0.34, 0.45, 0.45 and 0.35 for MgY, CaY, SrY and BaY respectively. Powder X-ray diffraction showed no collapse of the zeolite structures.

### 6.2.2 Infrared Spectroscopy

The zeolite powder (30mg) was pressed into a self-supporting wafer and analyzed *in-situ* during adsorption and reaction by means of transmission FTIR spectroscopy using a Bruker Vector22 FTIR spectrometer with a MCT detector. A miniature cell, equipped with NaCl transparent windows, which can be evacuated to pressure below 10<sup>-7</sup> mbar was used for the *in-situ* experiments. The temperature is variable from room temperature to 500°C. Each spectrum consists of 32 scans taken at 4cm<sup>-1</sup> resolutions.

The samples were activated in vacuum ( $<10^{-7}$  mbar) at  $500^\circ\text{C}$  (ramp  $10^\circ\text{C}/\text{min}$ ) for 2 hours, subsequently cooled down to  $200^\circ\text{C}$  (dwell 10 hours), and cooled to room temperature. Loading of reactants (propane and oxygen) was controlled by gas pressure. Propane was introduced into the IR cell until equilibrium was reached at 1 mbar in the gas phase, followed by addition of 40 mbar of oxygen. A calibration curve was made by adsorption of known amounts of acetone at room temperature in order to determine the quantity of produced acetone from propane and oxygen. The concentration of hydroxyl O-D sites was evaluated using the characteristic band at  $2685\text{cm}^{-1}$ . The molar extinction coefficients for this band  $\nu(2685) = 8.54 \text{ cm}/\mu\text{mol}$  was taken from literature<sup>17,18</sup>. The FTIR spectra in propane adsorption and reaction studies were corrected for absorption by the activated zeolite.

## 6.3 Results

### 6.3.1 Catalyst characterization

Transmission FTIR spectra of the activated MgY, CaY and SrY showed formation of an absorption band at  $3645\text{cm}^{-1}$ , which indicated the formation of Brönsted acid site<sup>12,19</sup>. Further, additional bands at  $3695\text{cm}^{-1}$  for MgY,  $3590\text{cm}^{-1}$  for CaY and  $3570\text{cm}^{-1}$  for SrY were attributed to  $M(\text{OH})_x$  species. BaY did not exhibit any Brönsted acid sites. Detailed results and interpretation can be found in our previous paper<sup>12</sup>. In addition,  $^{27}\text{Al}$  MAS NMR showed no extra-framework aluminum, even not after activation at  $500^\circ\text{C}$ .

### 6.3.2 Oxygen adsorption

Infrared spectra of oxygen adsorbed on alkaline-earth exchanged Y zeolite at room temperature are given in Figure 6-1. Clearly, at room temperature, bands appear in the  $1552\text{-}1555\text{cm}^{-1}$  region, which is in the O-O stretch frequency range<sup>14-16</sup>. The frequency of this peak slightly increases in the order BaY ( $1552\text{cm}^{-1}$ ) = MgY ( $1552\text{cm}^{-1}$ ) < SrY ( $1553\text{cm}^{-1}$ ) < CaY ( $1555\text{cm}^{-1}$ ). The shape of the band gets broader with increasing cation radius (i.e..  $\text{Mg}^{2+} < \text{Ca}^{2+} < \text{Sr}^{2+} < \text{Ba}^{2+}$ ). On

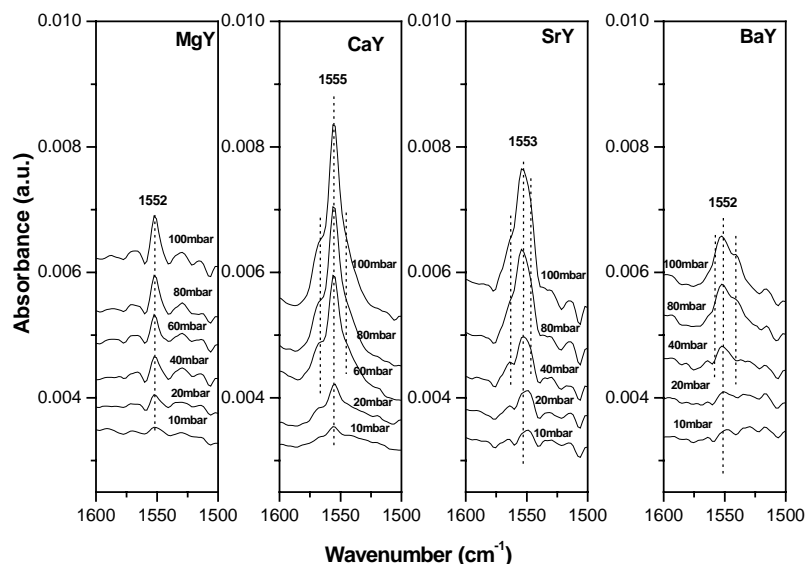


**Figure 6-1.** FT-IR spectra of adsorbed oxygen on alkaline-earth exchanged Y zeolite at room temperature at different oxygen partial pressure

MgY, only one sharp peak was found at  $1552\text{cm}^{-1}$  and which increased in intensity when oxygen pressure increased from 10mbar to 100mbar. While for CaY, SrY and BaY with increasing oxygen partial pressure two side bands appeared at the higher frequency side (about  $1564\text{cm}^{-1}$ ) and low-frequency side (about  $1542\text{cm}^{-1}$ ). Figure 1b shows the infrared spectra of activated Ca-NaY73 and Na-CaY71 samples having the same calcium content. A clear decrease of the band at  $3644\text{cm}^{-1}$  was observed for Na-CaY71 sample compared to both CaY and Ca-NaY73, which indicates that most of the protons were exchanged by sodium ions. Na-CaY71 and Ca-NaY73 showed similar intensities for the O-H vibration from both isolated silanol ( $3744\text{cm}^{-1}$ ) and  $\text{Ca}(\text{OH})_x$  species ( $3590\text{cm}^{-1}$ ).

### 6.3.3 D<sub>2</sub>-propane (CH<sub>3</sub>CD<sub>2</sub>CH<sub>3</sub>) adsorption

Figure 6-2a and b present the gas phase infrared spectra of propane and d<sub>2</sub>-propane. The infrared frequencies of the methyl and methylene C-H stretch vibrations of d<sub>2</sub>-propane are easily distinguished: methyl-CH stretch vibrations appeared between  $3100\text{cm}^{-1}$  and  $2800\text{cm}^{-1}$ , while the methylene-CD vibrations turned up between  $2300\text{cm}^{-1}$  and  $2000\text{cm}^{-1}$ . Figures 6-2c-f show the infrared spectra after adsorbing 1mbar d<sub>2</sub>-propane on the different alkaline earth exchanged Y-zeolites at room temperature. Two main methyl-CH stretch vibration areas were observed: one intense band at  $2963\text{cm}^{-1}$  which position hardly changed with different cation. This peak can be attributed to the methyl-CH asymmetric stretching<sup>20-22</sup>. With increasing cation radius from  $\text{Mg}^{2+}$  to  $\text{Ba}^{2+}$ , a shoulder appeared beside this band and increased intensity, while its frequency shifted to lower wavenumber (from  $2946$  to  $2930\text{cm}^{-1}$ ). At lower frequency one main band was found from methyl symmetric CH stretching<sup>20-22</sup>. This band clearly

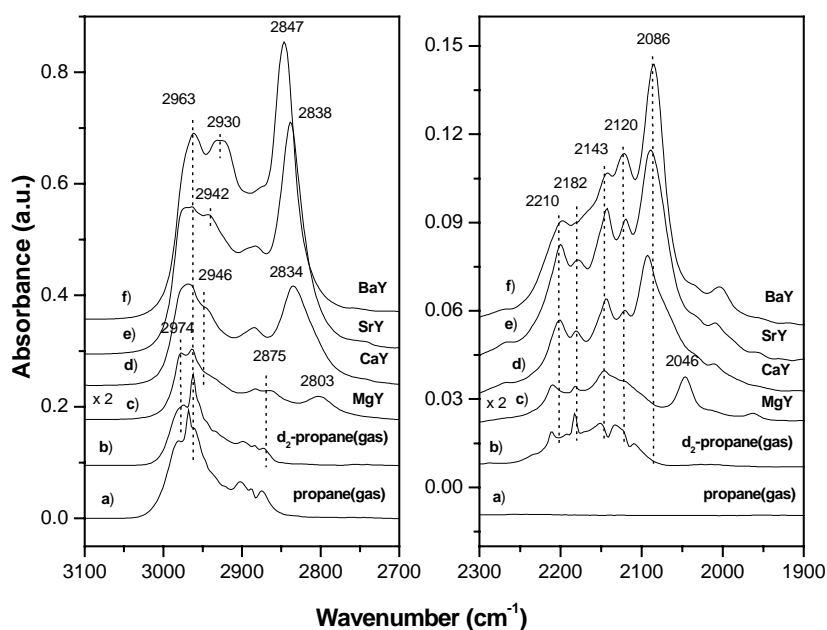


**Figure 6-2.** Infrared spectra of 10mbar gaseous a) propane, b) d<sub>2</sub>-propane, and c-f) 1mbar d<sub>2</sub>-propane adsorption on alkaline-earth exchanged Y zeolite

hardly changed with different cation. This peak can be attributed to the methyl-CH asymmetric stretching<sup>20-22</sup>. With increasing cation radius from  $\text{Mg}^{2+}$  to  $\text{Ba}^{2+}$ , a shoulder appeared beside this band and increased intensity, while its frequency shifted to lower wavenumber (from  $2946$  to  $2930\text{cm}^{-1}$ ). At lower frequency one main band was found from methyl symmetric CH stretching<sup>20-22</sup>. This band clearly



shifted towards lower wavenumber (from 2847 to 2803 $cm^{-1}$ ) with decreasing cation radius from  $Ba^{2+}$  to  $Mg^{2+}$ . Moreover, the intensity ratio of the high frequency band at 2963 $cm^{-1}$  to low frequency band at 2847-2803 $cm^{-1}$  decreased with increasing the cation radius.

The methylene CD stretch vibration appeared in the range 2210 - 2120 $cm^{-1}$  and showed almost identical frequencies for CaY, SrY and BaY, although the intensities varied with type of cation. Further, compared to the gas phase spectrum, one additional vibration at 2086 $cm^{-1}$  was found with high intensity. This frequency only slightly shifted ( $\sim 2cm^{-1}$ ) when the type of cation varied from  $Ca^{2+}$  to  $Ba^{2+}$ . Only for MgY a peak at 2046  $cm^{-1}$  was found. Moreover, for both methyl and methylene vibrations it can be seen that the spectrum obtained on MgY after adsorption of  $d_2$ -propane resembles the gas phase spectrum at high frequency, both in frequency and relative intensity. However, in addition bands were observed at much lower frequency, respectively at 2803 and 2046  $cm^{-1}$ . For CaY, SrY and BaY the spectra clearly showed many features different from the gas phase spectrum for both methyl and methylene CH stretch vibrations. Finally, the increase in overall intensity of the  $d_2$ -propane peaks in the order  $MgY < CaY < SrY < BaY$  is identical to normal propane adsorption and has been attributed to increasing basicity of the zeolite oxygen atoms <sup>12</sup>.

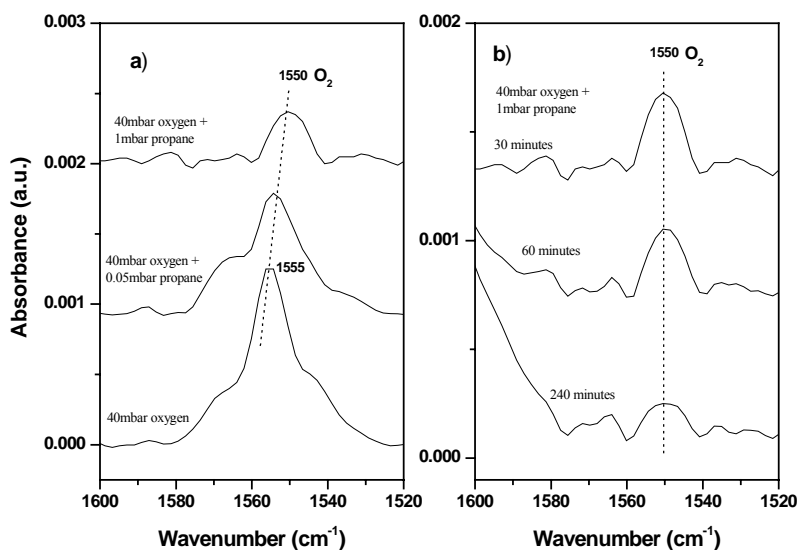


**Figure 6-3.** FTIR spectra of CaY after adsorption of oxygen and propane at room temperature. Peaks of adsorbed propane are subtracted. a) 40mbar oxygen (bottom), 40mbar oxygen and 0.05mbar propane for 30 minutes (middle), 40mbar oxygen and 1mbar propane for 30 minutes(top); b) 40mbar oxygen and 1mbar propane during reaction

### 6.3.4 Co-adsorption of oxygen and propane on CaY

After adsorption of O<sub>2</sub> on CaY the effect of co-adsorption of propane at room temperature was investigated. Figure 6-3a (bottom spectra) shows the infrared spectra of oxygen adsorption at 40mbar equilibrium pressure. Subsequently, 0.05mbar or 1mbar propane was introduced to the sample and equilibrated for 30 minutes to allow propane to diffuse into the zeolite pores. After 30 minutes only a very small amount of acetone was found, indicating that reaction just started. Middle and top spectra in Figures 3a show the differential spectra of the zeolites after subtraction of the intense propane band. Figure 6-3a distinctly shows that the intensity of the adsorbed oxygen peak at 1555cm<sup>-1</sup> decreased and shifted from 1555cm<sup>-1</sup> to 1550cm<sup>-1</sup> with increasing propane loading. In addition, the total peak became narrower since the two side bands disappeared after loading 1 mbar of propane. As propane oxidation reaction goes on, in Figure 6-3b, it clearly shows that intensity of adsorbed oxygen peak decreases.

### 6.3.5 Thermal oxidation of propane and d<sub>2</sub>-propane

Upon loading 1 mbar propane and 40 mbar oxygen on activated MgY, CaY and SrY zeolites, thermal reaction was noted at room temperature just minutes after introducing the gases into the pellet by infrared spectra. Reaction was much faster than if 40mbar oxygen is first adsorbed followed by 1 mbar of propane (as described in section 6.3.4) due to slightly diffusion of 1mbar propane in 40mbar oxygen in the system. On BaY zeolite, slow reaction was observed after 1 hour. All product absorptions can be attributed to acetone and water<sup>9;12;13</sup>. When loading 1mbar d<sub>2</sub>-propane and 40mbar oxygen on the activated zeolites, no reaction could be observed at room temperature within 5 hours.

In order to investigate the kinetic isotope effect on the thermal oxidation of propane for these catalysts, reaction was further carried out at 80°C. Figure 6-4 displays the acetone formation rate as a function of time for both normal propane and d<sub>2</sub>-propane at 80°C. A much higher acetone

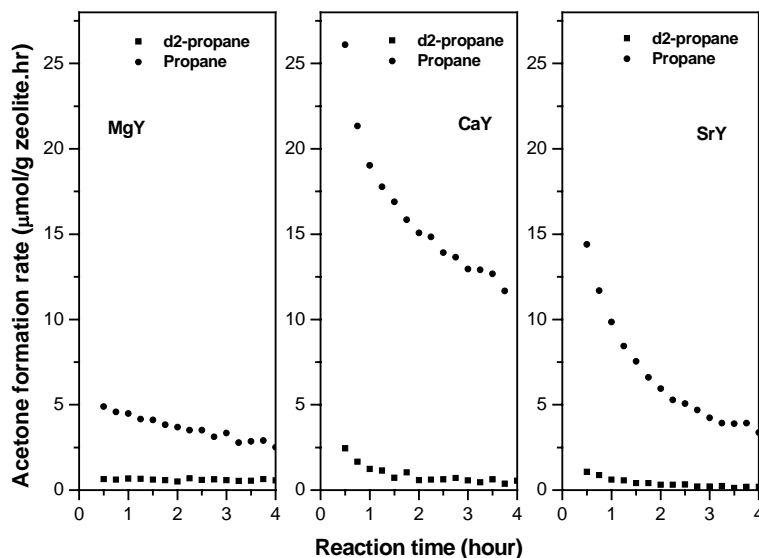


**Figure 6-4.** Acetone formation rate of propane and d<sub>2</sub>-propane oxidation at 80°C on alkaline-earth exchanged Y zeolite

formation rate was observed from propane than  $d_2$ -propane on MgY, CaY and SrY. On BaY only a very slow reaction was observed for propane, while no products could be detected for  $d_2$ -propane oxidation at  $80^\circ\text{C}$  (not shown). Based on the ratios of the initial acetone formation rate, the magnitude of the deuterium kinetic isotope effect increased in the order MgY (7.5) < CaY (10.7) < SrY (13.3). The observations are a clear indication of a substantial deuterium kinetic isotope effect in this system. The fact that the reaction rate decreased with time can be explained by product inhibition (water and acetone)<sup>13</sup>.

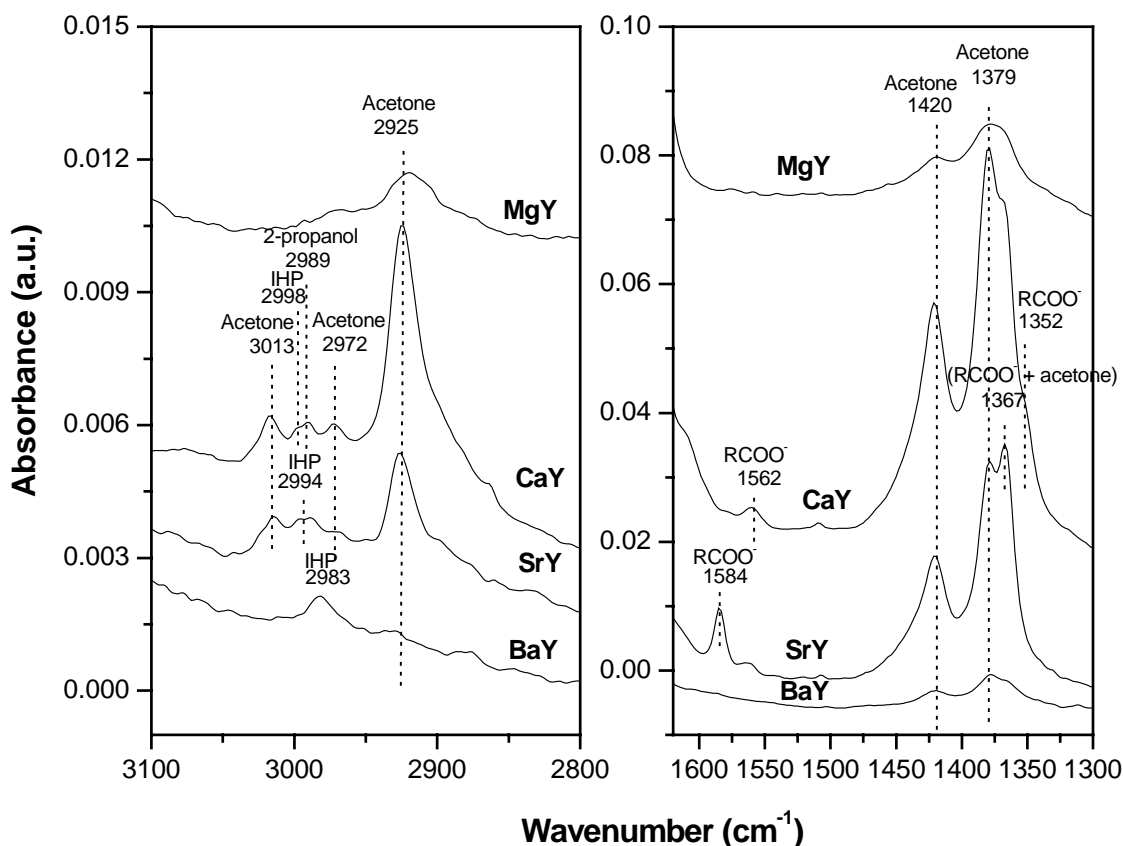


**Figure 6-5.** Infrared spectra of propane oxidation on alkaline-earth exchanged Y zeolite at  $80^\circ\text{C}$  for 4 hours, followed 5 minutes evacuation

After 4 hours of reaction at  $80^\circ\text{C}$  and subsequent removal of adsorbed propane under vacuum for 5 minutes, adsorbed species on the samples could be observed (Figure 6-5). To emphasize the smaller peaks below  $1600\text{ cm}^{-1}$ , the acetone C=O stretch peak at  $1682\text{ cm}^{-1}$  (CaY, SrY, BaY) and  $1694\text{ cm}^{-1}$  (MgY) is not shown, since this has a tenfold higher intensity than the other species observed. Below  $1600\text{ cm}^{-1}$ , the acetone CH deformation vibration can be observed as indicated in Figure 6-5. The

spectra for BaY and MgY were identical to reported spectra of propane oxidation at room temperature<sup>12</sup>. But on CaY and SrY new peaks were found in addition to the acetone and water bands previously reported. These peaks can be attributed to carboxylate species: bands at 1562, 1352 $\text{cm}^{-1}$  on CaY and 1584, 1367 $\text{cm}^{-1}$  on SrY are due to asymmetric and symmetric  $\text{COO}^-$  vibrations, respectively<sup>22;23</sup>. Moreover, 2-propanol (at 2989 $\text{cm}^{-1}$ ) was found<sup>24</sup>. Decomposition at elevated temperature of isopropylhydroperoxide (IHP) on CaY, SrY and BaY yielded exclusively acetone and water (not shown)<sup>12;25</sup>.

The infrared spectra after  $\text{d}_2$ -propane oxidation at 80°C for 4 hours, and subsequent 5 minutes evacuation are given in Figure 6-6 for MgY, CaY and SrY. The acetone C=O stretch vibration was found at the exact same frequencies as in the case normal propane was oxidized (1682 $\text{cm}^{-1}$  for CaY and SrY and 1694 $\text{cm}^{-1}$  for MgY), but it has much lower intensity due to the lower formation rate (Figure 6-4). For this reason, the acetone CH deformation vibration hardly can be observed in Figure 6-6. In addition, an O-D band at 2685 $\text{cm}^{-1}$ , a decrease of the O-H band at 3644 $\text{cm}^{-1}$  (not shown) and DHO bending vibrations (1445 $\text{cm}^{-1}$ ) were observed. Finally, for CaY and SrY carboxylate species were found at the same positions as for normal propane oxidation. Comparison of the asymmetric carboxylate vibration at 1584 $\text{cm}^{-1}$  (SrY) and 1562 $\text{cm}^{-1}$  (CaY) revealed that about 3 times more carboxylate species was formed from  $\text{d}_2$ -propane than from normal propane. Moreover, on SrY the concentration of carboxylate species was clearly higher than for CaY.

During the reaction, concurrent growth of acetone C=O, O-D and carboxylate species was observed. The molar ratio of acetone to hydroxyl O-D sites is  $1.0 \pm 0.2$  for all three zeolites during the whole reaction. No  $\text{CO}_x$  formation was found in the gas phase for either propane or  $\text{d}_2$ -propane oxidation at 353K as investigated by on-line mass spectrometer.

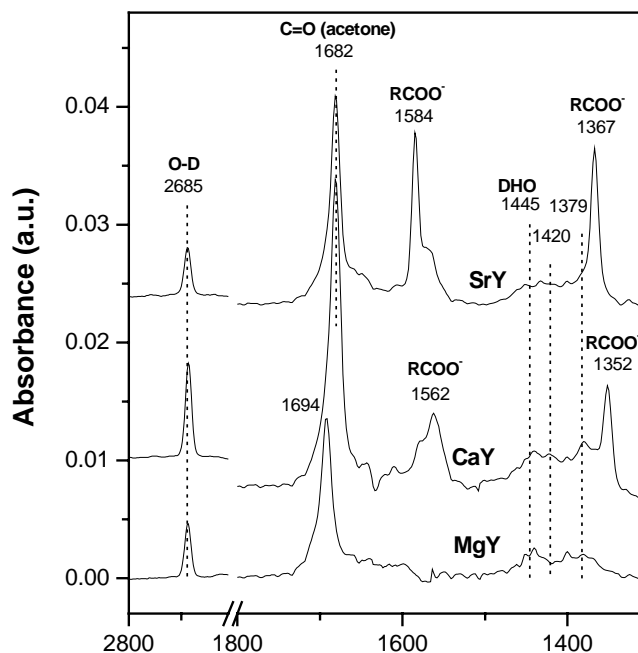


**Figure 6-6.** Infrared spectra of  $\text{d}_2$ -propane oxidation on alkaline-earth exchanged Y zeolite for 4 hours at 80°C, followed 5 minutes evacuation

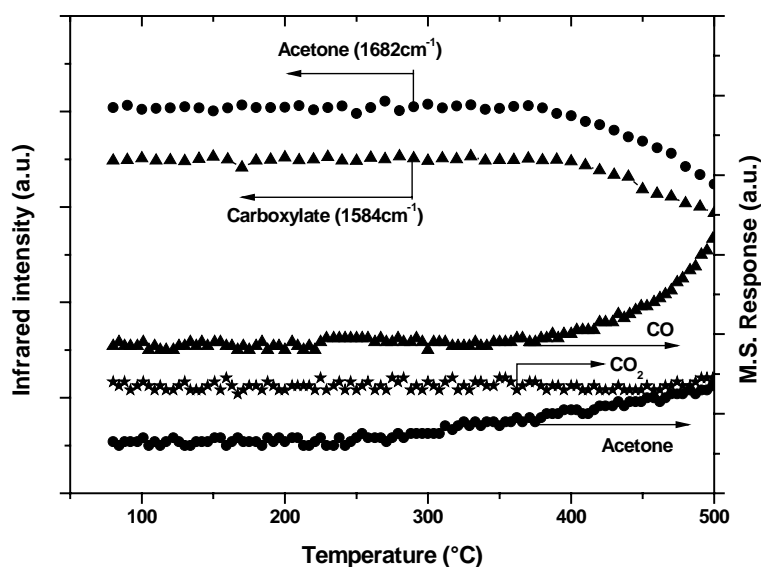


**Figure 6-7.** Change of IR band intensities on surface and mass responses in gas phase during TPD after  $d_2$ -propane oxidation on SrY

After  $d_2$ -propane oxidation at 80°C for 4 hours over SrY and subsequent 30 minutes evacuation, the sample was further heated to 500°C (10°C/min). Infrared spectra were taken simultaneously with on-line mass spectroscopy for detection of gas phase species. Peak intensities at 1682 $cm^{-1}$  (acetone) and 1584 $cm^{-1}$  (carboxylate) kept constant up to 400°C. With increasing temperature species started to desorb while acetone and CO in the gas phase were detected by mass spectroscopy after 350°C (Figure 6-7). No  $CO_2$  was detected. Based on the infrared intensities approximately 15% of the acetone and carboxylate species were removed from the surface after heating at 500°C.

### 6.3.6 Carboxylate formation on SrY

In order to better understand the formation of carboxylate several additional experiments were carried out. In most of oxidation reactions, carboxylate is produced via oxidation of a ketone. Since on SrY the largest amounts of carboxylates were found (Figures 6-5 and 6-6), this sample was selected to be further investigated.

First, 1 mbar of propane and 40 mbar of oxygen were reacted for 2 hours at room temperature to produce IHP adsorbed on the SrY zeolite. This was repeated for several pellets of SrY so that parallel experiments could be carried out. Excess propane and oxygen were removed by evacuation (Figure 8a). Infrared bands at 2994, 2942, 1396 $cm^{-1}$  belong to C-H vibrations of IHP, while the band at 873 $cm^{-1}$  is attributed to the O-O stretch vibration of IHP<sup>5;22</sup>. Also small amounts of acetone and water (not shown) were found. The following results were obtained:

1. Thermal decomposition of adsorbed IHP in the presence of acetone produced acetone and water exclusively at 80°C (Figure 6-8b).

- At 80°C, addition of 1mbar propane to the adsorbed IHP yielded a tiny amount of 2-propanol (at 2989cm<sup>-1</sup>, not indicated in spectra due to low intensity) together with acetone and water (Figure 6-8c). A very small amount of carboxylate can be observed as a shoulder at 1584 cm<sup>-1</sup>.
- Addition of 40mbar oxygen at 80°C to the adsorbed IHP resulted in production of acetone and water (Figure 6-8d), again with a small shoulder at 1584 cm<sup>-1</sup>.
- Significant carboxylate formation was observed together with acetone and water when both 1mbar propane and 40mbar oxygen were added to the adsorbed IHP at 80°C (Figure 6-8e). Moreover, in this experiment the carboxylate amount (exclude amount produced from IHP with propane or oxygen in Figure 6-8c and 6-8d) was found to be approximately 1.3 times higher than the amount of carboxylate produced on fresh SrY with 1 mbar of propane and 40 mbar of oxygen at 80°C without pre-production of IHP (not shown).

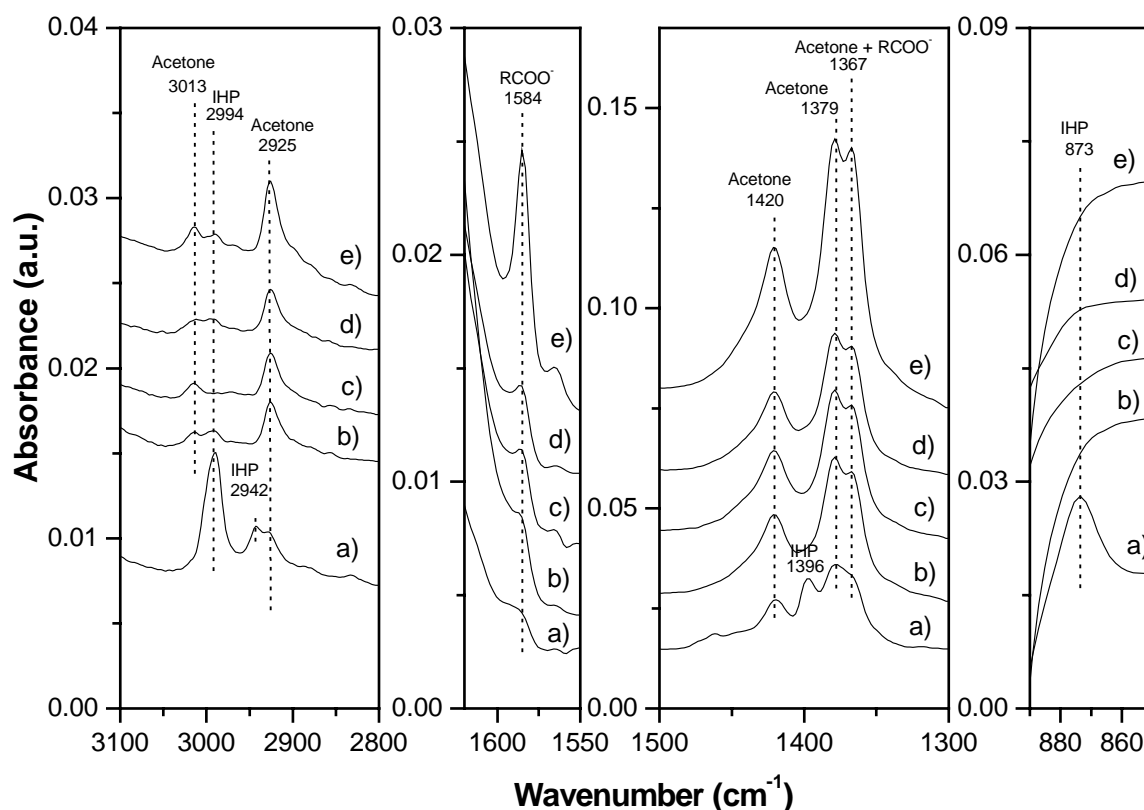


**Figure 6-8.** Infrared spectra on SrY zeolite a) after 1mbar propane and 40mbar oxygen at room temperature for 4 hours, followed 5 minutes evacuation; b) a. + 2 hours at 80°C; c) a. + 1mbar propane for 2 hours at 80°C, followed by 5 minutes evacuation; d) a. + 40mbar oxygen for 2 hours at 80°C, followed by 5 minutes evacuation; e) a. + 1mbar propane and 40mbar oxygen for 2 hours at 80°C, followed by 5 minutes evacuation

## 6.4 Discussion

### 6.4.1 Formation of $M^{2+}$ -adsorbate species in cation exchanged Y zeolite

Simultaneous adsorption of more than one molecule on a catalyst site is very important for many catalytic reactions because it facilitates reaction between adsorbed molecules. For exchanged Y-zeolites it was shown that only supercage cations (site II) are accessible for molecules such as CO, N<sub>2</sub>, oxygen and propane<sup>13;26</sup>. Recent DFT calculations and single-crystal X-ray diffraction studies on cation exchanged Y zeolite showed that the cations in the supercage are located above the three oxygen anions of the six-ring window which are facing the supercage<sup>27-29</sup>. As such a supercage cation could adsorb more than one molecule, so called geminal structure *via* electrostatic interactions<sup>30-32</sup>. The factors of influence on the formation of this geminal species are: (1) the electrostatic field of the cations; (2) the size of the cations and adsorbed molecules; (3) electron density (base properties) of the adsorbed molecules.

#### 6.4.1.1 Formation of $M^{2+}(O_2)$ species

This study convincingly shows that even at room temperature oxygen adsorption can be observed in the infrared spectra for alkaline earth exchanged Y zeolite (Figure 6-1). To our best knowledge, this is the first time that adsorbed oxygen species by transmission infrared spectroscopy were observed at this temperature. The fundamental vibration of the diatomic homonuclear molecule O<sub>2</sub> is infrared inactive for the free gas, but gains intensity when the molecule approaches a poorly shielded cation, because of the dipole moment induced by the electrostatic field of the cation<sup>14;16</sup>. Oxygen adsorption has been investigated mainly at very low temperatures by calculating the perturbation of the harmonic oscillator of the adsorbing molecule caused by interaction with the electrostatic field of the extra-framework cation<sup>14;15</sup>.

Our results showed that even at room temperature such a dipole interaction between O<sub>2</sub> and supercage cation gives rise to clearly observable infrared absorptions around 1552 -1555cm<sup>-1</sup> (Figure 6-1). We attribute this adsorption to the formation of  $M^{2+}(O_2)$  species at the supercage cation site above the 6-ring window. The electrostatic field of alkaline-earth cation increases with decreasing cation radius, which results in an increased polarization of adsorbed oxygen in the order BaY < SrY < CaY. It can be seen in Figure 6-1 that both intensity and frequency of the O<sub>2</sub> peak increases in the same order. By DRIFTS, a similar trend in frequency shift was reported for oxygen adsorption on alkali exchanged X zeolites with decreasing alkali cation radius<sup>16</sup>. The increase in intensity with higher oxygen partial pressure can be attributed to an increasing amount of  $M^{2+}(O_2)$  species, since TGA results showed that at these pressures

full  $M^{2+}(O_2)$  coverage is not reached yet (not shown). The side bands observed in the FTIR spectra of CaY, SrY and BaY were previously attributed to remaining rotational or librational freedom of adsorbed oxygen<sup>14</sup>. The fact that the intensity ratio of the sidebands relative to the main peak does not change with coverage is indeed an indication that the sidebands originate from the same molecule giving rise to the main frequency.

In contrast to  $Ca^{2+}$  (0.99Å),  $Sr^{2+}$  (1.13Å) and  $Ba^{2+}$  (1.35Å), the small ion radius of  $Mg^{2+}$  (0.65Å) allows the  $Mg^{2+}$  cation to be more closely to the plane of the six-ring windows, which lowers the effective electrostatic field of  $Mg^{2+}$  supercage cations<sup>32</sup>. Consequently, the frequency of the oxygen peak is at the same position as the main peak on BaY zeolite. Since  $Mg^{2+}$  is closer to the six ring window, the librational freedom of adsorbed oxygen will be limited compared to Ca, Sr or Ba cations. Consequently, side bands cannot be clearly observed (Figure 6-1). In addition, the lower intensity of the peak could also be partly due to the fact that MgY contains the lowest fraction of bare cations due to the applied activation procedure as was reported before<sup>12</sup>.

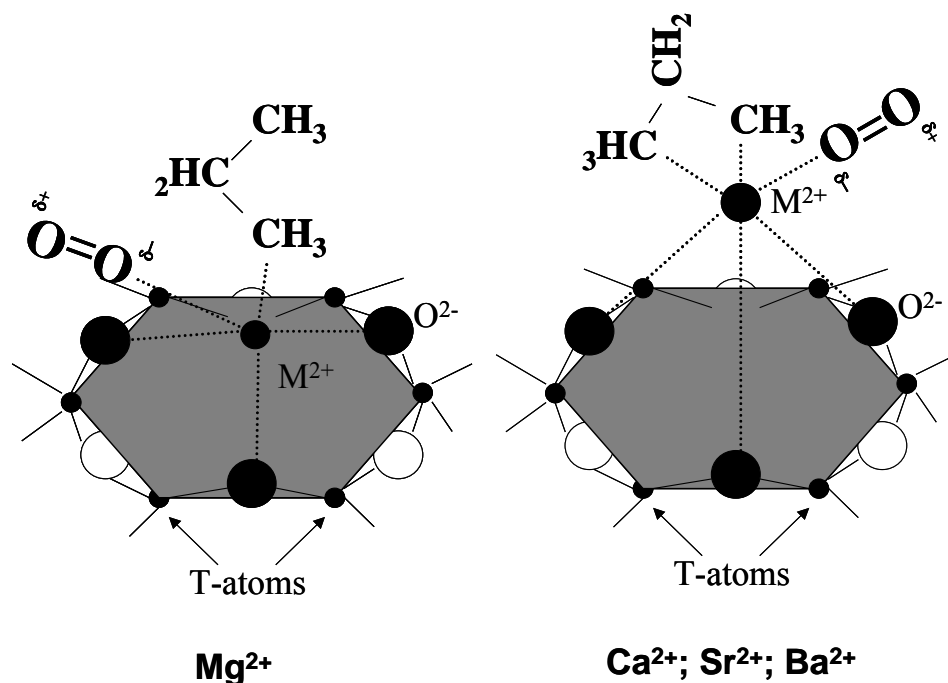
#### **6.4.1.2 Formation of $M^{2+}(C_3H_8)$ species**

The interaction of adsorbed alkane molecules with a zeolite is normally dominated by dispersive forces between alkane and zeolite oxygen atoms. Recent simulation results for alkane adsorption on Na-exchanged zeolites revealed that alkane adsorption is also strongly determined by the sodium cations at low and intermediate loadings, since they create additional single interaction centers, which act as “extra wall”<sup>33;34</sup>. At low coverage, this “extra wall” interaction is even more important since such adsorbate-adsorbent interaction is stronger than the adsorbate interaction with oxygen atoms of the zeolites<sup>35</sup>. The propane adsorption experiment in this study was carried out at low propane coverage. Thus, propane adsorption is mainly dominated by the interaction between propane and the alkaline-earth cations. Consequently, the cation induced dipole polarization in propane should affect the propane vibration modes observed in the infrared spectra.

In general, compounds containing methyl - metal atom coordination give rise to the normal  $CH_3$  vibrations, where the positions of bands due to asymmetric stretching and deformation vibrations are little affected by changing the metal atom, whereas the symmetric stretching and deformation vibration are very sensitive to such changes. The latter vibrations both move to lower frequencies compared to the gas phase, and the associated absorption band is characteristically getting intense and sharp<sup>22</sup>. Our observation that the propane symmetric stretching vibration shifts to lower frequency in the order BaY (2847 $cm^{-1}$ ) < SrY (2838 $cm^{-1}$ ) < CaY (2834 $cm^{-1}$ ) < MgY (2803  $cm^{-1}$ ), points to an increased interaction between the propane and the cations (Figure 6-2). Although the infrared intensities of the propane



methylene group in the adsorbed phase differ from the gas phase spectrum, the frequencies are only slightly affected by the type of cation except for  $Mg^{2+}$  (Figure 6-2). From this result we concluded that propane indeed interacts with the cation site *via* its methyl group.



**Scheme 6-1.** Geminal structures formed after adsorption of oxygen and propane on supercages in earth alkaline exchanged Y zeolite

Interestingly, the propane methyl vibrations on CaY, SrY and BaY clearly differ from the gas phase spectrum, while the spectrum for MgY resembles the gas phase much more, except for the band at  $2803\text{ cm}^{-1}$ . These observations can be explained by a propane molecule adsorption geometry in which for CaY, SrY and BaY both methyl groups are coordinating to cations, while for MgY only one end of the molecule is perturbed. In principle, two cations can be located in one supercage, however, the distance between two cations (about  $0.7\text{ nm}$ ) would be much larger than the size of the propane molecule ( $0.43\text{ nm}$ ). As a result, linear coordination of one propane molecule to two cations in the supercage is almost impossible. Therefore, we suggest a cyclic geometry of propane adsorbed on  $Ca^{2+}$ ,  $Sr^{2+}$  or  $Ba^{2+}$  (see Scheme 6-1). In such geometry, the methylene group will only be slightly affected by these cations, as has been found in the spectra (Figure 6-2). Similar to the oxygen adsorption results, for MgY a result different from the trend in the larger cations was obtained. Oxygen adsorption revealed that  $Mg^{2+}$  cations have a lower effective electrostatic field than expected on the charge to radius ratio, which could be explained by stronger shielding of the six-ring zeolite oxygen atoms. The large shift observed for

both the methyl and methylene stretch frequencies confirms the linear adsorption geometry of propane to  $Mg^{2+}$  cations, since only one methyl-group is perturbed via electrostatic interaction with the cation. As a consequence, most of the propane C-H vibrations resemble the gas phase spectrum. Since only one methyl group is close to the cation for MgY, the effective polarization on this group is larger than in the case of a circular geometry where two methyl groups contribute to a lower effective electrostatic field (Scheme 6-1).

#### **6.4.1.3 Formation of $M^{2+}(O_2)(C_3H_8)$ species**

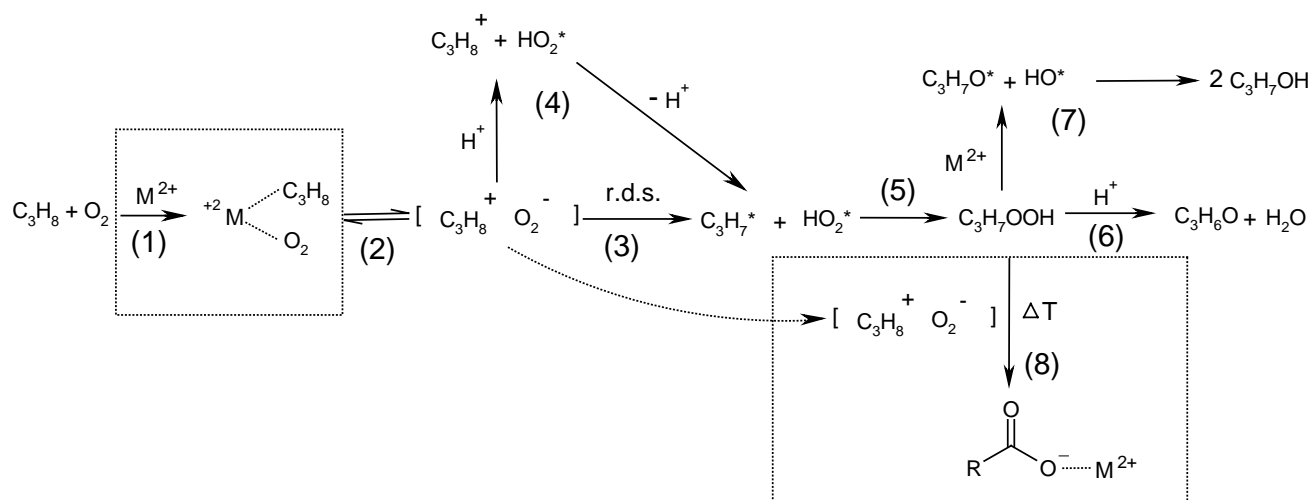
Co-adsorption of oxygen and propane on CaY clearly showed competitive adsorption between propane and oxygen since the intensity of the oxygen band decreased with increasing propane coverage (Figure 6-3). Since oxygen is a weaker base compared to propane, propane adsorption at the supercage cation is energetically favorable. Nevertheless, the space available at the  $Ca^{2+}$  supercage site could allow both propane and oxygen to adsorb simultaneously on a cation to form a so-called geminal species<sup>30-32</sup>. Due to the close proximity of the large propane molecule to the adsorbed oxygen, the oxygen molecule loses its librational or rotational freedom. This phenomenon is reflected by the disappearance of the side bands of the oxygen stretch vibration in the infrared spectra when increasing propane loading (Figure 6-3). Moreover, shielding of the electrostatic field by the adsorbed propane molecule weakens the electrostatic interaction between the remaining oxygen molecule and the  $Ca^{2+}$  site. Consequently, the infrared oxygen band decreased in intensity and shifted to lower wavenumber from  $1555\text{ cm}^{-1}$  to  $1550\text{ cm}^{-1}$ . Further, during the reaction, this band decreases its intensity (Figure 6-3b). Depletion of adsorbed propane infrared intensity has also been reported during the reaction, and was attributed to accumulation of adsorbed products acetone and water in the catalyst surface<sup>13</sup>.

In literature it was reported that oxidation reactions of olefins or alkyl benzenes could not be observed at room temperature<sup>6</sup>, even though the ionization potentials of these molecules are lower than for alkanes. Shielding of the cation electrostatic field as a result of hydrocarbon adsorption could account for this observation. Since olefins and alkyl-benzenes have a much higher electron density than alkanes, their adsorption could virtually diminish the electrostatic field of the cation. As a result, oxygen will not adsorb at the cation site to form a  $M^{2+}(O_2)(C_xH_y)$  complex and no reaction occurs.

Moreover, for MgY a much lower activity was reported than would be expected based on its charge to radius ratio. This can as well be explained by the fact that an active  $Mg^{2+}(O_2)(C_xH_y)$  complex is not easily formed. First, as discussed before,  $Mg^{2+}$  cations are located much closer to the six-ring window of the zeolite and therefore exhibit less possible coordination sites, resulting in a linear propane coordination. Second, as a result of its position, the electrostatic field is lowered to an effective field

similar to  $Ba^{2+}$  ions. Third, the lowest fraction of bare  $Mg^{2+}$  cations due to the applied activation procedure as was reported before<sup>12</sup>. All these facts slow down the oxidation reaction.

From these results we propose that the formation of a geminal  $M^{2+}(O_2)(C_3H_8)$  species with propane coordinated in a ring geometry with the cation (Scheme 6-1) is the precursor species for the thermal oxidation of propane by oxygen.



**Scheme 6-2.** Extended reaction mechanism of propane selective oxidation, in which formation of geminal precursor of the transition for electron transfer and parallel reaction for formation of monodenate carboxylate are emphasized

#### 6.4.2 Extended reaction scheme.

Although the formation of a charge transfer complex has been proposed to be the first step in the reaction mechanism of photon-induced selective oxidation of propane, until now no information was available of the species involved in the thermal oxidation of propane. Clearly, the results of this study point to the importance of a  $M^{2+}(O_2)(C_3H_8)$  complex as a first step in the reaction. The formation of a  $M^{2+}(O_2)(C_3H_8)$  precursor facilitates the selective oxidation of propane since both oxygen and propane are activated by the polarization induced by the electrostatic field of the  $M^{2+}$  cation. Further, in such a complex both molecules are close together facilitating their interaction. Providing the presence of a minimal required cationic electrostatic field, the  $M^{2+}(O_2)(C_3H_8)$  complex would decrease the activation energy to allow electron transfer from the polarized propane molecule to the activated oxygen molecule even at room temperature which results in the charge-transfer state  $[C_3H_8^+O_2^-]$ <sup>36</sup> (Scheme 6-2). Although it has been claimed that the charge-transfer state is stabilized in the electrostatic field of the

supercage<sup>6;37</sup>, until now no proof has been given for the existence of electron transfer in the thermal reaction mechanism. This will be subject of future calculations and experiments.

#### **6.4.2.1 Parallel reactions**

At room temperature, acetone and water were produced exclusively on cation exchanged Y zeolite at room temperature (from step 1 to step 6 in Scheme 6-2). However, increasing temperature to 80°C, selectivity decreased due to the formation of 2-propanol and carboxylate species (Figure 6-5 and 6-6). The formation of 2-propanol was explained recently by homolytic IHP decomposition at the cation site (step 7 in Scheme 6-2)<sup>24</sup>. The polarizing effect on IHP is larger for supercage Ca<sup>2+</sup> than for Sr<sup>2+</sup>, resulting in 2-propanol formation to increase in the order SrY < CaY (Figure 6-5). In the case of MgY, heterolytic elimination of water from IHP is dominated due to the combination of the low electrostatic field of Mg<sup>2+</sup> and its high Brønsted acidity<sup>25</sup>.

The pathway for formation of carboxylate species at 80°C is less clear. Comparison of formate and acetate adsorbed on CaY and SrY revealed that these species can be excluded. Unfortunately, the infrared intensity in the C-H stretching vibration range is too weak to be identified. However, both  $\nu_{as}(\text{COO})$  and  $\nu_s(\text{COO})$  frequencies of the carboxylate move to lower wavenumber for CaY compared to SrY. Further, the difference between the symmetrical and asymmetrical COO stretching vibration increases for SrY (217cm<sup>-1</sup>) compared to CaY (210cm<sup>-1</sup>). Same trends have also been observed for adsorbed monodentate carboxylate surface species on alkali ion exchanged X zeolites<sup>38</sup>. Moreover, TPD experiments after reaction showed that similar to acetone, this carboxylate species is also strongly adsorbed on the surface and less than 15% could be desorbed even at 500°C (Figure 6-7). CO was detected after 350°C and gained intensity with temperature (Figure 6-7), which is typical for monodentate carboxylate decomposition product<sup>39</sup>.

From Figure 6-8 it can be seen that the highest amount of carboxylate is produced when IHP is pre-adsorbed on SrY and propane and oxygen are added. Moreover, with additional IHP, more carboxylate is produced in the propane oxidation process compared to the reaction over clean SrY. For most oxidation reactions, carboxylates are produced by further oxidation of a ketone<sup>40</sup>. However, hardly any carboxylate could be observed from thermal reaction at 353K of either IHP or acetone (Figure 6-8). Moreover, carboxylate formation increased (MgY < CaY < SrY) with decreasing IHP decomposition rate (MgY > CaY > SrY), in other words, with higher IHP concentration on the catalyst surface. From this we conclude that the mechanism of carboxylate formation is most likely through a reaction of IHP with propane and oxygen. Further, it was also observed that carboxylate formation increased with decreasing proton transfer rate (propane < d<sub>2</sub>-propane) (Figure 6-5 and 6-6). In addition, it is known that

peroxides are capable of oxidizing alkanes at low temperature <sup>41</sup>. For this reason we propose the following side reaction, for the moment assuming that indeed a charge-transfer complex forms out of the precursor (step 8, scheme 6-2):



## 6.5 Conclusion

Unlike the normal redox property of metal oxides applied in traditional heterogeneous catalytic oxidation of alkanes, the nonredox alkaline earth cations in the supercage of Y zeolite provide a specific adsorption geometry to invoke reaction. Oxygen and propane are activated by simultaneous adsorption at the supercage cation site to form geminal species exclusively *via* electrostatic cation-adsorbate interaction. The extent of activation of propane and oxygen in Y-zeolites is determined by the high electrostatic field of supercage cations associated with the formation of a  $M^{2+}(O_2)(C_3H_8)$  complex in which propane forms a ring structure with the cation. This species facilitates both molecules interaction to initiate charge transfer, which product is stabilized in the supercage electrostatic field. The activity of propane selective oxidation to acetone increased in order BaY < MgY < SrY < CaY, which is in agreement with oxygen polarization induced by the electrostatic field of  $M^{2+}$  cations. The results also clearly demonstrate that the selectivity of propane oxidation is influenced by reaction temperature, cation Lewis acidity, rate of isopropylhydroperoxide (IHP) decomposition, and rate of proton abstraction from charge-transfer complex.

### Reference List

1. Centi, G.; Misono, M. *Catalysis Today* **1998**, *41*, 287-296.
2. Centi, G.; Cavani, F.; Trifiro, F. *Selective oxidation by heterogeneous catalysis*, Kluwer Academic/Plenum Publishers: New York, 2000.
3. Bielanski, A.; Haber, J. *Oxygen in catalysis*, Marcel Dekker, Inc.: 1991.
4. Mijs, W. J.; De Jonge, C. R. H. I. *Organic syntheses by oxidation with metal compounds*, Plenum Press, New York: 1986.
5. Blatter, F.; Sun, H.; Frei, H. *Chemistry-A European Journal* **1996**, *2*, 385-389.
6. Blatter, F.; Sun, H.; Vasenkov, S.; Frei, H. *Catalysis Today* **1998**, *41*, 297-309.
7. Larsen, R. G.; Saladino, A. C.; Hunt, T. A.; Mann, J. E.; Xu, M.; Grassian, V. H.; Larsen, S. C. *Journal of Catalysis* **2001**, *204*, 440-449.
8. Sun, H.; Blatter, F.; Frei, H. *Journal of the American Chemical Society* **1996**, *118*, 6873-6879.
9. Sun, H.; Blatter, F.; Frei, H. *Catalysis Letters* **1997**, *44*, 247-253.

10. Vanoppen, D. L.; DeVos, D. E.; Jacobs, P. A. *Progress in Zeolite and Microporous Materials, Pts A-C* **1997**, *105*, 1045-1051.
11. Vanoppen, D. L.; De Vos, D. E.; Jacobs, P. A. *Journal of Catalysis* **1998**, *177*, 22-28.
12. Xu, J.; Mojet, B. L.; Ommen, J. G. v.; Lefferts, L. *Phys.Chem.Chem.Phys.* **2003**, *5*, 4407-4413.
13. Xu, J.; Mojet, B. L.; Ommen, J. G. v.; Lefferts, L. *Journal of Physical Chemistry B* **2004**, *108*, 15728-15734.
14. Jousse, F.; Lara, E. C. D. *Journal of Physical Chemistry* **1996**, *100*, 233-237.
15. Jousse, F.; Lara, E. C. D. *Journal of Physical Chemistry* **1996**, *100*, 238-244.
16. Smudde, G. H.; Slager, T. L.; Weigel, S. J. *Applied Spectroscopy* **1995**, *49*, 1747-1755.
17. Hughes, T. R.; White, H. M. *Journal of Physical Chemistry* **1967**, *71*, 2192-2201.
18. Brugmans, M. J. P.; Bakker, H. J.; Lagendijk, A. *Journal of Chemical Physics* **1996**, *104*, 64-84.
19. Ward, J. W. *Journal of Physical Chemistry* **1968**, *72*, 4211-4223.
20. Gough, K. M.; Murphy, W. F. *Journal of Physical Chemistry* **1987**, *87*, 3332-3340.
21. Gayles, J. N.; King, W. T. *Spectrochimica Acta* **1965**, *21*, 543-557.
22. George Socrates *Infrared and Raman characteristic group frequencies : tables and charts*, 3rd ed.; 2001.
23. *The hand book of Infrared and Raman spectra of inorganic compound and organic salts*, San Diego, CA [etc.] : Academic Press: 1997.
24. Xu, J.; Mojet, B. L.; Ommen, J. G. v.; Lefferts, L. *Journal of Catalysis* **2004**, *Submitted*.
25. Xu, J.; Mojet, B. L.; Ommen, J. G. v.; Lefferts, L. *Journal of Physical Chemistry B* **2004**, *108*, 218-223.
26. Bajusz, I. G.; Goodwin, J. G. *Langmuir* **1998**, *14*, 2876-2883.
27. Se Bok Jang; Mi Suk Jeong; Yang Kim; Seong Hwan Song; Karl Seff. *Microporous and Mesoporous Materials* **1999**, *28*, 173-183.
28. Se Bok Jang; Mi Suk Jeong; Yang Kim; Seong Hwan Song; Karl Seff. *Microporous and Mesoporous Materials* **1999**, *30*, 233-241.
29. Vavssilov, G.; Staufer, M.; Belling, T.; Neyman, K.; Knozinger, H.; Rosch, N. *Journal of Physical Chemistry B* **1999**, *103*, 7920.
30. Hadjiivanov, K.; Ivanova, E.; Klissurski, D. *Catalysis Today* **2001**, *70*, 73-82.
31. Hadjiivanov, K.; Knozinger, H.; Ivanova, E.; Dimitrov, L. *Phys.Chem.Chem.Phys.* **2001**, *3*, 2531-2536.
32. Hadjiivanov, K.; Ivanova, E.; Knozinger, H. *Microporous and Mesoporous Materials* **2003**, *58*, 225-236.
33. Beerdsen, E.; Smit, B.; Calera, S. *Journal of Physical Chemistry B* **2002**, *106*, 10659-10667.
34. Beerdsen, E.; Dubbeldam, D.; Smit, B.; Vlugt, T. J. H.; Calera, S. *Journal of Physical Chemistry B* **2003**, *107*, 12088-12096.
35. Calera, S.; Dubbeldam, D.; Krishna, R.; Smit, B.; Vlugt, T. J. H.; Denayer, J. F. M.; Martens, J. A.; Maesen, T. L. M. *Journal of the American Chemical Society* **2004**, *126*, 11377-11386.

36. Li, P.; Xiang, Y.; Grassian, V. H.; Larsen, S. C. *Journal of Physical Chemistry B* **1999**, *103*, 5058-5062.
37. Frei, H. *3Rd World Congress on Oxidation Catalysis* **1997**, *110*, 1041-1050.
38. Rep, M. Side Chain Alkylation of Toluene with Methanol over Basic Zeolites. Thesis, University of Twente, 2002.
39. Borowiak, M. A.; Jamroz, M. H.; Larsson, R. *Journal of Molecule Catalysis A: Chemical* **1999**, *139*, 97.
40. Centi, G.; Corberan, V. C.; Perathoner, S.; Ruiz, P. *Catalysis Today* **2000**, *61*, 1.
41. Saul Patai *The chemistry of functional groups, The chemistry of peroxides*, Jone Wiley & Sons Ltd.: 1983.

## Chapter 7

### **Effect of Zeolite Geometry for Propane Selective Oxidation on Cation Electrostatic Field of $\text{Ca}^{2+}$ Exchanged Zeolites**

---

**Abstract:** *The effects of zeolite geometry on propane selective oxidation were studied by in-situ infrared spectrometry on  $\text{Ca}^{2+}$  exchanged Y, MOR and ZSM5 zeolites. Oxygen and propane adsorption at room temperature, revealed that the electrostatic field of  $\text{Ca}^{2+}$  increased in the order  $\text{CaY} < \text{CaMOR} < \text{CaZSM5}$ . The electrostatic field of  $\text{Ca}^{2+}$  cation in CaY and CaZSM5 was observed to correlate with propane selective oxidation activity and selectivity. At 353K, low activity but high selectivity to acetone was observed for propane oxidation on CaY zeolite, while high activity and a 2:1 mixture of 2-propanol and acetone on CaZSM5 zeolites revealed a typical homolytic peroxide decomposition. On CaMOR, the steric restriction for accommodating isopropylhydroperoxide (IHP) resulted in the lowest activity for propane oxidation. Further, the high Brønsted acidity combined with the large propane polarization in CaMOR resulted in propane deep oxidation to form CO and  $\text{CO}_2$ . It is convincingly showed that the electrostatic field of  $\text{Ca}^{2+}$  cations, the geometrical structure of a zeolite and the presence of Brønsted acid sites play important roles in determining activity and selectivity of propane partial oxidation on  $\text{Ca}^{2+}$  exchanged zeolites.*



## 7.1 Introduction

Recently, a new approach of photo or thermal selective oxidation of alkanes on alkali or alkaline-earth exchanged Y zeolite at low temperature was presented and gave an interest in the research of partial oxidation process<sup>1-7</sup>. It was proposed that the reaction involved the formation of an ion pair of hydrocarbon and oxygen ( $\text{C}_n\text{H}_{2n+2}^+\text{O}_2^-$ ), which stabilized in the electrostatic field of cation-exchanged Y zeolite. The alkyl hydroperoxide is produced from this charge transfer state and further goes on to form carbonyl containing product exclusively by elimination of water. The good activity and selectivity of this reaction is suggested to depend on both the electrostatic field at the cation site and the dynamics of the reactant molecules within the confined zeolite structure. Therefore, the zeolite structure, the framework composition, and the identity of the charge compensating cation are parameters that can be expected to impact catalytic activity and selectivity in zeolite catalyzed selective oxidation of alkanes.

Barium exchanged X, Y, ZSM5 and Beta have been used to investigate photo-oxidation of 1-alkenes, toluene and p-xylene<sup>2;6</sup>. However, selectivity was found to dramatically decrease in the order  $\text{X} > \text{Y} > \text{Beta} > \text{ZSM5}$ , which was attributed to the presence of residual Brönsted acid sites in these zeolites. The results also revealed that shape selectivity played an important role in determining product selectivity in side condensation reactions<sup>6</sup>.

Nevertheless, no results have been published for the influence of the zeolite host for the thermally activated alkane oxidation on cation-exchanged zeolites. Experimental results of CO adsorption showed that the electrostatic field increases with divalent cations versus monovalent cations for a given zeolite host, and for a given cation increases for zeolites with higher Si/Al ratios<sup>2;6</sup>. In our previous work, we

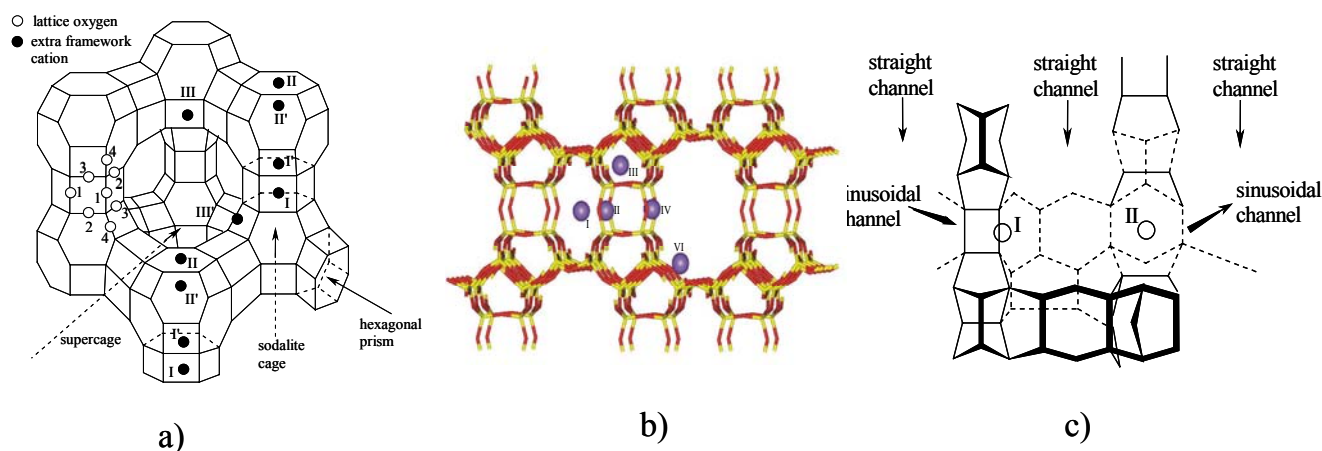


**Figure 7-1.** a) Framework structure of Y zeolite, with cation sites shown; b) Framework structure of mordenite, with cation sites shown; c) View of the [100] plane of MFI (ZSM5) with cation sites shown

have systematically investigated thermal propane selective oxidation to acetone on alkaline earth exchanged Y zeolite. The results have convincingly shown that activity and selectivity of propane oxidation to acetone were influenced not only by the electrostatic field of earth-alkali cations, but also the cation location and the Brønsted acidity of Y zeolite. So if oxidation of hydrocarbons in zeolites is a general phenomenon, then the shape and size of zeolites may potentially be used to better control activity and selectivity of the thermal propane selective oxidation reaction.

In this work, we have investigated two other types of  $\text{Ca}^{2+}$  exchanged zeolites: mordenite and ZSM5, in addition to  $\text{Ca}^{2+}$  exchanged Y zeolite. Zeolite Y is the synthetic form of faujasite and has a Si/Al ratio between 2 – 5. Its three dimensional framework has two main cages: the large supercage results from an assembly of the basic units, the sodalite cages (Figure 7-1a). The spherical supercages are approximately 1.3 nm in diameter. Access to supercages is afforded by four 12-membered ring windows about 0.74nm in diameter, which are tetrahedrally distributed around the center of the supercages. Cations can occupy three positions in Y zeolite (see Figure 7-1a). “Large pore” mordenite is a one-dimensional zeolite consisting of main channels parallel to the [001] crystal plane. The channels have a lightly elliptical cross section of a 12 membered ring with a diameter of 0.7 x 0.65nm (Figure 7-1b). Single crystal refinement of dehydrated NaMOR has revealed 5 different sites for cation location (see Figure 7-1b) <sup>8</sup>. Zeolite ZSM5 with medium pore sizes is characterized by a two-dimensional pore system with straight, parallel channels intersected by zigzag channels (Figure 7-1c). Both channels consist of 10 membered rings with diameter of 0.53 x 0.56nm in case of the straight channels and 0.51 x 0.5nm in case of the sinusoidal channels. IR studies of  $\text{H}_2$  and CO adsorption indicated that the cations are preferentially located at the intersections of the sinusoidal and straight channels at the edge of a 4-membered ring (site I) <sup>9;10</sup>. Additionally, small cations, like  $\text{Na}^+$  are also found in small cavities above the sinusoidal channel (site II), but MAS-NMR studies showed only a very low occupancy of this location (10%) (Figure 7-1c) <sup>11</sup>.

Propane selective oxidation on CaY zeolite at room temperature showed that  $\text{Ca}^{2+}$  in the supercage (site II) provided the specific adsorption geometry to invoke reaction <sup>12;13</sup>. Slightly increasing Brønsted acidity could enhance reaction activity, but induced lower selectivity to acetone due to a minor amount of 2-propanol formation. In this study, the activity and selectivity of thermal propane oxidation over  $\text{Ca}^{2+}$  exchanged MOR and ZSM5 zeolites were compared with CaY by infrared spectroscopy to resolve effect of zeolite geometry and Si/Al ratio on the selective propane oxidation mechanism.

## 7.2 Experimental

### 7.2.1 Materials

Zeolites CaY, CaMOR and CaZSM5 were prepared from respectively NaY (Zeolyst), NH<sub>4</sub>MOR (Zeolyst), NH<sub>4</sub>ZSM5 (Zeolyst). The parent zeolites were exchanged three times with 0.1M solution of calcium nitrate (Merck) for 20 hours at 90 °C under stirring. The resulting cation exchanged zeolites were washed three times with distilled water, filtered and dried overnight at 100 °C. The final form of CaMOR and CaZSM5 were obtained by calcination at 500°C under vacuum. The chemical compositions of catalysts (determined by X-ray fluorescence (XRF)), Ca<sup>2+</sup>/Al and NH<sub>4</sub><sup>+</sup>/Al ratio, as well as sample name are listed in Table 7-1.

**Table 7-1. Zeolite chemical composition (determined by XRF)**

<b>Zeolite<sup>(1)</sup></b>	<b><u>Chemical composition (wt%)</u></b>				<b><u>Molar ratio</u></b>			
	Na <sub>2</sub> O	Al <sub>2</sub> O <sub>3</sub>	SiO <sub>2</sub>	CaO	Si/Al	Na <sup>+</sup> /Al	Ca <sup>2+</sup> /Al	NH <sub>4</sub> <sup>+</sup> /Al <sup>(2)</sup>
CaY	1.087	21.76	65.99	11.12	2.6	0.08	0.47	/
CaMOR	0	7.31	88.66	3.14	10	0	0.39	0.22
CaZSM5(25)	0.03	3.32	95.32	1.29	25	0.01	0.35	0.29
CaHZSM5(38)	0	2.18	96.84	0.91	38	0	0.38	0.24

<sup>(1)</sup> CaY sample was prepared from Na type. CaZSM5 and CaMOR samples were prepared from NH<sub>4</sub> type. <sup>(2)</sup> NH<sub>4</sub><sup>+</sup> content was calculated based on the charge balance

### **7.2.2 Infrared Spectroscopy**

The zeolite powder (30mg) was pressed into a self-supporting wafer and analyzed *in-situ* during adsorption and reaction by means of transmission FTIR spectroscopy using a Bruker Vector22 FTIR spectrometer with a MCT detector. A miniature cell, equipped with NaCl transparent windows, which can be evacuated to pressures below 10<sup>-7</sup> mbar was used for the *in-situ* experiments. The temperature is variable from room temperature to 500°C. Each spectrum consists of 32 scans taken at 4cm<sup>-1</sup> resolution.

The samples were activated in vacuum (<10<sup>-7</sup>mbar) at 500°C (ramp 10°C/min) for 2 hours, subsequently cooled down to 200°C (dwell 10 hours), and cooled to room temperature. Loading of reactants (propane and oxygen) was controlled by gas pressure. Propane was introduced into the IR cell until equilibrium was reached at 1 mbar in the gas phase, followed by addition of 40 mbar of oxygen. A calibration curve was made by adsorption of known amounts of acetone and 2-propanol at room

temperature in order to determine the quantity of produced acetone and 2-propanol from propane and oxygen. The FTIR spectra were corrected for absorption of the activated zeolite.

## 7.3 Results

### 7.3.1 Catalyst characterization

Calibrated transmission FTIR spectra of the activated calcium exchanged zeolites are given in Figure 7-2. All samples showed an isolated silanol peak at  $3740\text{cm}^{-1}$  (ZSM5) and  $3744\text{cm}^{-1}$  (Y and MOR), which is either on the outer surface terminating the zeolite crystals or on silica impurities<sup>14;15</sup>. Bridging hydroxyl groups (SiOHAl groups, Brönsted acid sites) gave rise to IR absorption at  $3644\text{cm}^{-1}$  (Y),  $3616\text{cm}^{-1}$  (MOR) and  $3616\text{cm}^{-1}$  (ZSM5). High Brönsted acid site concentration was observed on CaMOR zeolite. For CaZSM5 with higher Si/Al ratio (CaZSM5(38)) the lowest amount of Brönsted acid sites were observed. The source of Brönsted acid sites is twofold. First, decomposition of  $\text{NH}_4^+$  ions due to incomplete exchange by  $\text{Ca}^{2+}$  cation (MOR and ZSM5) as determined by XRF elemental analysis (Table 7-1). Second, hydrolysis of water at  $\text{Ca}^{2+}$  sites during the activation procedure, according to:  $\text{Ca}^{2+} + \text{H}_2\text{O}(\text{ad}) + \text{Si-O-Al} \rightarrow \text{Ca}(\text{OH})^+ + \text{Si-O}(\text{H}^+)-\text{Al}$

This reaction is thought to occur during activation at elevated temperature (for all studied zeolites)<sup>1;14;15</sup>. The hydroxyl vibration at  $3590\text{cm}^{-1}$  for CaY results from  $\text{Ca}(\text{OH})_x$  species<sup>1</sup>. However, no  $\text{Ca}(\text{OH})_x$  species could be observed on CaMOR and CaZSM5, most likely due to the fact that this small peak is masked by the nearby high intensity hydroxyl vibration of Brönsted acid sites at  $3616\text{cm}^{-1}$ .

On ZSM5, a very broad band with maximum intensity around  $3470\text{cm}^{-1}$  belongs to perturbed hydroxyl groups that result from the presence of hydrogen bonding between OH groups and zeolite lattice oxygen<sup>15</sup>.

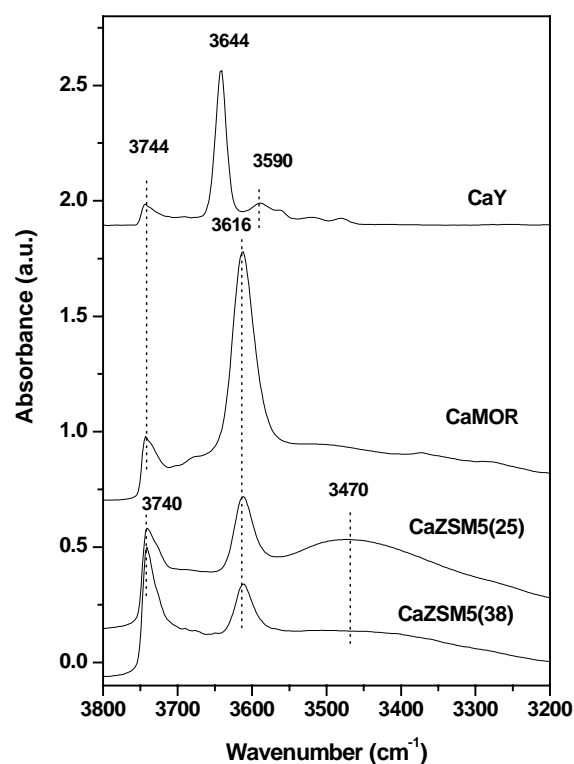


**Figure 7-2.** Infrared spectra of  $\text{Ca}^{2+}$  exchanged Y, MOR and ZSM5 zeolites.

### 7.3.2 Oxygen adsorption

Figure 7-3 shows the room temperature infrared absorption of  $\text{O}_2$  in  $\text{Ca}^{2+}$  exchanged Y, MOR and ZSM5 zeolites at 40mbar  $\text{O}_2$  equilibrium pressure. Clear broad bands appeared at  $1554\text{cm}^{-1}$  (CaZSM5),  $1555\text{cm}^{-1}$  (CaY) and  $1550\text{cm}^{-1}$  (MOR), which can be attributed to the O-O stretch vibration in adsorbed  $\text{O}_2$  <sup>13;16-18</sup>. High intensity of this band was found for CaZSM5, while with higher Si/Al ratio of CaZSM5, intensity slightly decreased. On CaMOR this band showed an asymmetric shape and could be separated to two peaks located at  $1554\text{cm}^{-1}$  and  $1550\text{cm}^{-1}$ . The peak intensity at  $1554\text{cm}^{-1}$  is slightly bigger than at  $1550\text{cm}^{-1}$ .

Further, two small side bands of adsorbed oxygen species were also found at high frequency side (about  $1570\text{cm}^{-1}$ ) and low frequency side (about  $1542\text{cm}^{-1}$ ) on the studied  $\text{Ca}^{2+}$  exchanged zeolites.

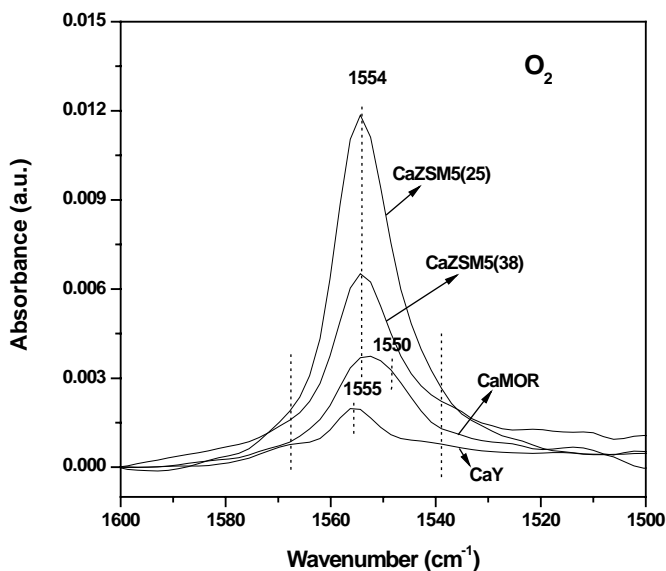


**Figure 7-3.** Infrared spectra of room temperature oxygen adsorption at 40mbar on  $\text{Ca}^{2+}$  exchanged zeolites

### 7.3.3 Propane adsorption.

Figure 7-4 displays the infrared spectra of propane adsorption on  $\text{Ca}^{2+}$  exchanged zeolites as function of propane partial pressure in the C-H stretch vibration range ( $3100\text{-}2600\text{cm}^{-1}$ ). Two main bands at  $2970\text{cm}^{-1}$  (methyl asymmetric stretching) and  $2838\text{cm}^{-1}$  (methyl symmetric stretching) were observed when propane adsorbed on CaY. Both band intensities steadily increase with increasing propane partial pressure. On CaMOR and CaZSM5, at the propane partial pressure below 0.2mbar, two main bands at  $2965\text{cm}^{-1}$  (both CaMOR and CaZSM5(25)), and  $2829\text{cm}^{-1}$  (CaMOR) or  $2826\text{cm}^{-1}$  (CaZSM5(25)) were found and increased in intensity with increasing propane partial pressure. With further increasing propane partial pressure the band intensities at  $2829\text{cm}^{-1}$  (CaMOR) and  $2826\text{cm}^{-1}$  (CaZSM5) did not vary significantly, however, an additional band at  $2875\text{cm}^{-1}$  was observed. With increasing propane partial pressure, this peak increased together with the high frequency band at  $2965\text{cm}^{-1}$ .

For CaZSM5(38) similar trends were observed, however with lower intensities at a given propane partial pressure (not shown).

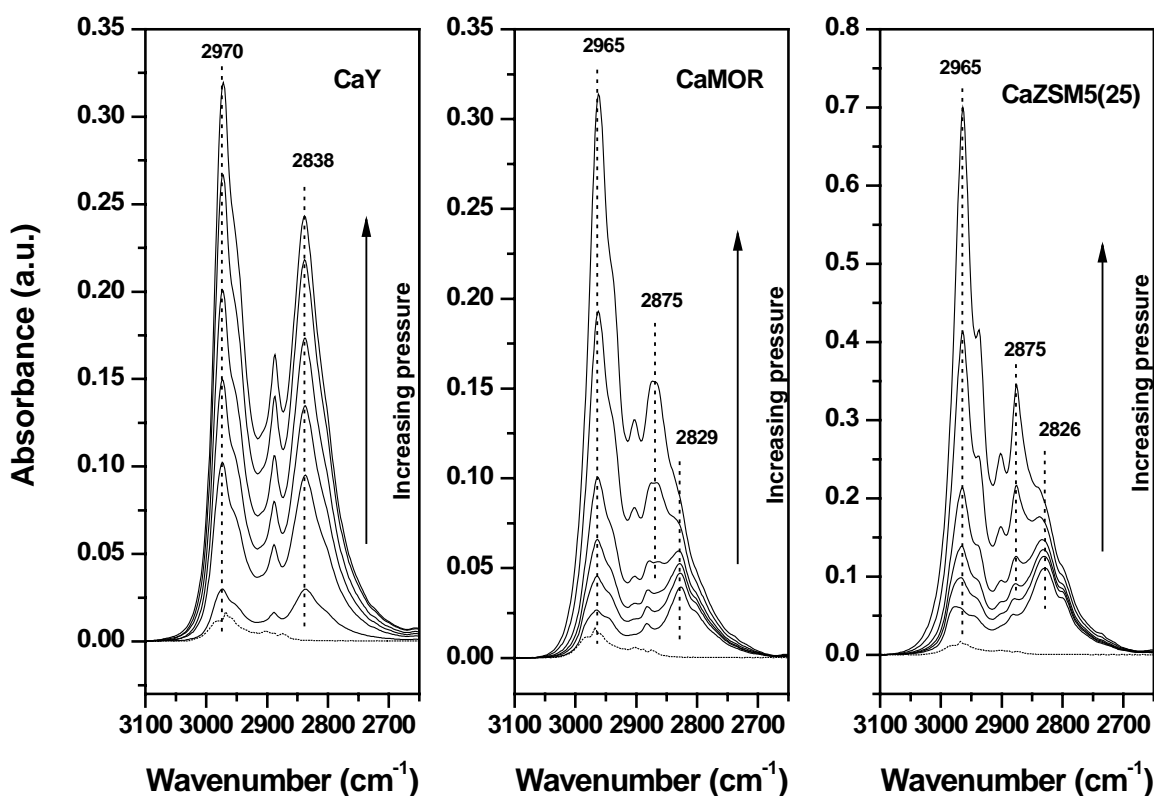


**Figure 7-4.** Infrared spectra of room temperature propane adsorption on  $\text{Ca}^{2+}$  exchanged zeolites with equilibrium propane partial pressure of 0.01, 0.05, 0.1, 0.2, 0.5 and 1 mbar. Dot line shows 1 mbar propane in gas phase.

### 7.3.4 Propane oxidation

Upon loading 1 mbar propane and 40 mbar oxygen on activated  $\text{Ca}^{2+}$  exchanged zeolites at  $80^\circ\text{C}$ , reaction was observed by following depletion of propane (band between  $3010$  and  $2600\text{cm}^{-1}$ ) and production of acetone (band at  $1682\text{cm}^{-1}$ ) and water (band at  $1634\text{cm}^{-1}$  (CaY),  $1640\text{cm}^{-1}$  (CaZSM5) and  $1627\text{cm}^{-1}$  (CaMOR)) (for experiment details see ref. 6 and 14). Figure 7-5 presents the infrared spectra after 20 hours reaction at  $80^\circ\text{C}$ . It is clear that acetone formation increased in the order  $\text{CaMOR} < \text{CaZSM5} < \text{CaY}$ . In addition to acetone and water, formation of  $\text{CO}_2$  and  $\text{CO}$  was found on CaMOR. From the infrared band structure it is clear that both  $\text{CO}$  and  $\text{CO}_2$  are trapped inside the CaMOR zeolite, since two single sharp bands appear near  $2215\text{cm}^{-1}$  ( $\text{CO}$ ) and  $2365\text{cm}^{-1}$  ( $\text{CO}_2$ ) in the infrared spectra. The vibrational band structure normally found for gas phase  $\text{CO}$  and  $\text{CO}_2$  is not observed. Also no  $\text{CO}_x$  was found in the gas phase by online mass spectrometry. No  $\text{CO}_x$  formation could be detected for CaY and CaZSM5 zeolites in both gas and solid phase. After 20 hours reaction, the systems with different

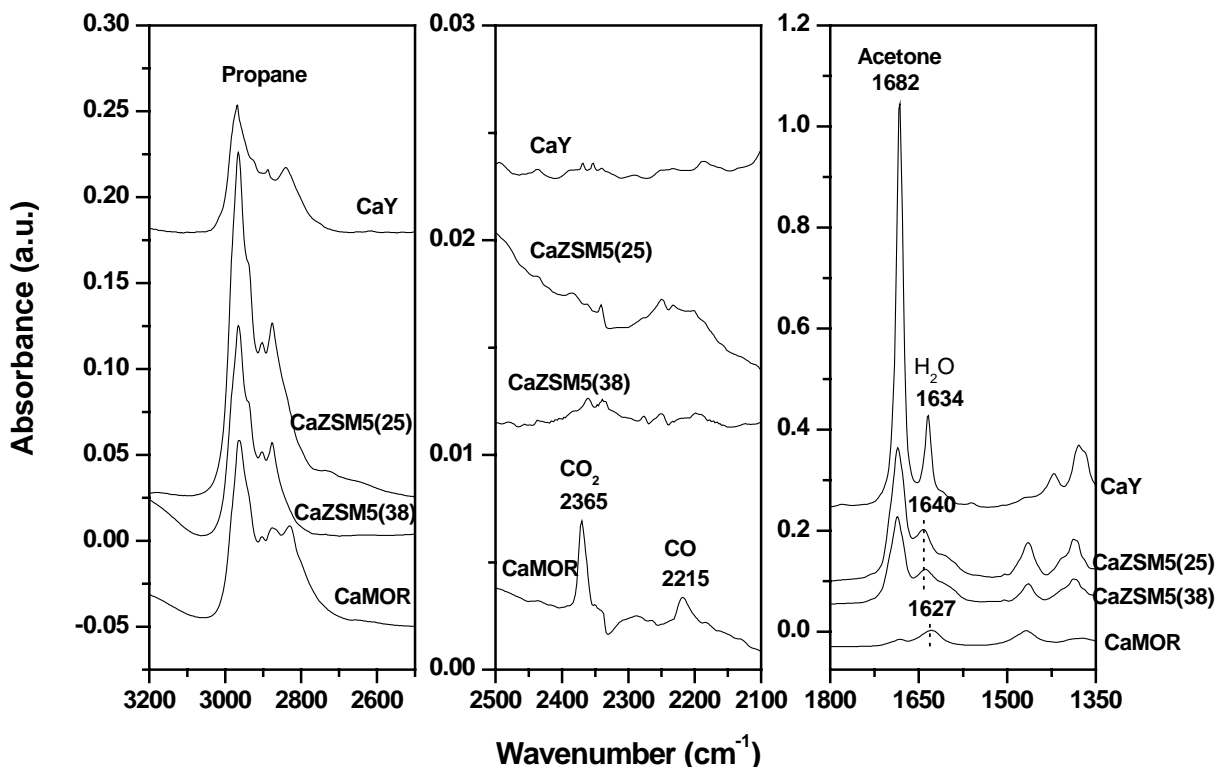


**Figure 7-5.** Infrared spectra after 20 hours propane oxidation at  $80^\circ\text{C}$  on  $\text{Ca}^{2+}$  exchanged zeolites.

zeolites were subsequently evacuated for 5 minutes to remove excess propane and oxygen. During evacuation, no acetone or 2-propanol were detected by on-line MS analysis. The infrared spectra afterwards are presented in Figure 7-6. Clearly bands can be observed between  $3100\text{-}2700\text{cm}^{-1}$  and  $1500\text{-}1300\text{cm}^{-1}$ , which were previously masked by the intensive bands of propane C-H vibration and deformation. The bands at  $3014$ ,  $2925$ ,  $1420$  and  $1379\text{cm}^{-1}$  can be attributed to acetone<sup>1</sup>. The frequencies at  $2989\text{cm}^{-1}$  for CaY (Figure 7-6a),  $2981$ ,  $2943$ ,  $2887$ ,  $1462$  and  $1385\text{cm}^{-1}$  for CaZSM5 (Figure 7-6b and 7-6c) match the bands of 2-propanol, which was confirmed by comparing the infrared spectra of 2-propanol loaded into the corresponding zeolites. On CaMOR, a small amount of propane is still left (band at  $2965$  and  $2829\text{cm}^{-1}$ , about 5% of total adsorbed propane before evacuation), even after evacuation for 30 minutes (Figure 7-6d). The intensity of CO ( $2215\text{cm}^{-1}$ ) and CO<sub>2</sub> ( $2365\text{cm}^{-1}$ ) on CaMOR decreased with evacuation (not shown). Evaluation of both intensities showed that about 30% of CO<sub>2</sub> and 15% CO desorbed after evacuation for 30 minutes. The CaMOR sample was then further heated to  $150^\circ\text{C}$  in vacuum (Figure 7-6e). Clearly, during this treatment propane desorbed as well as CO and CO<sub>2</sub> (not shown) No additional bands were observed within the noise level.

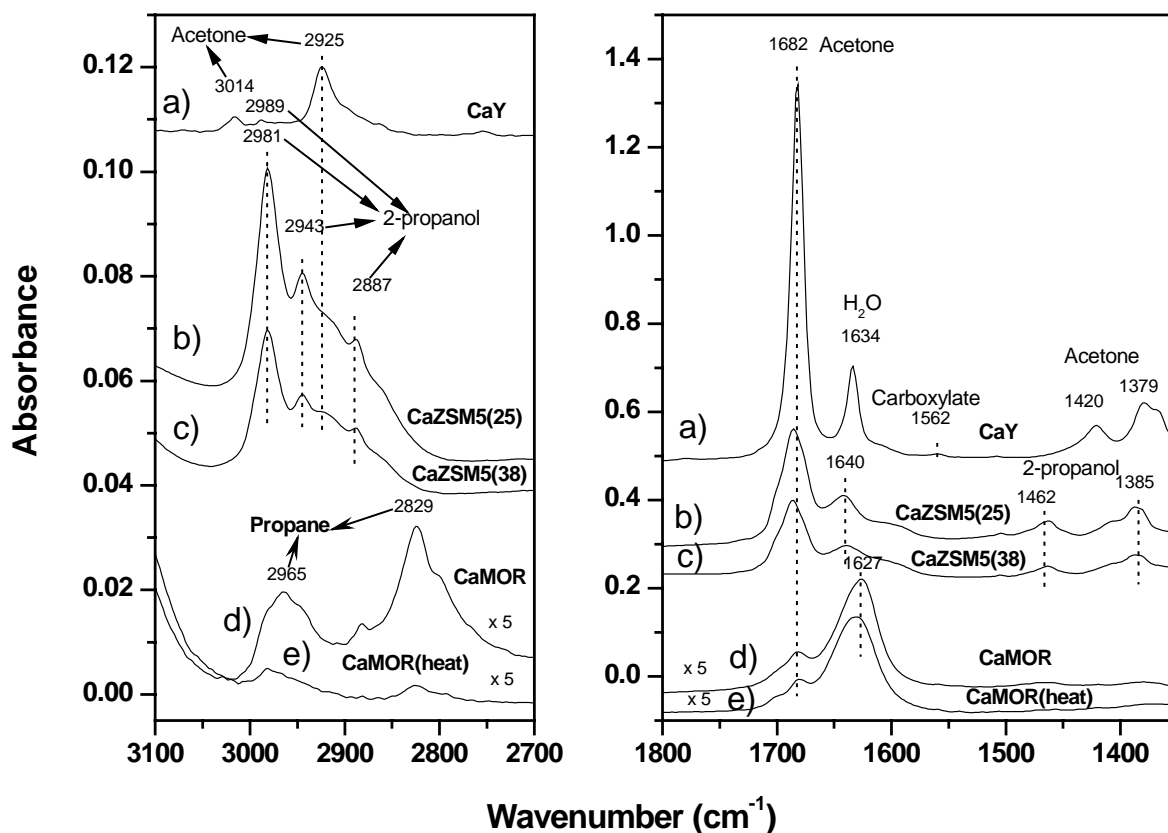


**Figure 7-6.** Infrared spectra a-d) after 20 hours propane oxidation at 80°C on Ca<sup>2+</sup> exchanged zeolites and subsequent evacuation for 5 minutes; e) after d, evacuated 30 minutes and followed heating to 150°C on CaMOR.

After 20-hour reaction at 80°C, lower acetone to water ratio was found on CaMOR than on CaY and CaZSM5 based on the infrared intensity of water (band at 1627-1640cm<sup>-1</sup>) and acetone (band at 1682cm<sup>-1</sup>). The amounts of acetone and 2-propanol produced on all zeolites after 20 hours reaction are listed in Table 7-2. High selectivity to acetone was found on CaY, while a 2:1 mixture of 2-propanol and acetone was observed on both CaZSM5(38) and CaZSM5(25) zeolites. Only 3% of acetone was produced on CaMOR compared to CaY. Further, based on amount of water produced on the catalysts in Figure 7-5, it also showed that much less propane was converted on CaMOR compared to CaY and CaZSM5.



**Table 7-2. Propane oxidation at 80°C on Ca<sup>2+</sup> exchanged zeolites**

Zeolite	Products (μmol/g)			(one + ol)/Ca <sup>2+</sup>
	Acetone	2-propanol	ol/one	(Molar ratio)
CaY	146.9	1.4	0.01	0.16 <sup>(1)</sup>
CaZSM5(25)	55.6	120.7	2.2	0.74 <sup>(2)</sup>
CaZSM5(38)	37.2	72.5	2.0	0.70 <sup>(2)</sup>
CaMOR	4.4	/	/	0.02 <sup>(3)</sup>

Note: Calculation based on <sup>(1)</sup> Ca<sup>2+</sup> cation in the supercage (site II); <sup>(2)</sup> all Ca<sup>2+</sup> cation; <sup>(3)</sup> Ca<sup>2+</sup> cation in the main channel (site IV)

## 7.4 Discussion

### 7.4.1 Effect of electrostatic field for reactants adsorption

In dried sodium and calcium exchanged Y zeolites, only 50-60% of the cations are located at site II, which is accessible to adsorbed molecules like propane<sup>12;19</sup>. For mordenite, the occupation of cation in five sites depends on the Si/Al ratio. The sodium cations in the MOR with Si/Al ratio of 10 has revealed that in each unit cell, 3 sodium cations located at site I (in side channel) and 2 cations occupied in site IV (in the intersection between inside eight-ring and main channel)<sup>20</sup>. The side channels are accessible only to small molecules like methane and oxygen. Larger hydrocarbons, like propane only access the main channels<sup>21</sup>.

This study shows that oxygen adsorption can be observed at room temperature in the infrared spectra between 1550-1555cm<sup>-1</sup> for calcium exchanged Y, MOR and ZSM5 zeolites (Figure 7-3). Study of oxygen adsorption on alkaline-earth exchanged Y zeolite revealed that oxygen could adsorb on alkaline-earth cation site *via* electrostatic interaction to form M<sup>2+</sup>(O<sub>2</sub>) species on the supercage Ca<sup>2+</sup> cations<sup>13</sup>. The dipole-induced polarization of oxygen by the cation electrostatic field results in an infrared active stretch vibration, which is infrared inactive in the free gas. It was shown that intensity and frequency increased with higher electrostatic field of cation. The side bands observed at 1570cm<sup>-1</sup> and 1542cm<sup>-1</sup> (Figure 7-3) were attributed to a combination of the O-O stretching vibration with a low-frequency motion of the molecule in its site, as proposed for oxygen adsorbed on CaA and alkaline earth exchanged Y zeolite<sup>13;18</sup>. From Figure 7-3 we can conclude that Ca<sup>2+</sup> cation in MOR and ZSM5 also provide a similar environment as CaY to form Ca<sup>2+</sup>(O<sub>2</sub>) species.

As pointed out in the introduction, the zeolites exhibit different cation positions. Only one site of  $\text{Ca}^{2+}$  cations in ZSM5 (site I) and Y zeolite (site II) (Figure 1) are accessible to oxygen<sup>14,22</sup>, while in MOR, oxygen can adsorb on  $\text{Ca}^{2+}$  at both sites I and IV<sup>21</sup>. The electrostatic field site I,  $\text{Ca}^{2+}$  in the small side pocket is shielded stronger than at site IV facing the main channel. Consequently, the infrared spectrum showed two  $\text{Ca}^{2+}(\text{O}_2)$  species at  $1554\text{cm}^{-1}$  and  $1550\text{cm}^{-1}$ , which can be attributed to oxygen adsorbed on  $\text{Ca}^{2+}$  at site IV and site I respectively (Figure 7-3). Further, for MOR the  $\text{Ca}^{2+}$  cations is distributed over site I and site IV exclusively, while in Ca-ZSM site I is 90% occupied<sup>20</sup>. However, for CaY zeolite approximately 50% of the total  $\text{Ca}^{2+}$  is located at site II in supercage<sup>12</sup>. Since also the  $\text{Ca}^{2+}$  cation concentration varied with Si/Al ratio in the different type of zeolite, the infrared spectra after oxygen adsorption are normalized per  $\text{Ca}^{2+}$  based on the amounts of  $\text{Ca}^{2+}$  at the accessible sites (Figure 7-7). Clearly, the electrostatic field per accessible  $\text{Ca}^{2+}$  is the lowest in CaY (multiplied by 2 in Figure 7-7). In addition, the electrostatic field on the CaZSM5 zeolites is much higher than on MOR and Y. This is in agreement CO adsorption results on different type of  $\text{Ba}^{2+}$  exchanged zeolites as published by Panov et al<sup>6</sup>. Compared to CaY and CaMOR, the unusual high electrostatic field of CaZSM5 can be attributed to the fact that  $\text{Ca}^{2+}$  locates at the isolated aluminum occupied oxygen tetrahedral sites with single negative charges due to high Si/Al ratios (25 or 38). This results in the formation of sites with only partially compensated excessive positive charges of  $\text{Ca}^{2+}$ <sup>23;24</sup>.

Recent results showed that on CaY, at low propane coverage, propane mainly adsorbed at supercage  $\text{Ca}^{2+}$  site. The size of  $\text{Ca}^{2+}$  was found to be large enough allowing both propane methyl groups to attach to  $\text{Ca}^{2+}$ , which resulted in the formation of cyclic geometry of propane adsorption structure<sup>13</sup>. Similar to the oxygen adsorption, the interaction between  $\text{Ca}^{2+}$  and the propane methyl groups is electrostatic in

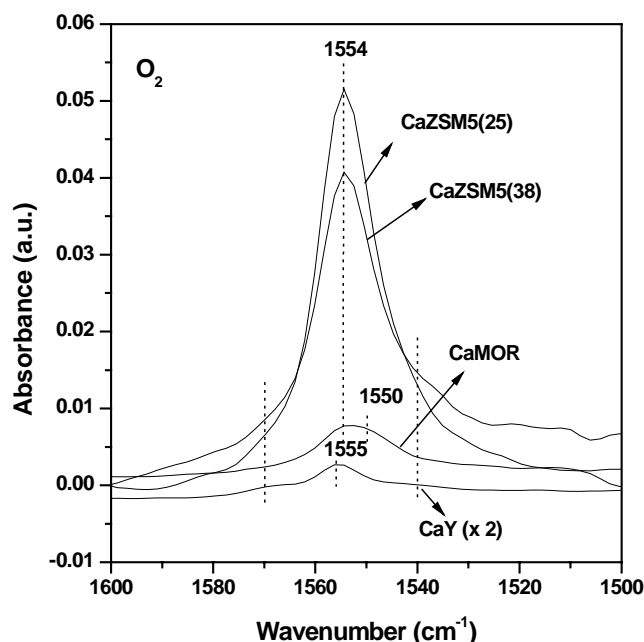


**Figure 7-7.** Normalized infrared spectra of oxygen adsorption at 40mbar on  $\text{Ca}^{2+}$  exchanged zeolites (Normalization based on the effective  $\text{Ca}^{2+}$  concentration in each zeolite. e.g. only  $\text{Ca}^{2+}$  cation in the supercage for CaY; all  $\text{Ca}^{2+}$  cation for CaMOR and CaZSM5)

nature. As a result, the  $\text{Ca}^{2+}$  induced polarization effect resulted in a shift of the symmetric stretching vibration of propane methyl group to the lower frequency ( $2838\text{ cm}^{-1}$ ) with increasing cation electrostatic field (figure 7-4).

Compared to the propane adsorption spectra on CaY, similar spectra were obtained on CaMOR and CaZSM5 below 0.2mbar equilibrium partial pressure (Figure 7-4), which suggests that adsorbed propane at  $\text{Ca}^{2+}$  site in all three zeolites had the same cyclic structure. Further, with increasing electrostatic field ( $\text{CaY} < \text{CaMOR} < \text{CaZSM5}$ ), the symmetric stretching vibration frequency of the propane methyl groups moved to lower wave number in the order  $\text{CaY} (2838\text{cm}^{-1}) > \text{CaMOR} (2829\text{cm}^{-1}) > \text{CaZSM5} (2826\text{cm}^{-1})$  (Figure 7-4).

On CaMOR and CaZSM5, the lower concentration of  $\text{Ca}^{2+}$ , due to the higher Si/Al ratio, and the stronger interaction of propane and  $\text{Ca}^{2+}$ , due to the higher electrostatic field, cause propane to saturate the  $\text{Ca}^{2+}$  site at lower propane partial pressure compared to CaY. As a result, with increasing propane partial pressure ( $>0.2\text{mbar}$ ) propane filled the zeolite pores *via* a dispersive force interaction with the zeolite framework oxygen atoms. Therefore the methyl groups are less affected by the cation electrostatic field and a peak appeared at  $2875\text{ cm}^{-1}$  (Figure 7-4) which can also be found in the gas phase propane spectrum.

Since the symmetric  $\text{CH}_3$  vibration at  $2838\text{-}2826\text{cm}^{-1}$  arises from the  $\text{Ca}^{2+}(\text{C}_3\text{H}_8)$  complex, the integrated area of this peak per effective  $\text{Ca}^{2+}$  site represents the normalized amount of propane adsorbed on  $\text{Ca}^{2+}$ . The

effective number of accessible  $\text{Ca}^{2+}$  sites for propane was calculated based on the fact that on CaY and ZSM5, the oxygen adsorption sites of  $\text{Ca}^{2+}$  are also accessible for propane. But on CaMOR, only site IV is accessible for both oxygen and propane. Site I only allowed to adsorb oxygen, because propane

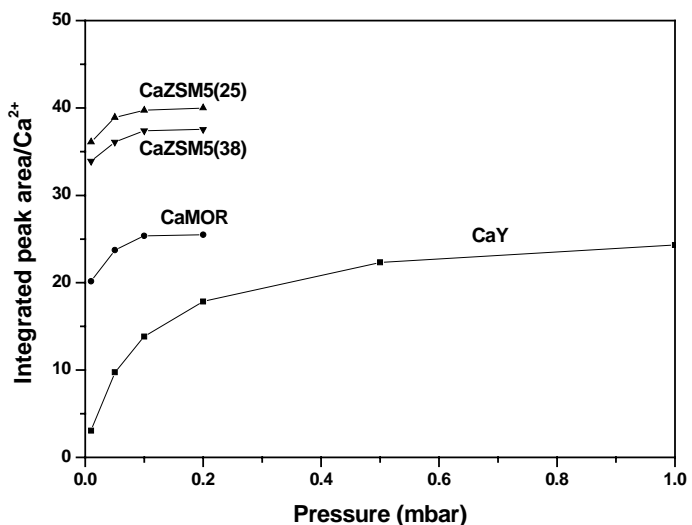


**Figure 7-8.** Propane adsorption isotherms on  $\text{Ca}^{2+}$  exchanged zeolites at 298K. (Propane adsorption was expressed as integrated area of infrared band at  $2838\text{-}2826\text{cm}^{-1}$  per effective  $\text{Ca}^{2+}$  sites in each zeolite. The effective  $\text{Ca}^{2+}$  sites used in calculation are  $\text{Ca}^{2+}$  cation in the supercage (site II) for CaY, in the main channel (site IV) for CaMOR and all  $\text{Ca}^{2+}$  cation for CaZSM5. For details see text)

(0.43nm) is too large to enter the side pocket (0.26 x 0.37nm) (Figure 7-1). The normalized propane adsorption isotherms of  $\text{Ca}^{2+}$  exchanged zeolites at room temperature are presented in Figure 7-8. Clearly, propane saturated the accessible  $\text{Ca}^{2+}$  sites on MOR and ZSM5 at much lower pressure than on CaY, where full coverage was not reached even at 1 mbar of propane pressure. In other words, the strength of adsorption increased from CaY to CaMOR to CaZSM5. Further, the normalized integrated peak area was found to decrease in the order  $\text{CaZSM5}(25) > \text{CaZSM5}(38) > \text{CaMOR} > \text{CaY}$ , which can be attributed to the decreasing electrostatic field in the samples. These results are in full agreement with the electrostatic field deduced from the oxygen adsorption experiments as shown in Figure 7-7.

#### 7.4.2 Effects of zeolite topology and Brønsted acid concentration on the reaction mechanism

In this study, on CaY zeolite high selectivity to acetone was observed in propane selective oxidation. The 2:1 mixture of 2-propanol to acetone observed on CaZSM5 is typical of homolytic peroxide decomposition, followed by a radical reaction pathway in the alkane autooxidation<sup>4</sup>. Finally,  $\text{CO}_x$  was observed for CaMOR, in addition to acetone and water. Therefore, it is clear that the type of zeolite has a large influence on the mechanism of propane oxidation.

Previous infrared result on CaY revealed that propane and oxygen could simultaneously adsorb at the supercage  $\text{Ca}^{2+}$  site to form  $\text{Ca}^{2+}(\text{O}_2)(\text{C}_3\text{H}_8)$  species *via* electrostatic interaction. Consequently, both molecules are activated by the polarization effect induced by the electrostatic field of  $\text{Ca}^{2+}$ , and their close proximity facilitates reaction. The similar propane and oxygen adsorption infrared spectra observed for the three types of  $\text{Ca}^{2+}$  exchanged zeolites (Y, MOR and ZSM5) in this study suggests that propane and oxygen adsorption results in similar  $\text{Ca}^{2+}(\text{O}_2)(\text{C}_3\text{H}_8)$  complexes which react to form isopropylhydroperoxide (IHP). Decomposition of IHP studied on CaY showed two parallel pathways. First, heterolytic elimination of water from IHP at Brønsted acid sites is the major path to result in acetone<sup>1</sup>. Second, homolytic decomposition of IHP at the  $\text{Ca}^{2+}$  site yields  $\text{C}_3\text{H}_7\text{O}^*$  and  $\text{HO}^*$  radicals which recombine with propane into 2 molecules of 2-propanol<sup>25</sup>. In the latter case,  $\text{Ca}^{2+}$  acted as a Lewis acid center to activate the O-O bond in IHP. The low amount of 2-propanol observed on CaY shows that its low electrostatic field is not capable to induce homolytic splitting of IHP to a large extent.

Contrast to CaY, homolytic decomposition of IHP showed to be an important reaction on CaZSM5. As discussed in previous section,  $\text{Ca}^{2+}$  cations in high Si/Al ratio ZSM5 are located at isolated aluminum occupied oxygen tetrahedral sites with single negative charges to form sites with only partially compensated excessive positive charges on  $\text{Ca}^{2+}$  cations. Those  $\text{Ca}^{2+}$  cations possess unusually high Lewis acidity, which results in strong activation of the IHP O-O bond, followed by homolysis. Moreover, IHP decomposition to acetone occurs at Brønsted acid sites. Protons are normally located at

the zeolite framework oxygen site next to the aluminum. However, the isolated Al sites in the high Si/Al ratio ZSM5 zeolites prevent the IHP at Ca<sup>2+</sup> sites to diffuse easily to the proton sites. Moreover, CaZSM has much less Brönsted acid sites compare to CaY (Figure 7-2), which again favours the IHP homolytic decomposition. Finally, the high amount of propane adsorbed in the ZSM5 zeolite pores contributes to a higher rate of 2-propanol formation.

Comparing the total of acetone and 2-propanol production per Ca<sup>2+</sup> cation site on CaY and CaZSM5 (Table 7-2), shows that Ca<sup>2+</sup> in CaZSM5 is about 5 times more active than in CaY (Table 7-2). Again, this attributed to the very high electrostatic field of Ca<sup>2+</sup> site in ZSM5. , Increasing Si/Al ratio of ZSM5 decreased the total amount of acetone and 2-propanol per Ca<sup>2+</sup> cation only slightly. Finally, 2-propanol to acetone ratio decreased with decreasing electrostatic field.

Although propane and oxygen adsorption showed a reasonable electric field of Ca<sup>2+</sup> in CaMOR, low acetone formation was observed on CaMOR. Moreover, over-oxidation to CO<sub>x</sub> was found. Over-oxidation of acetone was excluded, since no further oxidation occurred in the presence of acetone and oxygen at 80°C. We suggest that the full oxidation of propane can be due to the location Ca<sup>2+</sup> in the unique one-dimensional channel structure together with the high Brönsted acid concentration. As discussed above, in MOR, only Ca<sup>2+</sup> cation at site IV (Figure 7-1b) is accessible to both propane and oxygen molecules to allow reaction. The unique one-dimensional channel (0.65 x 0.7nm diameter) in MOR inhibits the formation of the bulky IHP molecule at the Ca<sup>2+</sup> site. Consequently, only minor amounts of acetone were found. On the other hand, acidic zeolites are well known as cracking catalyst for hydrocarbon molecules<sup>15</sup>. The high Brönsted acid concentration and the highly polarized propane molecule in CaMOR could induced propane cracking. In the presence of oxygen, the cracking intermediates (e.g. radicals or carbocation) may further oxidize to CO and CO<sub>2</sub>. Cracking is most likely inhibited in lower acidic zeolites such as CaY and CaZSM5. Further, although ZSM5 has small channels with diameter of 0.53 x 0.56nm in case of the straight channels and 0.51 x 0.5nm in case of the sinusoidal channels, preferential location of Ca<sup>2+</sup> is at the intersections of both channels (Figure 7-1c) providing enough space to accommodate IHP. Also the supercage in zeolite Y is large enough (Figure 7-1a) to allow propane selective oxidation.

In good agreement with our previous results, this study further confirmed that a high electrostatic field of Ca<sup>2+</sup> determines the propane oxidation activity and selectivity. However, also the geometrical restrictions affect the activity due to the limitation of formation transition-state complexes to IHP at Ca<sup>2+</sup>. The optimal ratio between Brönsted acid sites and Ca<sup>2+</sup> cation could enhance reaction activity, but too high concentration of Brönsted acid sites also affects selectivity due to hydrocarbon cracking. Nevertheless, the studies in this paper are limited to surface reaction because oxygenates are strongly

adsorbed in the zeolites. Therefore the catalytic cycle is not closed. Currently, further studies are undertaken in developing and extending this methodology in alkane partial oxidation by changing reactant composition in order to desorb products at reaction conditions.

## 7.5 Conclusion

Based on oxygen and propane adsorption at room temperature, the electrostatic field of  $\text{Ca}^{2+}$  was observed to increase in the order  $\text{CaY} < \text{CaMOR} < \text{CaZSM5}(38) < \text{CaZSM}(25)$ . The electrostatic field and Lewis acidity of  $\text{Ca}^{2+}$  cation in CaY and CaZSM5 was found to correlate with propane selective oxidation activity and selectivity. At 80°C, low activity but high selectivity to acetone was observed for propane oxidation on CaY zeolite due to the main reaction path of heterolytic  $\text{H}_2\text{O}$  elimination of reaction intermediate IHP. On CaZSM5, an unusual high electrostatic field and Lewis acidity of  $\text{Ca}^{2+}$  cation resulted in high activity, but favoured homolytic IHP decomposition pathway, which formed a 2:1 mixture of 2-propanol and acetone in the products. On CaMOR, the steric restriction for accommodating the transition-state complex to IHP resulted in the lowest activity of acetone formation. Further, the high Brønsted acid concentration with high propane polarization on CaMOR resulted in propane deep oxidation to form CO and  $\text{CO}_2$ . It is convincingly showed that the electrostatic field of  $\text{Ca}^{2+}$ , the zeolite structures and the presence of Brønsted acid sites play important roles in determining the reaction paths in propane partial oxidation on  $\text{Ca}^{2+}$  exchanged zeolites.

## Reference List

1. Xu, J.; Mojet, B. L.; Ommen, J. G. v.; Lefferts, L. *Phys.Chem.Chem.Phys.* **2003**, *5*, 4407-4413.
2. Xiang, Y.; Larsen, S. C.; Grassian, V. H. *Journal of the American Chemical Society* **1999**, *121*, 5063-5072.
3. Vanoppen, D. L.; DeVos, D. E.; Jacobs, P. A. *Progress in Zeolite and Microporous Materials, Pts A-C* **1997**, *105*, 1045-1051.
4. Vanoppen, D. L.; De Vos, D. E.; Jacobs, P. A. *Journal of Catalysis* **1998**, *177*, 22-28.
5. Sun, H.; Blatter, F.; Frei, H. *Catalysis Letters* **1997**, *44*, 247-253.
6. Panov, A. G.; Larsen, R. G.; Totah, N. I.; Larsen, S. C.; Grassian, V. H. *Journal of Physical Chemistry B* **2000**, *104*, 5706-5714.
7. Blatter, F.; Sun, H.; Vasenkov, S.; Frei, H. *Catalysis Today* **1998**, *41*, 297-309.
8. Schlenker, J. L.; Pluth, J. J.; Smith, J. V. *Materials Research Bulletin* **1979**, *14*, 751.
9. Kustov, L. M.; Kazansky, V. B. *Journal of the Chemical Society, Faraday Transactions* **1991**, *87*, 2675.

10. Bordiga, S.; Garrone, E.; Lamberti, A.; Zecchina, A.; Kazansky, V. B. *Journal of the Chemical Society, Faraday Transactions* **1994**, *90*, 3367.
11. Ohgushi, T.; Niwa, T.; Arakia, H.; Ichino, s. *Microporous and Mesoporous Materials* **2004**, *8*, 231.
12. Xu, J.; Mojet, B. L.; Ommen, J. G. v.; Lefferts, L. *Journal of Physical Chemistry B* **2004**, *108*, 15728-15734.
13. Xu, J.; Mojet, B. L.; Ommen, J. G. v.; Lefferts, L. *Journal of Physical Chemistry B* **2005**, *Submitted*.
14. Donald W. Breck *Zeolite molecular sieves: structure, chemistry, and use*, Wiley: New York, 1974.
15. H. van Bekkum *Introduction to zeolite science and practice*, Elsevier: Amsterdam, 2001.
16. Smudde, G. H.; Slager, T. L.; Weigel, S. J. *Applied Spectroscopy* **1995**, *49*, 1747-1755.
17. Jousse, F.; Lara, E. C. D. *Journal of Physical Chemistry* **1996**, *100*, 238-244.
18. Jousse, F.; Lara, E. C. D. *Journal of Physical Chemistry* **1996**, *100*, 233-237.
19. Calera, S.; Dubbeldam, D.; Krishna, R.; Smit, B.; Vlugt, T. J. H.; Denayer, J. F. M.; Martens, J. A.; Maesen, T. L. M. *Journal of the American Chemical Society* **2004**, *126*, 11377-11386.
20. Rep, M. Side Chain Alkylation of Toluene with Methanol over Basic Zeolites. PhD thesis, University of Twente, 2002.
21. Beerdsen, E.; Smit, B.; Calera, S. *Journal of Physical Chemistry B* **2002**, *106*, 10659-10667.
22. Bajusz, I. G.; Goodwin, J. G. *Langmuir* **1998**, *14*, 2876-2883.
23. Kazansky, V. B.; Serykh, A. I. *Phys.Chem.Chem.Phys.* **2004**, *6*, 3760-3764.
24. Kazansky, V. B.; Serykh, A. I. *Microporous and Mesoporous Materials* **2004**, *70*, 151-154.
25. Xu, J.; Mojet, B. L.; Ommen, J. G. v.; Lefferts, L. *Journal of Catalysis* **2004**, *Submitted*.

## Chapter 8

### Epitome

---

#### 8.1 Extended reaction mechanism of propane oxidation on cation exchanged zeolites

The research presented in this thesis has provided information to better understand the mechanism of propane selective oxidation to acetone over alkaline earth exchanged zeolites. The information includes 1) the location of active sites; 2) the formation of an adsorbed reaction precursor; 3) the functioning of active sites in reaction activity and selectivity; 4) the water-assisted low temperature acetone desorption.

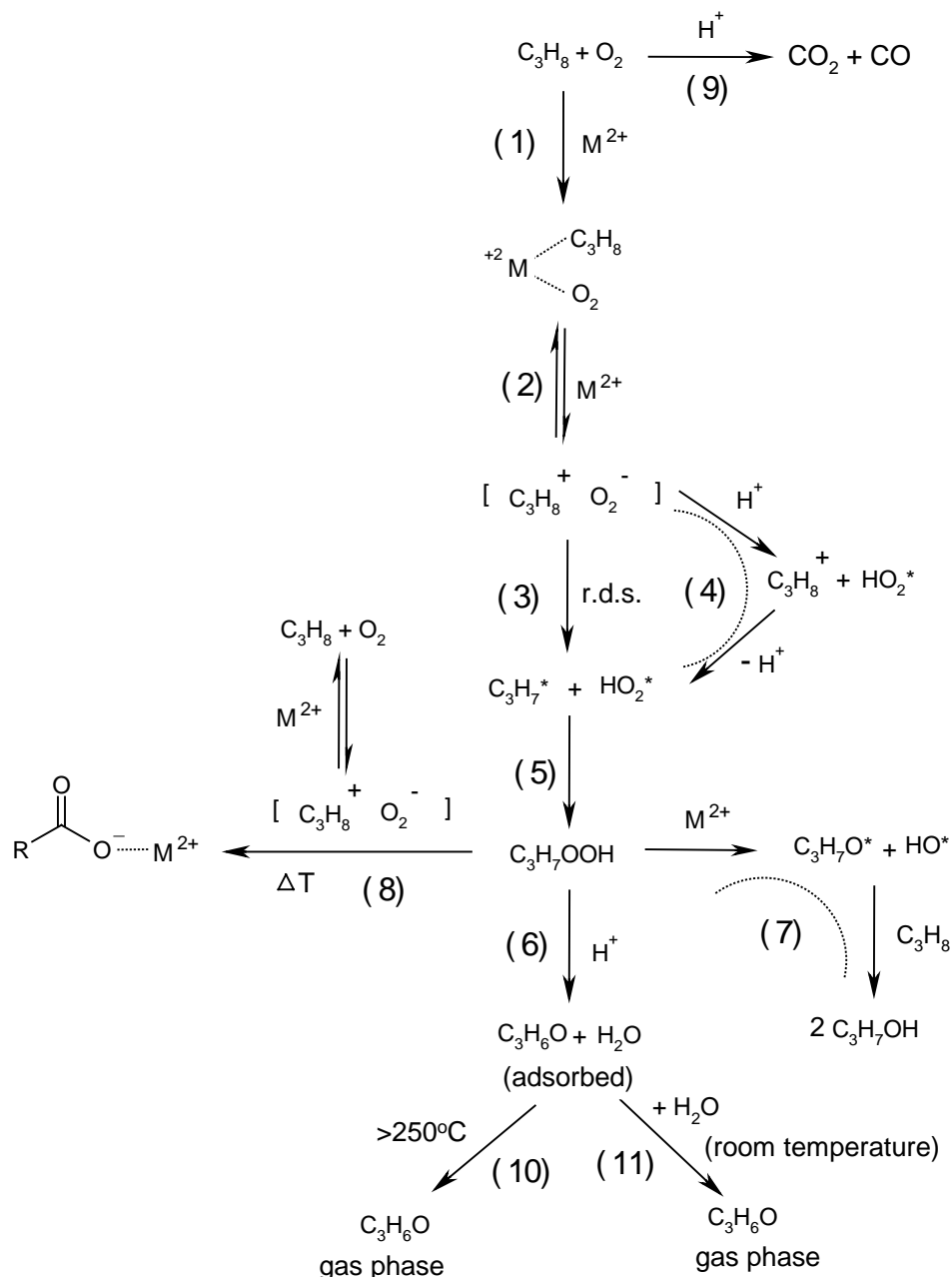
As an example, variation of exchanged  $\text{Ca}^{2+}$  content in CaNaY zeolites showed that more than 50%  $\text{Na}^+$  exchange levels with  $\text{Ca}^{2+}$  resulted in sudden property changes for the zeolites: a dramatically increased amount of Brönsted and Lewis acid sites accompanied with increased adsorbed propane quantity and initial acetone formation rate<sup>1</sup>. These phenomena can be fully attributed to the location of  $\text{Ca}^{2+}$  in the supercage of Y-zeolite above 50% exchange level. It turned out convincingly that only alkaline earth cations located in the supercage contributed to the formation of Brönsted and Lewis acidity as well as selective oxidation activity at room temperature<sup>1</sup>.

Infrared results on reactants adsorption revealed that the non-redox alkaline earth cation in the supercage of Y zeolite provides a specific adsorption geometry to invoke reaction<sup>2-3</sup>. Oxygen and propane are activated by simultaneously adsorption at supercage cation site to form a  $\text{M}^{2+}(\text{O}_2)(\text{C}_3\text{H}_8)$  complex *via* exclusively electrostatic cation-adsorbate interaction<sup>3</sup>. The activity of propane selective oxidation increased in the order  $\text{BaY} < \text{MgY} < \text{SrY} < \text{CaY}$ , which is in agreement with oxygen polarization induced by electrostatic field observed in infrared spectra<sup>3-4</sup>. The much lower electrostatic field of  $\text{Mg}^{2+}$  than expected based on its charge to radius ratio, was attributed to the small ion radius of  $\text{Mg}^{2+}$  (0.65Å) allowing the  $\text{Mg}^{2+}$  cation to be more closely to the plane of the six-ring windows, which shields electric field of  $\text{Mg}^{2+}$  cation more strongly<sup>3:5</sup>. As a result, linear propane adsorption was





(IHP) (**step 5**)<sup>4,6</sup>. However, the formation of IHP is slowed down if the zeolite channels are not big enough to accommodate this large branched molecule as was found for mordenite<sup>9</sup>.



**Scheme 8-2.** Reaction network for propane selective oxidation over cation-exchanged zeolite

Decomposition rate of IHP into acetone increased in the order BaY < SrY < CaY (< MgY) which was attributed to an increase in number of Brönsted acid sites in the samples<sup>4,10</sup>. Moreover, to FTIR data of acetone adsorbed on Brönsted acid sites<sup>4</sup> pointed out IHP decomposition into acetone occurred at Brönsted acid sites (**step 6**). Specifically, with increasing concentration of Brönsted acid sites on calcium exchanged Y zeolite, Volcano type of plots were observed for: (1) initial acetone formation

rate; (2) total amount of acetone produced after 20 hours of reaction <sup>11</sup>. The results clearly showed that Brönsted acidity increases IHP formation rate, most likely *via* a catalytic H<sup>+</sup>-abstraction (**step 4**) <sup>11</sup>, as well as IHP decomposition into acetone and water (**step 6**). Since acetone formation from propane and oxygen involves two active sites (bare cation and Brönsted acid site), a subtle balance between the numbers of supercharge Ca<sup>2+</sup> ions and Brönsted acid sites determines the reaction activity.

However, high Brönsted acidity should be avoided because this could result in propane cracking, and consequently over-oxidation to CO and CO<sub>2</sub> (**step 9**) <sup>9</sup>. Moreover, increasing IHP formation rate by increasing Brönsted acidity on CaY zeolite also decreases selectivity due to 2-propanol formation <sup>11</sup>. After its formation, IHP is first adsorbed close to the cation sites <sup>4</sup> where the bare cation acts as a Lewis acid center <sup>12</sup>. It was found that with longer IHP residence time or higher IHP concentration the bare cation activates the peroxide bond in IHP, thus catalyzing homolytic IHP decomposition to form C<sub>3</sub>H<sub>7</sub>O\* and HO\* radicals. Subsequently, an alkyloxyl radical reacts with propane, followed by radical recombination into two molecules of 2-propanol (**step 7**) <sup>11-12</sup>. In cation exchanged Y zeolite, formation of 2-propanol is a minor parallel reaction in addition to IHP decomposition into acetone and water. Increasing the cation electrostatic field by increasing the Si/Al ratio of the zeolite (e.g. from Y to ZSM5) strongly enhances propane oxidation activity<sup>9</sup>. Since both electrostatic field and Lewis acidity of the cation increase (or decrease) simultaneously, selectivity to acetone dramatically decreased on ZSM5 due to homolytic IHP decomposition to form 2-propanol <sup>9</sup>. A 2:1 mixture of 2-propanol and acetone was observed for propane oxidation on CaZSM5 with a Si/Al ratio of 25.

Further, increasing reaction temperature leads to the formation of monodentate carboxylate ions most likely *via* reaction of IHP and the charge-transfer complex, which is adsorbed at the cation site (**step 8**) <sup>3</sup>. Decreasing both IHP decomposition rate and proton transfer rate an increased amount of carboxylate was produced.

Finally, thermal desorption of produced acetone needs very high temperatures (> 250°C) on alkane-earth exchanged zeolites (**step 10**) <sup>10</sup>. At such a high temperature, overoxidation occurs under reaction conditions, which dramatically decreases reaction selectivity. Release of oxygenated hydrocarbons from cation exchanged zeolites can be achieved by extraction with polar organic solvents <sup>4;8</sup>. However, a solvent free method would be environmentally and economically preferable. It was discovered that acetone can be desorbed even at room temperature by simply adding water to the sample after reaction (**step 11**) <sup>10</sup>. Consequently, water-assisted desorption of acetone opens up a route to practical application of this type of samples for partial oxidation of small alkanes.

## 8.2 Recommendations for future work

Although a lot of efforts have been made in this thesis to explore this novel method of selective oxidation of small alkanes, there are still open questions remaining. Thus it is worthwhile to further investigate such a system experimentally and theoretically.

First and most important is to turn such a reaction into a real catalytic system. Since regeneration of wet zeolites can be done at much lower temperatures than for acetone-saturated zeolites, the water-assisted low temperature desorption of acetone opens up a route for practical application of this type of samples<sup>10</sup>. Nevertheless, continuous operation would be more preferable. Thus, it is sensible to perform experiments to determine the delicate balance between good activity, selectivity and desorption of products by tuning zeolite properties, feed composition and reaction temperature.

Second, in this thesis, we only focused on the thermal activation. However, experimental results from literature and our project partner (Leiden University, Dr. Mischa Bonn and Dr. Otto Berg) showed that activity of propane selective oxidation on CaY zeolite is higher by photo-activation than by thermal-activation. Although it has been claimed that the charge-transfer state is stabilized in the electrostatic field of the supercage in the photoreaction<sup>7</sup>, until now no proof has been given for the existence of electron transfer in the thermal reaction mechanism. In the thermal reaction, the adsorption complex could also lead to an alternative mechanism with hydrogen transfer instead of ion-pair formation. Therefore, the full mechanisms involved in both photo and thermal activation oxidation need to be clarified better understand the system and to further improve catalyst performance. This will be a subject of future calculations and experiments.

Third, an effective method to estimate the number of active cation sites need to be developed. The active cation sites are only poorly shielded bare cation sites with high electrostatic field, and need to be accessible for both propane and oxygen molecules. At low propane coverage, extra framework cations act as an “extra wall” and create extra interaction centers in the zeolites which have favorable electrostatic interactions with propane molecules<sup>3</sup>. Therefore, we expect that the strength of such interaction differ from the interaction *via* dispersive force with lattice oxygen at higher loading. To quantify the active sites, TGA-DSC could be applied, while it simultaneously provides information on the role of the cation in alkane and oxygen adsorption.

#### Reference List

1. Chapter 4 in this thesis
2. K. Hadjiivanov, E. Ivanova, Klissurski, D, *Catalysis Today* **2001**, 70 73-82
3. Chapter 6 in this thesis
4. Chapter 2 in this thesis

5. K. Hadjiivanov, E. Ivanova, H. Knozinger, *Microporous and Mesoporous Materials* **2003**, 58 225-236
6. H. Sun, F. Blatter, H. Frei, *Catalysis Letters* 44, 247-253 (1997)
7. F. Blatter, H. Sun, S. Vasenkov, H. Frei, *Catalysis Today* 41, 297-309 (1998)
8. R. G. Larsen et al., *Journal of Catalysis* 204, 440-449 (2001)
9. Chapter 7 in this thesis
10. Chapter 3 in this thesis
11. Chapter 5 in this thesis
12. D. L. Vanoppen, D. E. De Vos, P. A. Jacobs, *Journal of Catalysis* 177, 22-28 (1998)

## Acknowledgements

First I would like to extend my deepest gratitude to my Promotor, Prof. dr. ir. Leon Lefferts, for having offered me this Ph.D. position, and your guidance and encouragement throughout the whole process of my PhD project.

And I also would like to express my humble regards to my Assistant Promoter, Dr. Barbara L. Mojet. Thank you so much for your valuable time and advises in my scientific research, presentations, posters and paper. It has been a really hard time for you in the last four years.

Thanks

To everyone who is working or worked in CPM group

To many who have become friends along the way

To those whose help is highly appreciated

Finally special thanks to my wife Weiqun and my son Andy for your love and support.

Thank you so much for all you have done!

Wishing you all the best in your life,

Jiang

## List of publications

Propane selective oxidation on alkaline earth exchanged zeolite Y: room temperature in situ IR study

Jiang Xu, Barbara L. Mojet, Jan G. van Ommen and Leon Lefferts

*Physical Chemistry Chemical Physics*, 2003, 5, 4407-4413

Desorption of acetone after room temperature propane oxidation

Jiang Xu, Barbara L. Mojet, Jan G. van Ommen and Leon Lefferts

*The Journal of Physical Chemistry B*, 2004, 108, 218-223

The effect of Ca<sup>2+</sup> position in zeolite Y on selective oxidation of propane at room temperature

Jiang Xu, Barbara L. Mojet, Jan G. van Ommen and Leon Lefferts

*The Journal of Physical Chemistry B*, 2004, 108, 15728-15734

The effects of Brønsted acidity in the mechanism of selective oxidation of propane to acetone on CaY zeolite at room temperature

Jiang Xu, Barbara L. Mojet, Jan G. van Ommen and Leon Lefferts

*The Journal of catalysis*, 2005, accepted

Formation of M<sup>2+</sup>(O<sub>2</sub>)(C<sub>3</sub>H<sub>8</sub>) species in alkaline-earth exchanged Y zeolite during propane selective oxidation

Jiang Xu, Barbara L. Mojet, Jan G. van Ommen and Leon Lefferts

*The Journal of Physical Chemistry B*, 2005, to be submitted

Effect of zeolite geometry for propane selective oxidation on cation electrostatic field of Ca<sup>2+</sup> exchanged zeolites

Jiang Xu, Barbara L. Mojet, Jan G. van Ommen and Leon Lefferts

*Microporous and Mesoporous Materials*, 2005, to be submitted

Selective oxidation of propane to acetone at room temperature in modified CaY zeolite: effect of active sites for catalysis preparation

Jiang Xu, Barbara L. Mojet, Jan G. van Ommen and Leon Lefferts

In preparation

Changes in electronic properties of the zeolite framework induced by the extra framework cation: A <sup>27</sup>Al MAS and <sup>27</sup>Al MQ MAS NMR study

Jiang Xu, Barbara L. Mojet, Peter C. M. M. Magusin, Jan G. van Ommen and Leon Lefferts

In preparation

## Curriculum Vitae

Jiang Xu was born on 12 March 1972 in Changshu, a very beautiful city in China. From 1990 to 1994, he majored in Applied Chemistry in the Department of Chemistry at Xiangtan University, China. In 1994, he joined the catalysis group in State Key Laboratory of Catalysis, Institute of Dalian Physical Chemistry, China Academy of Sciences. He worked in the area of the preparation of new material of molybdenum nitride catalyst and its application in the HDN and HDS for fuels. After getting his master degree in June 1997, he joined UPM-Kymmene, the world third largest paper manufacturer and worked there for four years in the Department of Power and Utilities as Engineer in the beginning and promoted as Project Manager later on.

In July 2001 he started his PhD project in Heterogeneous Catalysis in the CPM group at the University of Twente, the Netherlands, under the supervision of Prof. Leon Lefferts and Dr. Barbara, L. Mojet. He devoted his four years in the research of “selective oxidation of light alkanes over zeolites”. The main findings are described in this thesis.